Slope Stability analysis of Selected Slope Sections along Jinka to Mendir road,south omo zone,SW Ethiopia

LIYA ZELEKE FAGE

A Thesis Submitted To The Department Of Applied Geology

School Of Applied Natural Science

Presented In Partial Fulfillment Of The Requirement For The Degree Of Master Of Science In Engineering Geology

Office Of Graduate Studies

Adama Science And Technology University

January,2023

Adama, Ethiopia

Slope Stability analysis of Selected Slope Sections along Jinka to Mendir road,south omo zone,SW Ethiopia

LIYA ZELEKE FAGE

Major advisor: Bayisa Regassa (Ph.D.)

Co-advisor: Tola Garo (MSc.)

A Thesis Submitted to the Department of Applied Geology

School of Applied Natural Science

Presented In Partial Fulfillment of the Requirement for the Degree of Master's in Engineering Geology

Office of Graduate Studies

Adama Science and Technology University

January, 2023

Adama, Ethiopia

Declaration

I hereby declare that this Master Thesis entitled is "**Slope Stability analysis of Selected Slope Sections along Jinka to Mendir road,south omo zone,SW Ethiopia"** my original work. That is, it has not been submitted for the award of any academic degree, diploma, or certificate in any other university. All sources of materials that are used for this thesis have been duly acknowledged through citation

______________________________	__________________________	__________________
Name of the Student	Signature	Date

Recommendation

We, the advisors of this thesis, hereby certify that we have read the revised version of the thesis entitled "**Slope Stability analysis of Selected Slope Sections along Jinka to Mendir road,south omo zone,SW Ethiopia**" was prepared under our guidance by **Liya Zeleke** and submitted in partial fulfillment of the requirements for the degree of Masters of Science in **Engineering Geology**. Therefore, we recommend the submission of a revised version of the thesis to the department following the applicable procedures.

______________________	______________________	______________________
Major Advisor	Signature	Date
______________________	______________________	______________________
Co-advisor	Signature	Date

Approval Page

We, the advisors of the thesis entitled "**Slope Stability analysis of Selected Slope Sections along Jinka to Mendir road,south omo zone,SW Ethiopia**" and developed by Liya Zeleke, hereby certify that the recommendation and suggestions made by the board of examiners are appropriately incorporated into the final version of the thesis.

Major Advisor	Signature	Date
Co-Advisor	Signature	Date

We, the undersigned, members of the Board of Examiners of the thesis by **Liya Zeleke** have read and evaluated the thesis entitled "Slope Stability Analysis Along the Selected Road Sections of Jinka-Mendir Road, South Omo Zone Southwestern Ethiopia" and examined the candidate during the open defense. This is, therefore, to certify that the thesis is accepted for partial fulfillment of the requirement of the degree of Master of Science in **Engineering Geology**.

Chairperson	Signature	Date
Internal Examiner	Signature	Date
Ephrem Getahun(PHD)	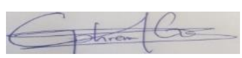	15/3/03/2024
External Examiner	Signature	Date

Final approval and acceptance of the thesis is contingent upon the submission of its final copy to the Office of Postgraduate Studies (OPGS) through the Department Graduate Council (DGC) and School Graduate Committee (SGC).

Department Head	Signature	Date
School Dean	Signature	Date
Office of Postgraduate Studies, Dean	Signature	Date

ACKNOWLEDGMENT

First of all, I would like to express my greatest praise to the Almighty God who strengthened, encouraged, mentored, and helped me to accomplish this thesis. Next, I would like to express my special gratitude to my advisor Dr.Bayisa Regasa as well as to my co-advisor Mr. Tola Garo who made this work possible.

I would extend my acknowledgment to the Addis Ababa Science and Technology University Department of Civil Engineering Geotechnical Laboratory & Geology Department for their commitment during laboratory work lastly; I offer a great thanks to Adama Science and Technology University for their financial help and the Department of Geology for providing different materials like field equipment.

Table of Contents

LIST OF TABLE

LIST OF FIGURE

List of Abbreviations and Acronyms

AASHTO = America Association of State Highway and Transportation Officials

ASTM = American Society for Testing Materials Standard

DEM = Digital elevation model

SNNP =South Nation, Nationality, and Peoples Region

FEM = Finite element method

FOS = Factor of safety

GLEM= General Limit Equilibrium method

ISRM = International Society of Rock Mechanics‟ Standards

LEM = Limit equilibrium method

D =Disturbance factor

E = Modulus of Elasticity

R =Rebound number

V =Poisson Ratio

JCS= Joint Wall Compressive Strength

JV = Volumetric Joint Count

RQD = Rock Quality Designation

SRF = Strength reduction factor

UCS = Uniaxial Compressive Strength

USCS=Unified Soil Classification System

ABSTRACT

Slope failures are among the most common geo-environmental natural hazards in the world's hilly and mountainous terrain causing damage to human life and the destruction of civil engineering infrastructure such as roads and open-pit mines. The road which connects Jinka to Mendir is also frequently affected by slope instabilities. Hence, this study is aimed at identifying and analyzing critical slope sections along this road by using Kinematic, Limit Equilibrium Method (LEM) and Finite Element Method (FEM). The input parameters for the analysis were determined through field investigation methods such as discontinuity surveying, in-situ Schmidt hammer test, sampling, and laboratory testing of samples. From field investigation, two critical structural controlled and one critical non-structural controlled and 2 soil slope sections were identified. Schmidt hammer rebound test conducted on the study area revealed that the Uniaxial Compressive Strength (UCS) value ranges from 68.3MPa to 72.8MPa and 95 MPa for rocks of structural and non-structural controlled slope sections, respectively. The stability analysis of structurally controlled slope sections is first done via kinematic analysis and the results showed that RSS3 and RSS4 are unstable for planar mode of failure. Further stability analysis of planar mode of failure in terms of Factor of Safety (FOS) using Rocplane 2.0 software revealed that RSS3 is unstable under static and dynamic saturated conditions due to JSS1 and JSS2. A similar analysis of planar mode of failure in terms of Factor of Safety (FOS) using Rocplane 2.0 software revealed that RSS4 is unstable under static and dynamic saturated conditions due to JSS2. Similarly, stability analysis using both LEM-based Slide 6.0 and FEM-based Phase 2.0 software has also shown that non-structural controlled, structural controlled, and soil slope sections are unstable under saturated conditions. This illustrates that rainfall/or saturation is the major factor contributing to slope failure in the study area. Moreover, the FOS obtained from LEM-based Slide 6.0 software and SRF obtained from FEM-based Phase 2.0 software are in very close agreement which validated slope instability problems in the study area. Depending on the analysis of results, a total bolt capacity of 290 and 198 t/m were designed for RSS3 to stabilize planar failure due to JS1 and JS2 respectively. Similarly, rock bolts with a total capacity of 198 t/m at RSS4 stabilize planar failure due to JS2. Moreover, for non-structural controlled sections, it is designed to reduce slope angle and height. The safety factors were computed by lowering the slope angle from the original condition and by lowering the slope height according to research increasing the factor of safety. For soil sections it is designed to flatten the slope angle from the original slope angle was modeled as (1H: 1V) and the analysis was then carried out by subsequently reducing the slope angle from (1H:1V) to (1.5H:V), (2H:1V) and (2.5H:1V),(3H:1V) by keeping the height (V) constant that enhances the factor of safety. Moreover, surface and subsurface drainage systems are also recommended in these slope sections for better control of water effects.

Keywords: *Slope stability analysis, Critical section, Factor of safety, Kinematic analysis, Limit Equilibrium, and Finite element method*

CHAPTER ONE

1. INTRODUCTION

1.1 Background

Slope stability analysis is critical for the long-term development and safety of mining, civil, and environmental engineering projects around the world. Around the world, many geological and geotechnical difficulties occur that cause slope failures to damage civil engineering projects such as dams, irrigation canals, highways, and railroads (Khandker et al., 2013). Slope failures are natural events that occur frequently along cut slopes of highways built in hilly places around the world, resulting in the loss of life, injury, and major property damage each year (Aleotti & Chowdhury, 1999). Most of the time, inappropriate adjustments to the natural slope during road construction and widening can disrupt the cut slope's stability.

Slope instability is induced by a mixture of internal and external causes that reduce or enhance the shear strength of the slope material (Searom, 2017). Although many geotechnical engineers and engineering geologists have conducted numerous investigations on slope stability analyses in the past, stability issues persist as a result of human and natural disturbances that disrupt the delicate nature of the soil and rock slope (Abramson et al., 2001). The characteristics and orientation of a discontinuity in the rock mass are the most essential requirements for rock slope stability (Vatanpour et al., 2014). Additional effective criteria that contribute to instability include the type and filler material qualities of joints, external force conditions, weathering, and groundwater level in tensional fractures (Regmi et al., 2013; R. K. Sharma et al.,2013). The varieties of slope failure can be planer, wedge, or topple depending on the orientation discontinuities (Hoek & Bray, 1981).

The problem of slope instability was also prevalent along roads that run through the country's mountainous regions. Because of mountain and roadside cutting, the majority of the Ethiopian plateau in the north, south, and western regions has a history of slope instability, both in superficial materials and at bedrock (Ayalew, 1999).The study area was also located on the southwestern Ethiopia plateau, where slope instability is a major problem. There are many ways to perform slope stability analysis, each with advantages and disadvantages. Several researchers have studied slope stability using analytical and numerical modeling methods such as limit equilibrium, kinematic, and finite element methods.

Slope stability evaluations utilizing the limit equilibrium method or the finite element approach applying the shear strength reduction (SSR) technique can be performed to analyze the factor of safety (Kumar et al., 2020). The slope stability factor of safety (FoS) is defined as the ratio of resisting forces to driving forces. Furthermore, the slope stability study was performed on the Rocscience Slide and Phase2 software utilizing the limit equilibrium method (LEM) and the finite element method (FEM) (Komadja et al., 2021).

For slope stability analysis, numerous LEMs can be characterized as rigorous or non-rigorous. The rigorous approach for satisfying any slip surface(Morgenstern & Price, 1965) and the complete equilibrium conditions appeared to be correct (Zhang et al., 2013), hence they were used in this investigation.

Kinematic analysis was used to analyze failure modes by demonstrating the geometrical relationship between numerous joint sets and the slope face (Khanna & Dubey, 2021).FEM can solve complex problems with stress and movement data, which the limit equilibrium method cannot (Cheng et al., 2006). Griffiths & Lane, (1999) further show that the FEM-SRF can accurately simulate a slope and provide the FOS for the critical slip surface without making any assumptions. The SRF technique, which is equivalent to FOS, gradually decreases the shear strength parameters (cohesion and angle of friction) of the slope's materials until the slope becomes unstable (Bushira et al., 2018). Slope instability engineering solutions require a thorough understanding of analytical methods, investigation tools, and stabilization procedures.

The selected site is in Jinka town, in the South Omo Zone of Ethiopia's South Nation, Nationality, and People's Region, 563 kilometers from Addis Ababa. This research will enable designers, administrators, and planners to make judgments about the safety of local citizens and the harm caused by slope instability to road infrastructure in the study area.

To describe the engineering characteristics of materials along the road sections, a complete field survey, discontinuity measurements, in situ tests, and laboratory experiments were used. The primary purpose of the research is to calculate the factor of safety, identify critical slope sections, and develop corrective procedures. Limit equilibrium and finite element methods are used to determine the stability of the slope in the area of study and to recommend some remedial measures based on the analysis results.

1.2 Statement of the problem

Slope instability is one of the most hazardous processes in the world which is caused by failure of soil, rock, or a combination of soil and rock along the road section (Cheng and Lau, 2008). The highlands of Ethiopia are highly susceptible to slope instability due to heavy rainfall and land-use change, including the effect of road construction(Woldearegay,2013). The present study was undertaken along the road Jinka to Mendir, South Omo Zone, Southwestern Ethiopia. Southwestern Ethiopia passes through an extremely rugged terrain characterized by steep hill slopes and deep valleys. However, the road was affected by frequent slope instability problems during and after its construction. There is different manifistaion of slope stability in study area such as spring,development of crack,damage on different stractures.The problem was intense mainly during the rainy season when different rock and soil slope failures occur. The stated slope stability problem along the road section hinders day-to-day traffic activities by blocking and damaging the road. In addition, there was no research or other investigation done on slope stability along the road section to identify, analyze, and recommend proper remedial measures. Therefore, the present study was intended to identify, locate, and analyze slope stability problems along selected road sections using different approaches such as kinematic deterministic, Limit Equilibrium, and Finite Element approach and recommended proper remedial measures based on the analysis result.

1.3 Significance of the Study

The current research will be used to design slope instability countermeasures for future road improvements and maintenance. The study's findings are expected to improve understanding of the rock and soil slope stability conditions, engineering characteristics of rock and soil slopes, failure mechanisms, and triggering factors in the study area.

The current study tried to identify areas that may be sensitive to future slope problems in addition to investigating the causes of slope instability. Furthermore, preventive stabilization and remedial procedures are required for potentially unstable slope sections where the stability study results show that the roadway slope does not meet the factor of safety criterion. Furthermore, the findings of this study will be utilized to guide the construction of other highways in comparable or related topographic and geological environments.

1.4 Limitations of the Study

The research location was discovered along the road from Jinka to Mendir in the South Omo Zone, Southern Ethiopia. Also, the current study area lacks appropriate secondary data to comprehend the subsurface geology, such as drill log geophysical data, geotechnical reports, and trial test pit inside depth. Furthermore, no regular groundwater monitoring wells were found in the research area, making it impossible to evaluate groundwater level variations and their impact on slope stability. Similarly, no borehole log data were available to analyze subsurface lithology, and even if a borehole log was provided, a trial test pit was located inside the depth**.**

1.5 Description of the Study Area

1.5.1 Location and Accessibility

Figure 1 shows the study area for research work in the South Omo Zone of Ethiopia's South Nation, Nationality, and People's Region. It is bounded by longitudes ranging from 36 30' to 37 30' E 30' E and latitudes ranging from 5°30' to 6°00' N. It is defined topographically by a variety of mountains and gorges. There are two approaches to the research area. Addis Abeba-Ziway/Batu-Shashemene-Awassa-Sodo-Araba Minch-Konso-Jinka asphalt road; and Addis Abeba-Butajira-Sodo-Araba Minch-Konso-Jinka asphalt road.

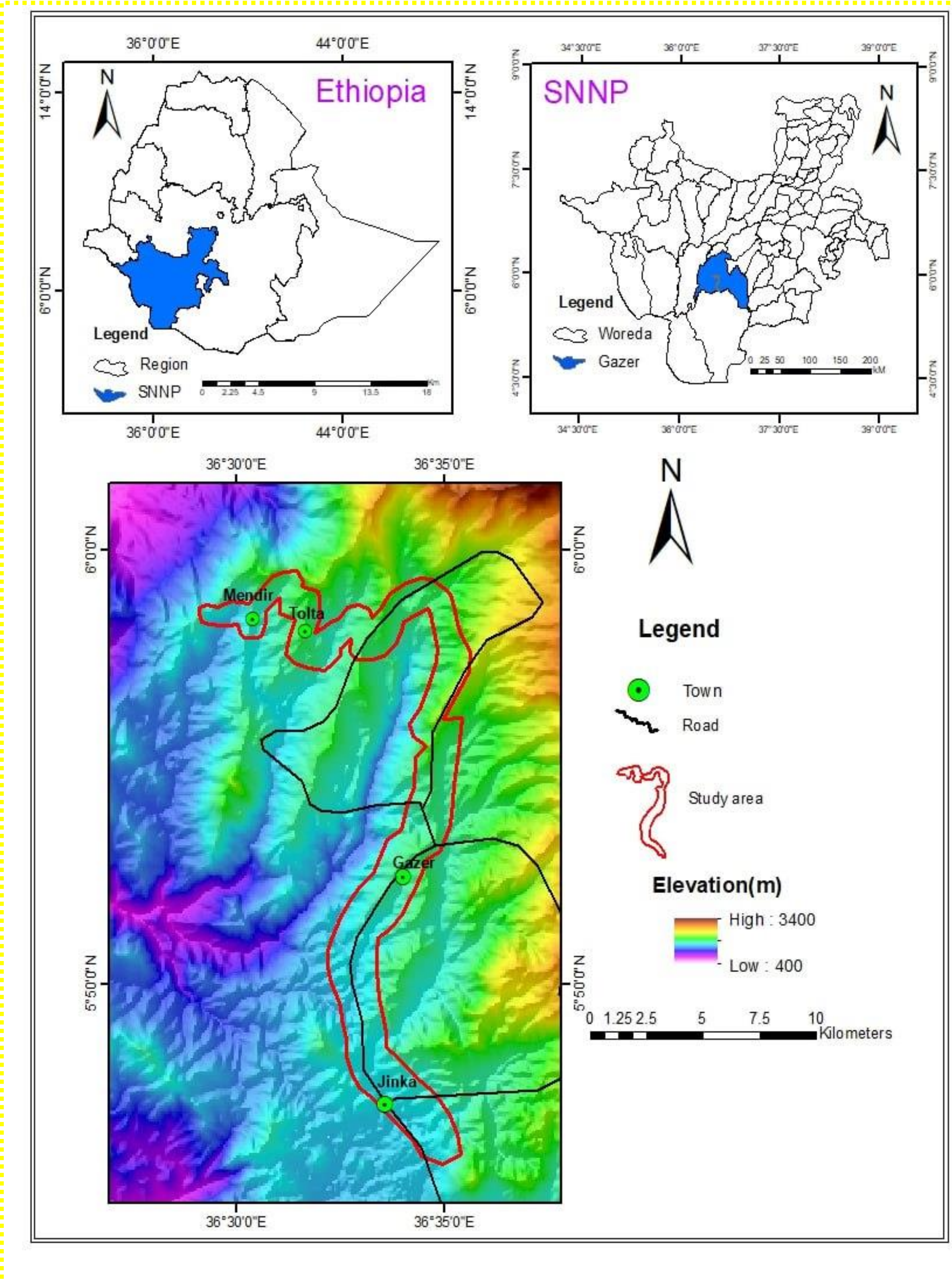

Figure 1. 1: Location map of study area

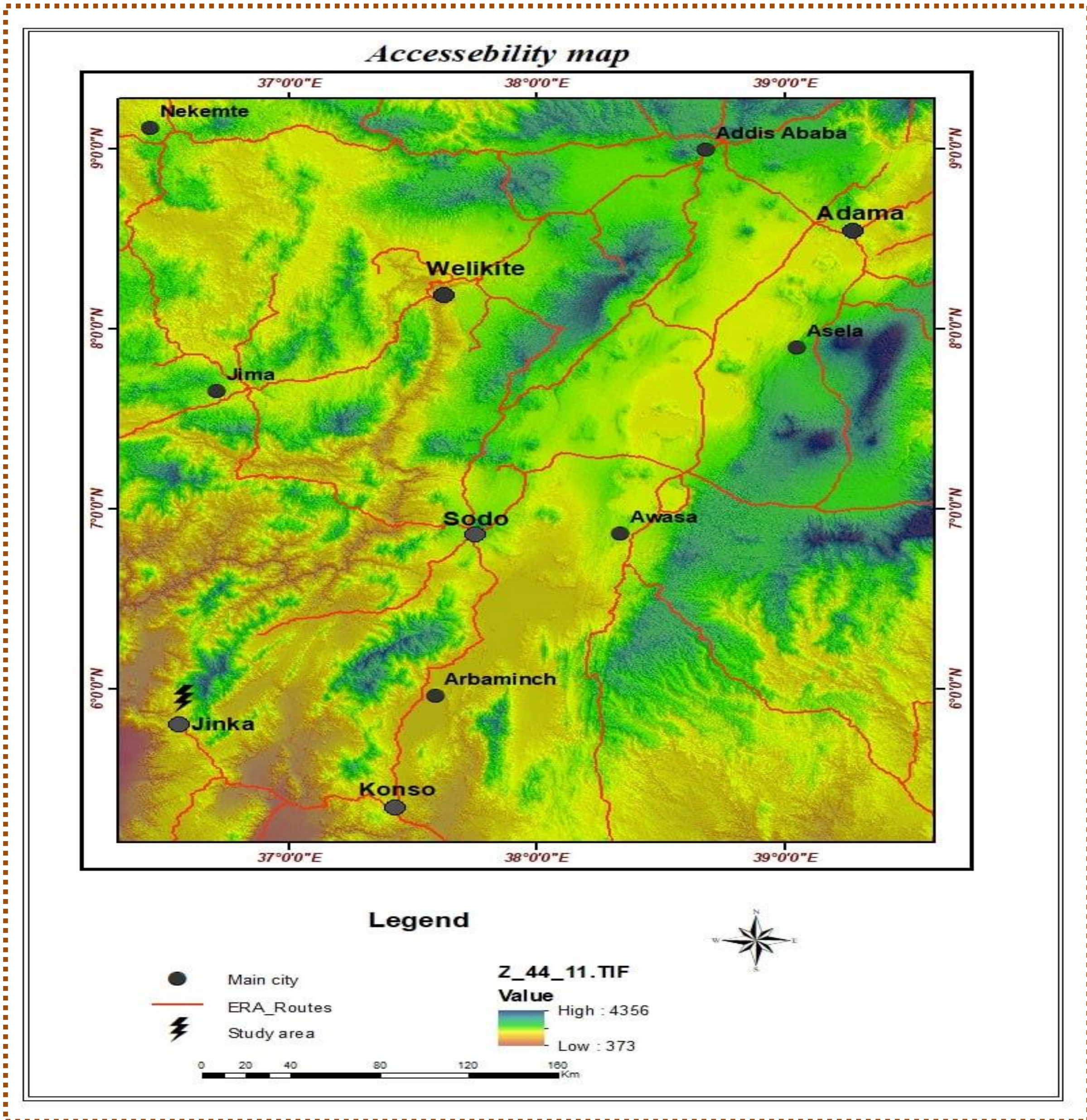

Figure 1. 2: Accessibility map of the study area

1.5.2 Physiography

The research area begins at Jinka Town at 1400 meters above sea level, ascends to Tolta Village at 1730 meters above sea level, and then progressively declines to Mendir Village at 1450 meters above sea level. It is characterized by highly varied and spectacular topographic settings. Physiography is strongly related to the geological setting and geomorphological history of rocks(Huggel et al., 2008). The highlands of Wellega, Illuababor, Jimma, Kaffa, Gamo, and Gofa are included in the physiography subdivision of southwestern Ethiopia.

The research area contains a variety of physiographic features, including flat, rolling, mountains, and escarpments. The southern plateau of Ethiopia is the wettest region. The Dabus, Deddessa (Abay tributaries), Baro, Akobo, and Ghibe/Omo rivers drain it.

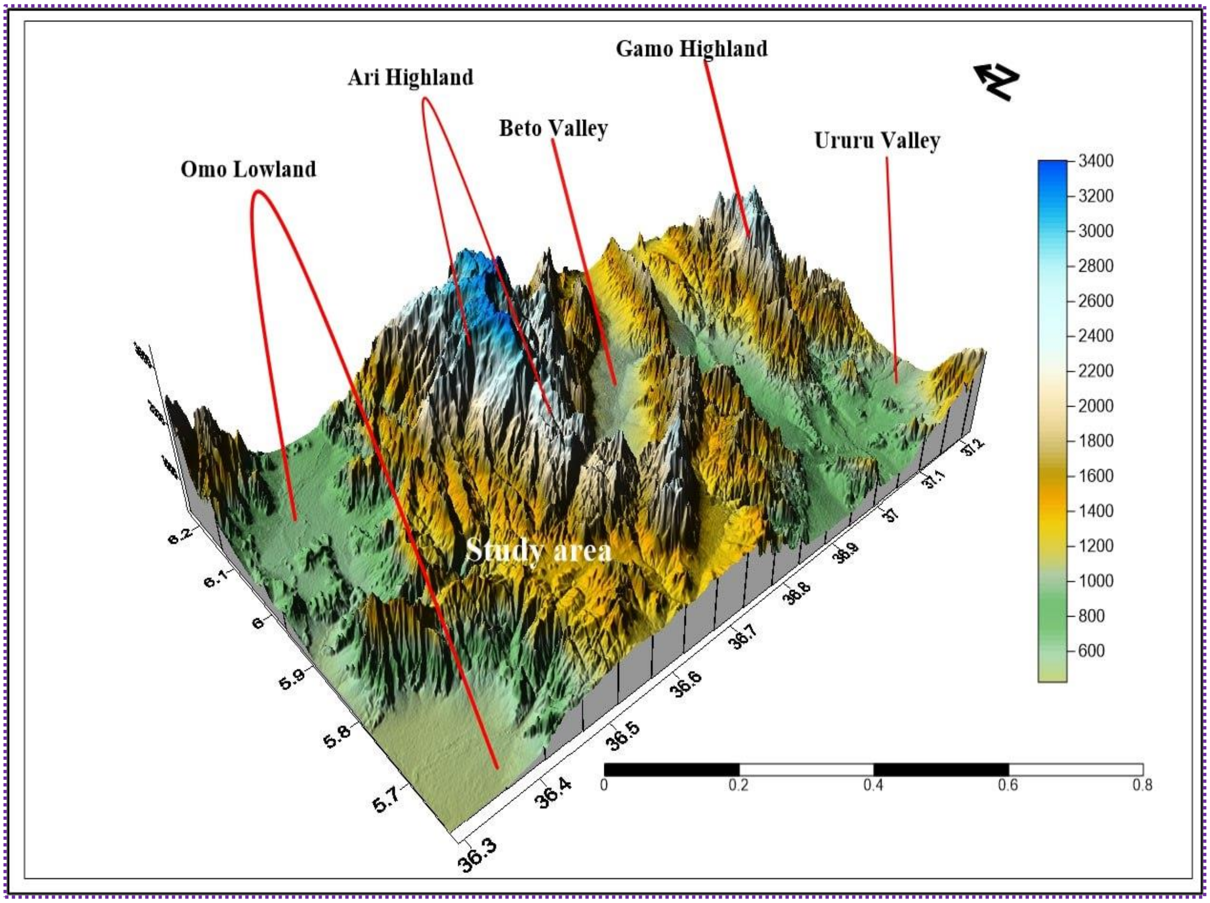

Figure 1. 3: 3D View a physiographic map of the study area

1.5.3 Climate of the Study Area

Ethiopia has a wide range of rainfall patterns. Lowland locations have lower precipitation records, while highland areas receive more than 70% of the yearly rainfall, according to(Ayalew, 1999).

There are two recognized climate components: precipitation amounts and temperature distribution conditions. Ethiopia is divided into three separate seasons. These are known as "Bega", "Belg", and "Kiremt" and occur between October and January, February and May, and June and September, respectively. There are two acknowledged climate components, according to(Ayalew, 1999) precipitation amount and distribution temperature conditions.

A) Rainfall

Rainfall is one of the external and triggering variables that induce slope instability, and it is the most prevalent cause of slope failure(Ayalew et al., 2004). A variety of topographical, geological, hydrological, and land use factors can influence slope instability in the Ethiopian highlands, while heavy rainfall is the most prevalent cause of landslides(Woldearegay, 2013). The Ethiopian National Meteorological Agency provided rainfall data for the research region of Jinka Station. The average monthly rainfall was 199.1 mm and 43.76 mm respectively.

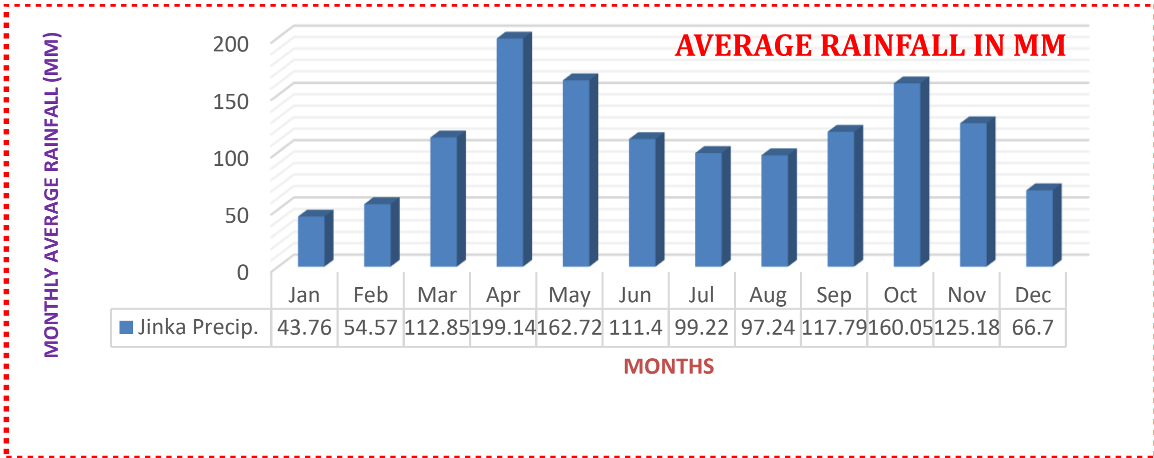

Figure 1. 4: Monthly rainfall data of the study area from (1970-2021)

(Source: Ethiopia National Meteorological Agency, 2022).

B) Temperature

The maximum and minimum mean annual temperature data for the study area were obtained from the Ethiopian National Meteorological Agency's Jinka Station. Jinka's maximum and minimum average temperatures are 29.52 and 14.74 degrees Celsius, respectively.

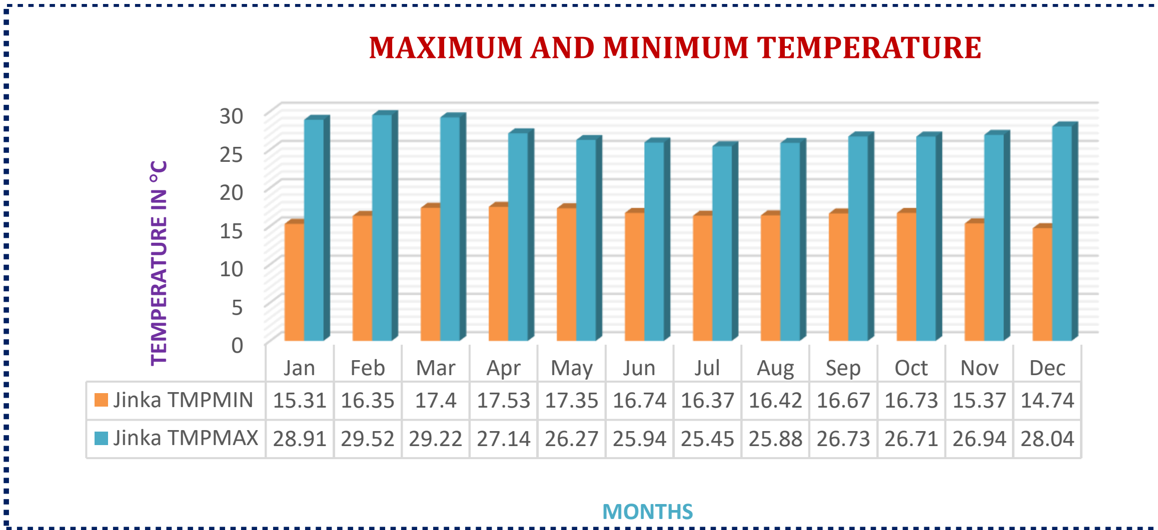

Figure 1. 5: Monthly Temperature data in the study area (1970-2021)

(Source: Ethiopia National Meteorological Agency, 2022).

1.5.4 Seismicity of the Study Area

Seismic activity is one of the factors that contribute to slope instability, particularly in seismically active areas (Hoek & Bray, 1981). The minimal magnitude of an earthquake required to trigger slope failure is 4-5M (Pantelidis, 2009). Because horizontal seismic acceleration contributes to the driving force along the failure plane, planar rock slope failures are easily destabilized under seismic loading circumstances (Raghuvanshi, 2019). South Ethiopia's seismic hazard (6,0°-8,5°N, 37,5°-39,5°) is influenced by the region's rift characteristics. According to the seismic risk map (Dulbal, 2020), the study area is in a seismic zone 2 and a horizontal seismic acceleration of 0.07g.

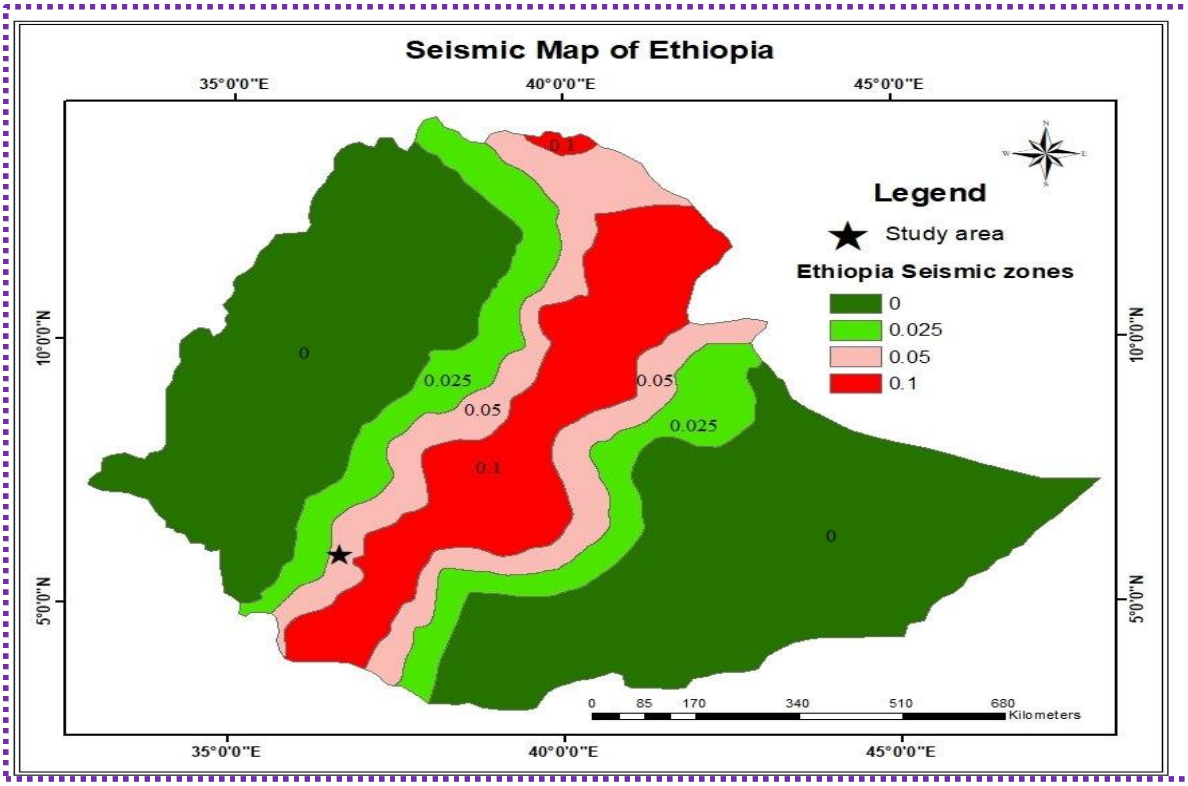

Figure 1. 6: Seismic map of the study area (Source: Dulbal, 2020)

1.6 The Objective of Research

1.6.1 General objective

The main objective of this study is to conduct the slope stability analysis for the critical slope section along selected section of Jinka to Mendir in the south Omo Zone of Southwestern Ethiopia.

1.6.2 Specific Objective

- ✓ Identifying and locating potential slope instability issues for specific road sections.
- ✓ To determine the geological and geotechnical parameters of critical unstable rock and soil slope sections.
- ✓ Critical rock slope failures will be analyzed kinematically.
- ✓ To determine the factor of safety/or Stress Reduction Factor of the critical slope sections.
- ✓ Cmputing slope stability analysis using LEM and FEM methods on selected slope sections
- ✓ Provide proper recommendation based on stability analysis model

1.7. Thesis Organizations

The content of the present research is organized into six chapters

Chapter 1: Deals with the general background of the research and the statement of the problem, objectives, description of the study area, significance, and limitations of the research

Chapter 2: Discusses the literature review including the mode of slope rock mass failure, factors influencing rock slope stability, slope Stability analysis method, previous works related to slope stability, and the remedial measures for slope stability.

Chapter 3: Discusses the methodology, data collection, and parameters used in the slope stability analysis in the study area.

Chapter 4: Describes the regional and local geological settings and structures of the study area.

Chapter 5: Briefly describe the results and discussions obtained from the laboratory and slope stability analysis and interpretations. After that, there was an evaluation discussion on the analyzed outcome.

Chapter 6: Deals briefly with the conclusions and recommendations.

CHAPTER-TWO

2. LITERATURE- REVIEW

2.1 INTRODUCTION

Slope failures are a significant natural hazard in most places of the world. Slope stability issues are widespread in highway, canal, and dam construction, as well as on some natural slopes that may become unstable due to the presence of water, which influences soil qualities. Ground slope instability, rock slope instability, surface floods, soil erosion, and natural geological variations all cause damage to infrastructure in Ethiopia such as as roads, buildings, and dams. Road construction is one of the most essential investments in Ethiopia. However, slope instability was a common issue along roads that passed through mountain regions. Because of the cutting of hills and roadsides, most of the north, south, and western portions of the Ethiopian plateau have a history of slope instability, both in superficial materials and bedrock (Ayalew, 1999).

Geological activities such as rock slope failures are governed by natural physical processes. (Hoek et al.,2002). These failures have caused huge economic losses, property damage, maintenance costs, and injuries. Rock slope failures can occur when driving forces exceed resisting forces. (Raghuvanshi, 2019). Rainfall-induced slope failure is common in Ethiopia's hilly and mountainous terrains, which have a diverse set of topographical, geological, hydrological (surface and groundwater), and land-use circumstances (Woldearegay, 2013).

2.2 Factors Affecting Slope Stability

Slope stability is influenced by a variety of things. A change in any of these characteristics, or their combination, could modify the slope's steady-state condition, reducing its stability and leading to slope failure. Slope failures occur not only on the steepest slopes but also on the flattest. In general, factors that cause instability are categorized based on their effect on slopes. responsible for slope instability by increasing shear stress or decreasing shear strength of the soil or rock mass (Matthews et al., 2014).

2.2.1 Geologic Factors

When considering slope stability, geology is one of the most significant aspects to consider. Depending on the type of origin, there is a strong relationship between the geology of the material and slope instability in a certain area. The geology's slope determines the mechanical behavior of rock slopes. Rock slopes made up of distinct geologic units have varying strengths and weathering resistance. Rocks with great strength are less prone to erosion. (Hamza & Raghuvanshi, 2017). Lithology and geological structures have an impact on slope stability.

2.2.1.1 Lithology: Weathering processes, water percolation, and rock mass interaction all contribute to slope instability. Water can percolate through joints and fractures in the weathered rock, causing slope failure. The degree of weathering and the internal structure of the rock affect rock material qualities such as strength and permeability.

2.2.1.2 Geological structures: The most important criteria for assessing rock slope stability is discontinuity strength rather than direction(Zare & Jimenez, 2015). The properties of discontinuities, as well as their relationship with slope geometry, determine rock slope stability(Searom, 2017). The area's tectonic setting contributes to slope instability through fracturing, faulting, jointing, and foliation structures (Hoek & Bray, 1981). Because fault and fracture zones represent weak zones, they may be advantageous planes of weakness where failures occur.

2.2.2 Geomorphic Factor

Geomorphology also has a significant impact on slope stability and susceptibility. In terms of slope grade, aspect, and slope shape, it is connected with topography and slopes.

- ✓ **Slope gradient**: Shear stress increases due to gravity's influence when the slope gradient increases, resulting in increasing material flow downslope.
- ✓ **Slope aspect**: The slope aspect is the orientation of the slope. Through differential evaporation, altering weathering, and root formation, it has a substantial impact on hydrological processes, particularly in arid areas. (Sidle & Ochiai, 2006).
- ✓ **Slope shape:** By concentrating surface and, more significantly, subsurface water, the slope geometry has a substantial impact on the slope stability of steep terrain.

The geometry of a slope, according to Dai and Lee(2002), impacts the direction and volume of surface runoff or subsurface drainage. The inclination of a slope in proportion to the strength of the slope materials and the direction of discontinuities determines its stability (Price, 2009). Steeper slopes are more prone to instability than gentle slopes (Hamza & Raghuvanshi, 2017).

2.2.3 Rainfall (Hydrological Factor)

The most common cause of slope failure is rainfall, which is one of the external and triggering factors that contribute to slope instability(Raghuvanshi et al.,2014; Woldearegay, 2013). Rainfall that infiltrates the slope reduces shear strength, increasing the instability of the probable failure plane(Pantelidis,2009; Raghuvanshi,2019). Slope failures are typical following heavy rainfall for an extended length of time. This is a triggering factor that is often considered in dynamic slope failure models. Rainfall has the effect of raising the level of groundwater. Groundwater, in turn, impacts rock slope stability for the following reasons(Wyllie & Mah,2004). Water pressure influences rock slope stability by decreasing resistive force and increasing the failure plane.

- ✓ increase the degree of weathering in the rock, which weakens the slope's toe.
- ✓ The freezing of groundwater and surface water in tension fractures generates a buildup of water pressure, which reduces the slope's stability.
- ✓ A change in the moisture content of the rock accelerates weathering and reduces the rock's shear strength.
- ✓ Groundwater flows into the slope face.

Groundwater flow into the slope face determining recharge and discharge area for the location of unstable rock slope is one of the methods in evaluating the impact of groundwater on slope stability (Wyllie & Mah, 2004).

2.2.4 Anthropogenic Factor

The consequences of human activities on slope stability are significant. Farming, habitation, ditch construction, road cutting, building stone quarrying, and mining all have a substantial impact on hilly and mountainous terrain(Raghuvanshi et al., 2014).

- ✓ During highway and road construction, undercutting and slope alteration create an artificial slope that exceeds the angle of repose. As a result, the average gradient of the slope increases. As a result, the likelihood of slope failure rises.
- ✓ Rapid slope failure is caused by the modification of a slope during engineering projects, such as increasing the slope angle from gentle to steep or removing the slope toe.
- ✓ During mining and quarrying operations, slope overloading occurs. This additional weight may increase the likelihood of slope failure, and changes in hydrology may have a considerable impact on slope stability. (Chen, 2001)
- ✓ Soil slope failure is caused by human-induced deforestation because tree roots no longer hold the soil together and are unable to protect it from heavy rainfall.
- ✓ Machine activity and subsurface explosions created vibrations, which resulted in major floods and sediment failure in large reservoirs.

2.2.5 Dynamic Forces (Seismicity)

Natural slopes fail as a result of earthquake shaking and vibration (Ermias et al., 2017; Pantelidis, 2009). The minimal magnitude of an earthquake required to produce slope failure is 4-5 MM (Pantelidis, 2009). Seismic waves in rock raise stress, which may result in fracturing (Hack & Huisman,2002). Ground accelerations have a substantial impact on slopes made of rock masses with significant structural discontinuities. When ground acceleration is applied to discontinuous rock slopes, structural discontinuities open. The slopes that are stable under static seismic loading can fail under dynamic seismic stress, according to (Hoek and Bray(1981).

2.2.6 Force of gravity

The primary cause of mass waste is gravity. Gravity is the force that pulls everything on the earth's surface towards the center. The force of gravity acts downward on a flat surface. The substance will not move under the force of gravity as long as it is on a flat surface(Nelson, 2013). Slightly steeper slope angles increase shear stress, as does anything that diminishes shear strength, such as lowering particle cohesiveness or frictional resistance. The safety factor, FS, is a commonly used shear strength-to-shear stress ratio.

Fs = shear strength/shear stress

The force that holds the material on the slopes together, which may include friction and cohesive forces that hold the rock or soil together, is referred to as shear strength. The slope is likely to collapse if the safety factor goes below 1.0. Gravity would tend to flatten slopes if it weren't for the cohesion and friction forces of rocks and soils. A landslide may be initiated, however, due to temporary changes in equilibrium or external perturbations (Gholipoor, 2015). The stabilization conditions may change.

2.2.7 Geotechnical Properties of Soils and Rocks

Porosity, gradation factors, dry density, saturated permeability, and shear strength have been identified as geotechnical parameters that contribute to the physical-based approach's prediction of slope collapses(Park et al.,2016; Shepheard et al.,2019). Mechanical and chemical weathering modify the rock's strength properties. Some of the important geotechnical parameters of soils that control slope stability are soil composition depth shear strength (which is dependent on density, cohesion, plasticity, dilatancy, and the angle of internal friction), porosity, permeability, grading, moisture content, and organic matter content(Kumar et al., 2020). The shear strength parameters of the slope material are cohesion and angle of internal friction, and they are the fundamental elements that define the resistive force acting normally to the failure plane(Raghuvanshi, 2019).

2.3 Mode of Rock Slope Failure

Slope failures can appear in a variety of forms, depending on the origin of the failure, geometry, material qualities, and velocity of movement (Searom, 2017). There are four types of rock slope failure: planar, wedge, toppling, and circular.

2.3.1 Planar Failure

Planar failure occurs when the strike of the discontinuity plane is almost parallel to the strike of the slope and daylight on the slope face (Raghuvanshi,2019). The failure surface is typically a structural discontinuity such as bedding planes, faults, joints, or the contact between bedrock and an overlying layer of weathered rock. The following conditions are favorable for plane failure:

- ✓ The strikes of both the sliding plane and the slope face lie parallel (±20°) to each other.
- ✓ The dip of discontinuity is less than the dip of the slope, and the failure plane is daylight on the slope face.
- ✓ The dip of the planar discontinuity is greater than the angle of friction on the surface.

2.3.2 Wedge Failure

The wedge mode of failure occurs when two structural discontinuity planes strike obliquely against each other and their line of junction is oriented in the direction of the slope face. On these two crossing planes, the rock mass will slide in the direction of the line of junction, into which the line of intersection plunges(Pantelidis, 2010). A rock slope's wedge failure happens when two weak planes intersect to form a wedge.

The following conditions favor wedge failure:

- ✓ The dip of the slope is at a steeper angle than the dip of the line of intersection of the two discontinuities.
- ✓ The line of intersection daylight on the slope face, and the dip of the line of intersection must be greater than the angle of friction of the surface.
- ✓ The plunge of the line of intersection is less than the inclination of the slope face, and thereby the line of intersection must daylight in the slope.

2.3.3 Toppling Failure

According to(Goodman, 1991), The overturning of rock strata or discontinuities that are deeply into the slope face causes the rock slope to topple Furthermore, (Hunt, 2007) defines toppling failure as a rock block overturning through an axis point placed below its center of gravity. It is the most common type of failure in rock masses that have been separated into a series of columns by a sequence of fractures that strike parallel to the slope face and steeply dip into the rock mass (Norrish & Wyllie,1996). A tightly spaced, jointed rock mass and a sharply dipping discontinuity that sets that dip away from the slope are required for toppling failure.

There are two types of toppling.

- ✓ Flexural: When a series of beds are steeply inclined away from a rock face, flexural toppling occurs.
- ✓ Block: when there are numerous close joints in the rock mass, causing the weighted centroid to fall outside the base of the column or block.

2.3.4 Circular (Rotational) Failure

According to Taheri(2013), circular failure is best understood on slopes with fully weathered rocks, substantially disturbed rocks, and many crossing weak planes or joints sliding down a curved surface to form a circular arc. This type of failure is the most common in soils, although it can also occur in weak, extensively jointed, or fractured rock masses.

Circular slips are associated with homogenous soil conditions, whereas non-circular slips are associated with non-homogeneous soil conditions. When the presence of surrounding strata of significantly varying strength affects the morphology of the failure surface, translation, and compound slides occur. When the next stratum is near the surface and the neighboring stratum is planar and often parallel to the slope, translational slips are most common. When the next stratum is at a larger depth, compound slips occur, with the failure surface comprising curved and planar parts. A revolving slide represents the movement of material along a curved surface.

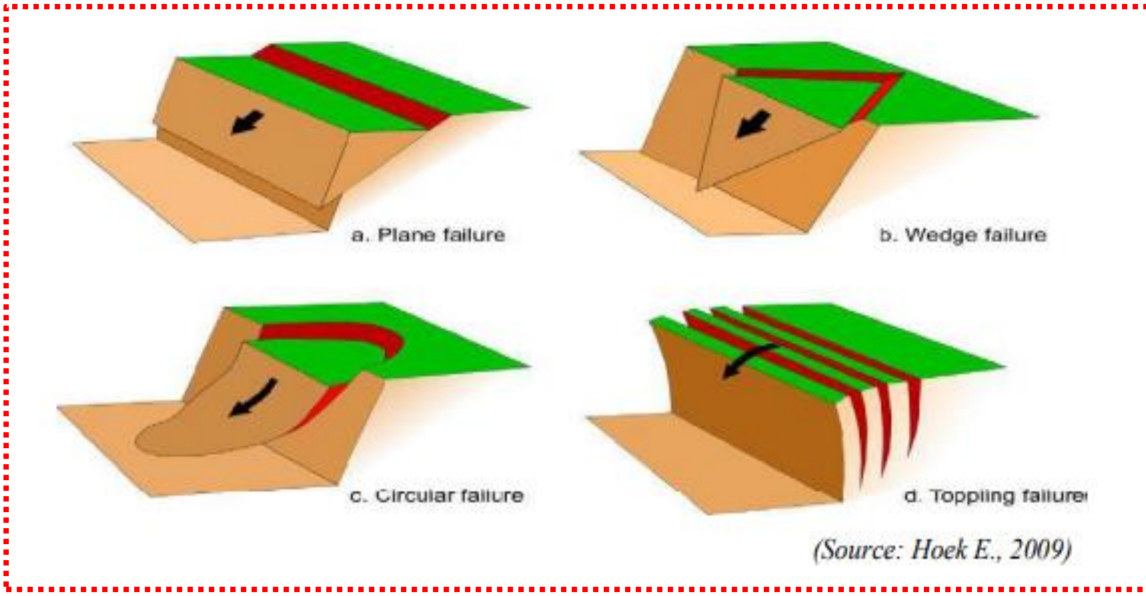

Figure 2. 1: Simplified illustrations of most common slope failure modes

2.4 Rock Mass Failure Criteria

In rock mechanics and engineering, the rock failure criterion is critical for forecasting the failure of rock masses(Zhu et al., 2015). A variety of criteria, including those listed below, can be used to characterize failure processes.

2.4.1 Mohr-Coulomb Strength Criteria

The Mohr-Coulomb criterion, or the criterion established by (Barton, 1973)is used in soil mechanics. The Mohr-Coulomb failure or strength criterion has been widely used in geotechnical applications (Hammah et al., 2004).

The Mohr-Coulomb criterion can be written as follows: (2.1)

$$\tau = c + \partial n \tan\phi \qquad \text{Eq (2.1)}$$

Where τ = is the shear stress, σ= is the normal stress, c= is the cohesion of the material, and ϕ is the material angle of friction.

Effective stress governs soil shear strength regardless of whether the failure occurs under drained or undrained conditions. The strength envelope of Mohr-Coulomb displays the relationship between shear strength and effective stress.

2.4.2 Hoek Brown Strength Criteria

Hoek and Brown(1997) developed a link between the maximum and minimum primary stresses to forecast the failure of intact and fragmented rocks. Relationships between the criterion and rock mass rating elements were introduced to characterize the qualities of the rock mass. (Hoek et al., 1998) presented the Geological Strength Index (GSI), a generalized Hoek-Brown criterion.

Use the following equation in the (Hoek et al., 2002) edition

$$\sigma 1' = \sigma_3 ' + \sigma c_i \left(m_b \frac{\sigma 3'}{\sigma c_i} + s\right)^{a} \qquad \text{Eq (2.2)}$$

Where σ1 is the maximum and σ3 is the minimum effective principal stresses at failure respectively, mb, s, and α are the values of Hoek-Brown constants for the rock mass, and ∂ci is the uniaxial compressive strength of the intact rock.

$$mb = mi \exp(\frac{\mathrm{GSI}-100}{28-14D} \qquad \text{Eq (2.3)}$$

$$S = \exp \frac{(\mathrm{GSI}-100)}{(9-3\mathrm{D})} \qquad \text{Eq (2.4)}$$

$$\alpha = \frac{1}{2}+\frac{1}{6}\left(e^{\frac{-GSI}{15}} - e^{\frac{-20}{3}}\right) \qquad \text{Eq (2.5)}$$

2.4.3 Barton-Bandis Failure Criterion

(Barton, 1973) proposed an empirical law of fundamental friction angle to predict the shear strength of discontinuities. The combined effects of surface roughness, rock surface strength, applied normal stress, and shear displacement determine the shear strength of discontinuity surfaces in rock slopes. The Barton-Bandis failure criterion, according to(Barton, 1973), can be stated as follows:(Barton, 1973)

$$\tau = \partial n * \tan \{\mathrm{JRC} * \log 10(\frac{jcs}{\sigma n}) + \phi r) \qquad \text{Eq (2.6)}$$

Where: τ = Peak shear strength, ∂n = Effective normal stress, JRC = Joint roughness coefficient, JCS = Joint wall compressive strength, ϕr = Residual friction angle

JCS is the compressive strength of a layer of rock near a junction that determines the rock mass's strength and deformation qualities.

According to (Barton and Choubey(1977), the joint roughness coefficient (JRC) is the coefficient of joint surface roughness with a value ranging from 0 to 20 (smoothest to roughest). A basic friction angle (b) is a 25° to 35° angle with a flat, planar, unweathered rock surface.

2.5 Slope Stability Analyses Approaches

As the demand for a better knowledge of the failure mechanisms of both man-made and natural slopes grows, slope stability analysis is becoming more common in geotechnical engineering. Various scientists and groups have created several rock slope stability evaluation procedures or techniques**.**

2.5.1 Kinematic Analysis

Kinematic stability analysis methodologies deal with slope stability by focusing on the geometric requirements needed for the rock block to move along the discontinuity plane without accounting for any forces that cause sliding. (Hoek & Bray,1981).

In the kinematic analysis, stereographic projections are utilized to evaluate the possible modes of rock slope failure (planer, wedge, and toppling) by taking into account the strike angle, dip angle, dip direction of the slope, and discontinuity surface(Lamessa & Meten, 2021a). According to Gischig et al.(2011), kinematic analyses are quite helpful for evaluating the various failure modes of rock masses with discontinuities.

Dips software may be used to determine the kinematic acceptability of each mode of failure using input data such as:

- ✓ Friction angle,
- ✓ Dip and dip directions of the slope,
- ✓ Discontinuities orientations.

The probabilities of various types of failure are determined by the angular relationship between structural discontinuities in rocks and the gradient, as well as the aspect of topography(Wyllie & Mah, 2004b).

- ✓ **Planar:** If the strike of the discontinuity is nearly parallel (±20º) the trend of the slope and dip of the discontinuity are gentler than those of the slope, then planar failure is likely to occur.
- ✓ **Toppling**: If the strike of discontinuity is nearly parallel (±20º) to the trend of the slope but discontinuity is dipping steeply in the opposite direction to that of the slope direction, it will give rise to a toppling failure mode.
- ✓ **Wedge:** When two discontinuities do not form any failures individually but intersect in such a way that the line formed by their intersection daylights into a slope face, i.e., the amount of plunge is less than the angle of slope provided the intersection's plunge also exceeds the friction angle, wedge failure is likely to occur.

2.5.2 Limit Equilibrium Method

The Mohr-Coulomb formula is used to determine the shear strength along the sliding surface in slope stability utilizing limit equilibrium(Aryal, 2006).The limit equilibrium technique is based on the concept of the factor of safety(Alzo'ubi, 2016).A state of limit equilibrium is obtained when the mobilized shear stress is expressed as a percentage of the shear strength (Janbu, 1973). According to Duncan et al.(2014), the limit equilibrium approach only offers an estimate of slope stability but no information about the magnitude of movement.

Several limit equilibrium (LEM) techniques have been developed for assessing slope stability. GLE is an extension of the Spencer and Morgenstern-Price methods, which satisfy both moments and force equilibrium conditions(Abramson et al., 2001). Software for analyzing limit equilibrium slope stability, such as phase, slide, swedge, and Rocplane, is now widely used in engineering procedures outlined in the Rocscience computer program (ROCSCIENCE, 2004).A limit equilibrium analysis was performed on structures having the potential for kinematic instability, and the shear strength parameters (friction angle and cohesion) were used to determine the factor of safety (Park & West, 2001).

The factor of safety of a slope subject to shear failure can be defined as the ratio of shear strength (resisting force) to shear stress (driving force) (Alzo'ubi, 2016; Stead & Wolter, 2015). According to Christian(2004), if the factor of safety value is larger than one, the slope is stable; if it is less than one, the slope is unstable; and if FOS equals one, the slope is in a critical condition of equilibrium.

2.5.2.1 Analytical Methods of Limit Equilibrium

- ✓ **Method of slice**

The slicing method is the most widely used limit equilibrium approach. This method separates the majority of the soil into vertical parts. The approach can be applied in a variety of ways. Because of differing assumptions and inter-slice boundary limits, these changes can produce different results (factors of safety).

- ✓ **Morgenstern price Method**

This method was developed by (Morgenstern and Price, 1965), and takes into account not only the normal and tangential equilibrium but also the moment equilibrium for each slice. This approach makes a simplifying assumption about the relationship between the interslice shear force and the normal force. Morgenstern presented a complete and rigorous solution approach that is applicable to slip surfaces of any shape and meets all static equilibrium conditions. In that, both force and moment equilibriums are satisfied and the interslice force function is assumed, the Morgenstern approach is identical to the other. They advocated for making assumptions about interslice force relations to attain statical determinacy of the problem and avoid any numerical difficulties that may develop throughout the procedure.

- ✓ **Spencer’s method**

(Spencer, 1967) based his findings on the slicing procedures of Fellenius and Bishop (1927). Spencer's method for slope stability analysis with arbitrary failure surfaces is reasonably accurate. This method fulfills both the sliding mass moment and the force equilibrium.

2.5.3 Finite Element Method

According to (Stark et al., 2005) In engineering, the finite element method is used to validate newly proposed analysis methods. Furthermore, FEM is a current and powerful engineering computational method that can reproduce the physical behaviors of a problem without the requirement for specialized computational tools to simplify it. The finite element approach considers the soil's linear and nonlinear stress-strain behavior when predicting shear stress for the analysis (Burman et al., 2015). Slope failure happens in a finite element model when zones are unable to withstand the applied shear loads.

Previous study has discovered that the FEM yields a lower global safety factor (FS) than the LEM and better measures slope stability (Pradhan & Siddique,2020) and (Bushira et al., 2018). These approaches offer various advantages, including the capacity to represent slopes with high realism (complex geometry, loading sequences, reinforcement material presence, water action, and complex soil behavior laws) and to better observe soil deformations in situ. Because the engineer has a greater number of variables at his disposal, interpreting the analysis outcome is critical. FEM slope analysis is the shear strength reduction approach used by(Gurocak et al., 2008). Phase2 software can be used to perform finite element analysis.

2.5.3.1 The Shear Strength Reduction (SSR) Technique

A new finite element method technique for estimating the factor of safety of earth slopes is the shear strength reduction method. The SSR method reduces soil shear strength to the bring slope to the verge of failure(Duncan et al., 2014).

In the finite element technique, such a condition is detected by the failure to attain equilibrium. In the SSR technique, the slope materials are thought to have elastic-plastic behavior. The material's strength is gradually reduced until failure occurs.

2.6 Rock Mass Classification System

The primary purpose of rock mass classification is to provide quantitative data and technical instructions for upgrading previously conceptualized geological formation representations. (Liu & Chen,2007). Many scientists have developed or used rock mass classification systems as an experimental method for analyzing rock slopes (Hack et al.,2003; Liu & Chen,2007; Pantelidis,2010).The system's purpose is to classify rock masses based on qualitative factors such as strength, discontinuity, weathering, and structural orientation. These qualitative parameters will be converted into rated parameters that will be used to estimate deformability and strength properties, provide measurable data for support estimation, and serve as a communication platform for researchers, designers, engineers, and contractors. (Bieniawski,1989).

Furthermore, (Pantelidis, 2009), claims that rock mass categorization is effective for evaluating the performance of rock-cut slopes by utilizing the most essential inherent and structural factors.

Many engineers have utilized and obtained international recognition for rock mass classification systems such as Rock Mass Rating (RMR), Rock Mass Quality Designation (RQD), and Geological Strength Index (GSI)(Gurocak & Alemdag,2012; Karaman et al., 2015).

2.6.1 Rock Quality Designation Index (RQD)

The rock quality designation is an important factor in classifying rock mass. The Rock Quality Designation (RQD) index was developed by Deere et al. (1967).

The RQD index is influenced by several factors, including joint orientation, joint spacing, fracture frequency, and joint roughness (Azimian, 2016).RQD is defined as the percentage of intact drill core bits longer than 10cm recovered following a single core run(Abzalov, 2016), The general equation is represented by the symbol.

$$RQD = \sum \frac{\text{Core pieces} > 10\text{cm}}{\text{The total length of the core run}} \times 100\% \qquad \text{Eq (2.7)}$$

The volumetric joint count (Jv) is a measure of jointing degree or inter-block size that can be used to describe rock mass jointing (Palmstrom, 2005).

Joint spacing (S) is the distance between two consecutive discontinuities measured along a line on the rock surface, as used by the Jv. The number of joints that intersect one m3 volume is known as the Jv count. The correlation between RQD and volumetric discontinuity joints Jv according to (Palmstrom, 1974) can also be used to estimate the RQD, as follows

$$\text{RQD} = 115 - 3.3\text{Jv} \qquad \text{Eq (2.8)}$$

Where the volumetric discontinuity joints Jv is the sum of the number of discontinuities per unit length for all discontinuity sets, which can be determined from the discontinuity set spacings within a volume of the rock mass (Palmstrom, 1982), as follows

$$\text{JV} = \frac{1}{s1} + \frac{1}{s2} + \frac{1}{s3} \cdots + \frac{1}{sn} \qquad \text{Eq (2.9)}$$

Where s1, s2, and s3 are the mean discontinuity set spacings. (Palmstrom, 2005) Suggests that r= 5 m be assumed.

As a result, the volumetric discontinuity frequency Jv can be generalized as

$$JV = \frac{1}{s1}+\frac{1}{s2}+\frac{1}{s3}\cdots+\frac{Nr}{5} \quad \text{Eq (2.10)}$$

Where Nr is the number of random discontinuities.

2.6.2 Rock Mass Rating (RMR) (Bieniawski)

Bieniawski (1973) established the Rock Mass Rating (RMR) classification system, and(Bieniawski, 1979) published the specifics of a rock mass classification system known as the Geomechanics Classification or the Rock Mass Rating (RMR) system. In 1989, Bieniawski also developed a modified rating that comprises five categorization factors and one rating adjustment. The parameters are uniaxial compressive strength intact material, rock quality designation (RQD), discontinuity spacing, discontinuity condition, and groundwater condition, and the rating is altered in the direction of the discontinuities.

In addition, the orientation of the discontinuity and slope is measured in the field with the Brunton compass. The five main parameters of the RMR are those described above, and they can be used in the field to estimate discontinuity spacing, discontinuity condition, and groundwater condition utilizing visual observation and equipment such as a tape meter(Bieniawski, 1973).

Deere et al. (1967) proposed an equation that can be used to calculate the RQD. Uniaxial compressive strength (UCS) of the intact rock can be estimated from the point load strength index Is (50) using the empirical formula (Broch and Franklin,1972), and Schmidt hammer rebound hardness value(R) measurements both in the laboratory and in the field tests (Aydin, 2009).

Table 2.1 Rock Mass Rating System (After Bieniawski 1989).

1.	Strength of intact rock material	Point load strength index (MPa)	> 10	4 – 10	2 – 4	1 – 2			
		Uniaxial compressive strength (MPa)	> 250	100 – 250	50 – 100	25 – 50	5 – 25	1 – 5	< 1
	Rating		15	12	7	4	2	1	0
2.	RQD (%)		90 – 100	75 – 90	50 – 75	25 – 50	< 25		
	Rating		20	17	13	8	3		
3.	Joint spacing (m)		> 2	0.6 – 2	0.2 – 0.6	0.06 – 0.2	< 0.06		
	Rating		20	15	10	8	5		
4.	Condition of joints		not continuous, very rough surfaces, unweathered, no separation	slightly rough surfaces, slightly weathered, separation <1 mm	slightly rough surfaces, highly weathered, separation <1 mm	continuous, slickensided surfaces, or gouge <5 mm thick, or separation 1–5 mm	continuous joints, soft gouge >5 mm thick, or separation >5 mm		
	Rating		30	25	20	10	0		
5.	Ground-water	inflow per 10 m tunnel length (l /min), or	none	< 10	10 – 25	25 – 125	> 125		
		joint water pressure/major in situ stress, or	0	0 – 0.1	0.1 – 0.2	0.2 – 0.5	> 0.5		
		general conditions at excavation surface	completely dry	damp	wet	dripping	flowing		
	Rating		15	10	7	4	0		

2.6.3 Slope Mass Rating (SMR)

Slope mass rating (SMR) was proposed by (Romana, 1985) which was the extension of RMR after Beniawski (1979), It was only used for a planar and toppling mode of failure before (Anbalagal et al., 1992) and modified to account for wedge mode of failure. It was calculated from basic RMR by adding adjustment factors derived from joint slope relationships and factors depending on the method of excavation. Finally, stability class and probability of failure of rock slope can be indicated by using the following equation.

$$SMR = RMRbasic + (F1 * F2 * F3) + F4$$

Where, RMR basic is rock mass rating after (Beniawski, 1989), F1- depends upon parallelism between joints and slopes face strikes. ($\alpha j - \alpha s$) where, αj is a joint strike and αs is a slope strike. F2- refers to joint dip angle (βj) or plunge of a line of intersection of two wedge forming planes (βj). F3- depends upon the relationship between joint dip or plunge of a line of intersection of two wedge forming planes and slope inclination. (βj - (βs) or ($\beta i - \beta s$) where, βs is the inclination of slope. F4- is considering about method of excavation. It includes the natural slope or the cut slope excavated by pre-splitting, smooth blasting, normal blasting, poor blasting, and mechanical excavation.

2.6.4 Uniaxial Compressive Strength (UCS) of Intact Rock

In rock engineering practice, uniaxial compressive strength is recognized as one of the most essential characteristics in the characterization of rock material (Beran, 2008). The uniaxial compressive strength of intact rock material can be determined using rock cores in a laboratory test. The UCS can be calculated using the empirical formula (Broch & Franklin, 1972) from the point load strength index (50), as well as Schmidt hammer rebound hardness value (R) data in laboratory and in-situ experiments.In rock mechanics, Schmidt hammer hardness values are used to assess the uniaxial compressive strength (UCS) and modulus of elasticity (E) of intact rock in laboratory and situ tests(Rahim et al., 2022). (Nazir et al., 2013)presented a correlation with the rebound number for determining UCS from the Schmidt hammer rebound value for use in rock quality.

Furthermore, using the equation below, (Barton and Choubey(1977) determined the rock's uniaxial compressive strength (UCS) by multiplying the rebound number by the dry density of the rock.

$$\log 10\ (UCS) = 0.00088\gamma R + 1.01 \qquad \text{Eq (2.11)}$$

Where UCS is the uniaxial compressive strength in Mpa, γ is the dry rock densities in KN/m3 and R is the average Schmidt rebound value.

Table 2. 2 Classification of UCS of rock according to Deere and Miller (1966).

(UCS) (MPa)	Description of strength
Over 224	Very High strength
112-224	High strength
56-112	Medium strength
28-56	Low strength
Less than 28	Very low strength

2.6.5 Point Load Strength Index

In the point load test, core specimens or irregular rock pieces are placed between the conical platens and the applied force (P) and distance (D) between them are measured at failure. Because of its ease of testing straight, cut blocks, or irregular lumps, the point load test is one of the cheapest and most useful processes for measuring the strengths of rocks.

Many experiments have been carried out to investigate the relationship between uniaxial compressive strength (UCS) and point load index (Is) for different rock types. (Broch & Franklin, 1972) characterized the relationship between uniaxial compressive strength and point load strength index in the equation as follows:

$$UCS = 24 * Is_{(50)} \qquad \text{Eq (2.12)}$$

Where $_{(50)}$ is the size corrected point load strength.

2.6.6 Geological Strength Index (GSI)

The geological strength index (GSI) is a field-based method for determining the strength of rock masses to build tunnels, caves, and other underground structures, which includes geological data about the rock mass, inputs from qualified and experienced field geologists and engineers about the visual impression of the rock structure, such as block and surface condition of discontinuities represented by joint characteristics (roughness and alteration), and reliable data in the form of an of rock mass strength properties that are used as input parameters for numerical analysis.(Hoek et al., 2013;Zhang et al., 2019).Based on field observations of the rock mass structure, which ranges from blocky to fragmented, the GSI approach categorizes the rock mass environment into five categories, ranging from very good to very poor(Hoek & Brown, 1997).(Marinos & Hoek,2000) proposed a quantitative GSI chart for estimating GSI.

2.7 Remedial Measures of Slope Instability

The rock and soil slope stabilization method keeps the slope stable. The slope stabilization method reduces driving force by excavating material from unstable ground, establishing proper drainage procedures, and increasing resistive force by building retaining structures or supports and using chemical treatments to strengthen the soil(Abramson et al., 2001). Before deciding on an effective slope stabilization strategy, a complete investigation of the existing slope conditions and an assessment of the primary causes of slope instability are required (Kazmi et al., 2017). The most appropriate slope corrective measure is chosen based on feasibility, stability, and cost when the reasons for slope stability are identified (Kazmi et al., 2017). These remedial measures help minimize the chances of slope failures by addressing their causes.

Slope stabilization methods can be placed in one of two broad categories:

- ✓ **Preventive stabilization methods**: are applied to stable but potentially unstable natural slopes and slopes to be cut.
- ✓ **Remedial or corrective treatments:** are applied to existing unstable slopes or failed slopes.

There are several methods for stabilizing an unstable rock slope (Abramson et al., 2001), and some of the methods are described below.

2.7.1 Retaining structures

Structures are generally constructed near the slope's toe to prevent slope failure, overturn, or collapse. Retention nets for rock slope faces, rockfall attenuation or stopping systems (rock trap ditches, benches, fences, and walls), and protective rock or concrete blocks against erosion are all examples of gravity retaining walls, gabion walls, and reinforced earth retaining structures with strip metallic reinforcement elements(Mite and Zenebe, 2020).

2.7.2 Modification of Slope Geometry (scaling)

Removing material from the area that triggered the landslide (perhaps using a lightweight fill) and adding material to the area to maintain stability and reduce the overall slope angle. According to(Kazmi et al., 2017) modifying the geometry of a steep slope to a gentler slope, either by flattening the slope or backfilling at the slope's toe, can increase the slope's stability. The slope is shortened to remove excessive strain in this technique. Scaling is frequently beneficial as a stabilizing or mitigation approach for two to ten years, depending on site conditions; as a result, it is not regarded as a permanent mitigation tool. It is, nevertheless, relatively inexpensive and serves as an excellent short-term technique. It is frequently integrated with other mitigation activities such as new rock excavation, rock reinforcement, or draped mesh due to how it improves site safety.

2.7.3 Rock Reinforcement Supports:

A rock reinforcement support involves the use of external materials such as rock bolts, anchors, and shotcrete to strengthen the rock and prevent failure(Cheng & Lau, 2014).

2.7.3.1 Rock bolts and anchors

The most useful supports are rock bolts and anchors, which keep blocks of rock from sliding away from the discontinuity planes(Hoek & Bray, 1981). In the case of fractured rock slopes, rock bolts, and anchors are utilized in conjunction with concrete walls to cover up the fractured rock areas.

2.7.3.2 Shotcrete:

It is primarily composed of fine aggregates and mortar. A layer of shotcrete applied to the rock face can help protect zones or beds of closely fractured rock.

Furthermore, shotcrete prevents small rock blocks from falling. Shotcrete increases the tensile and shear strength of slopes, lowering the risk of slope failure.(Wyllie & Mah, 2004).

2.7.4 Drainage Method:

The drainage method works when surface and subsurface drains are adequately maintained (Chen, 2001). Drainage is used to decrease the amount of water that might accumulate over rock mass discontinuities and cause hydrostatic pressure (Abramson et al., 2001). With proper surface and subsurface drainage system design, the hazards of pore water pressure and subsoil saturation building up can be mitigated by improving slope stability (Kazmi et al., 2017).

2.8 Slope Stability Analysis Software

Slope stability analyses can now be conducted using a range of computer-based geotechnical programs. Limit equilibrium designs have been utilized in software for a long time. Both LEM and FEM-based software are extensively used in geotechnical computations.

2.8.1 Phase software

Rocscience Inc. of Toronto, Canada, created Phase2 Software, which has been used in geotechnical and mining engineering as a tool for the design and study of tunnel surface excavation and supports. Furthermore, it is based on the finite element approach for determining the stability of soil and rock slopes. This software contains numerous FEM models as well as four basic sub-procedures.Inputs, calculations, outputs, and curve charts are examples of these procedures. It is used to analyze deformation and stability for a variety of geotechnical applications (Maula & Zhang, 2011).

2.8.2 Slide software

Rocscience Inc.'s slide software, developed in Toronto, Canada, can be used to analyze slope stability studies for soil and rock slopes. It includes a two-dimensional limit equilibrium (LEM) computer tool for testing the stability of circular or noncircular failure surfaces (Rocscience 2004, slide 6). For various research, external loading, groundwater, and forces such as surcharge and pseudo-static earthquakes can all be represented in the Slide software.

2.9 Previous and Related Slope Stability Study in Ethiopia

Rainfall-caused slope failures are common in Ethiopia's hilly and mountainous terrains, which have diverse topographical, geological, hydrological, and land use conditions(Woldearegay, 2013).Numerous researchers undertake various investigations, as stated below, to evaluate the slope stability condition of the underlying components and give necessary corrective activities.

1.Saed (2005) conducted limit equilibrium method slope stability evaluations along the main route from Gohatsion to Dejen towns by assessing the geological and geotechnical parameters of the geological material that composes the slope section. The investigation found slope instability difficulties such as rock fall, toppling, planar and wedge rock failure modes in rock slope sections, and circular rock failure modes in soil slope sections. During the wet season, the difficulties were more severe along the road's sides.

2.Molla(2011) investigated slope stability analysis on a specific slope segment of the Gohatsion-Dejen route. The deterministic slope stability analysis approach was utilized to conduct a detailed slope stability investigation of the specified slope section. The factor of safety for the specified slope sections was calculated using the SLOPE/W program. According to the results of this thesis study, the slope section is only stable in a static state under dry conditions with an FOS of 1.28. The sloping segment was unstable, with an FOS of less than 1.0 in all other static and dynamic saturation circumstances.

3.Beyene(2013) evaluated slope stability for selected sections of the Blue Nile Gorge Road in central Ethiopia using a combination of probabilistic and deterministic methodologies. He evaluated the stability of four critical slope sections, two of which were failed colluvium sections and the other two rock slopes.

The SLIDE software was used to analyze the stability of colluvium slopes under current and expected worst-case conditions, as well as rock slopes having a planar mode of failure. ROCPLANE software, which supports both deterministic and probabilistic approaches, was used. In conclusion, the results of this analysis indicated that the important colluvium slope sections in this area would be unstable during anticipated adverse conditions, and damage would be unavoidable in the event of failure. Under the worst anticipated condition, the deterministic and probabilistic analytical results showed the probability of rock block failures.

4.Lamesa and Meten (2021) studied the slope stability of the route from Gutane Migiru to Finca'a Sugar Factory. This study identified wedge and planar failure as the principal forms of rock failure based on kinematic analysis. The factors of safety and probability of failure for planar and wedge modes of rock failure were calculated using the Roc plane and Swedge software, respectively. Slide software was also utilized to assess the stability of soil slopes. Critical rock and soil slopes were more unstable under dynamic saturated conditions than in dry ones, according to deterministic and probabilistic stability models.

CHAPTER THREE

3. METHODOLOGY AND MATERIALS

3.1 General

The following approach, involving several systematic techniques and materials, was employed to successfully meet the general and specific objectives this research includes several components, including an integrated methodology and approach that includes investigating and analyzing existing data, extensive fieldwork, rock, and soil sampling, the kinematic analysis method, limit equilibrium, and finite element slope stability analysis methods, as well as laboratory testing and data processing methods.

3.2 Desk study

During this phase, relevant literature reviews and information on the study area were carried out. To understand the geological and geotechnical conditions in the study area, as well as the preparation of field material for this study, a thorough evaluation of past studies, books, and literature connected to the study, including published and unpublished reports, was also undertaken. Finally, the knowledge collected from the literature review, field surveys, laboratory testing, and analysis was used to create a conceptual framework and a general methodological flow chart for the study's slope stability analysis.

3.3. Data collection

The Ethiopian Geospatial Agency, the National Metrological Agency, and the Ethiopian Geological Survey provided data for the slope stability analysis. The Ethiopian Geospatial Information Agency (EGIA) provided a 1:50,000 scale topographic map of the research area, which was utilized to construct the study area base map with ArcGIS 10.8 software. The Ethiopian Geological Survey provided regional geological maps and reports, and the Ethiopian National Meteorological Agency provided climatic data for the research area. The most common cause of slope failure is heavy rainfall (Abebe et al., 2010; Woldearegay, 2013). At Jinka Station, graphs of average monthly precipitation data from 1970 to 2021 were created using Microsoft Excel (Fig1.4). Similarly, temperature data for the same time in the study area were provided for Jinka Station in Microsoft Excel (Fig1.5).

3.4 Field survey

Following reconnaissance research and an extensive literature review on various causes and mechanisms of slope failure, a detailed field investigation was carried out to identify the slope's instability state and collect data for future stability analysis. Primary data from the study area, as well as information on geological structures, discontinuity characteristics, rock mass characteristics, and drainage conditions, were obtained during the fieldwork. The purpose of this work was to identify probable failure phenomena such as slope inclination, drainage status, slope material type, weathering conditions, and the direction of the discontinuity that favors rock and soil slope failures. Additional field observations related to slope stability analysis were done following the identification of critical slope sections. In addition, the relevant primary data on various parameters was gathered.

3.4.1 Activities during Field Work

During the fieldwork, efforts were made to identify the various manifestations of instability existing on the slope, as well as to identify and gather data on possible causal factors contributing to slope instability. Field manifestations include slope toe removal, tension crack formation, slope face tilting, and discontinuity orientation, which all contribute to rock slope failures and spring stains across the slope face.

- Efforts were made during the fieldwork to assess and identify the different manifestations of instability present on the slope, as well as to identify and gather data on probable causative factors for slope instability. In addition, information was acquired through informal interviews with residents. In addition, it was attempted to identify the infrastructure damages caused by the landslide.

Figure 3. 1 a) Damaged church b) Tilt electric pole c) Damaged agricultural land (d) and (e)Springs observed

3.4.1.1. Discontinuity survey

The discontinuity surveys were largely done on rocks found along the road part of the research area. During the field investigation, possible slope instabilities were identified based on the failure mechanism, which might be structurally controlled or non-structurally controlled. The orientations of the discontinuities and the slope face orientation were measured using a Brunton compass. slope height was measured using a tape meter. The strength and orientation of discontinuities are the most essential factors for determining rock slope stability (Naghadehi et al., 2011).

3.4.1.2. In Situ Strength Tests

In this study, the Schmidt hammer strength test is employed in the field to estimate the uniaxial compressive strength (UCS) of the intact rock at the critical slope section(Barton & Choubey,1977). Schmidt hammer tests on rock samples in laboratories are influenced by sample size and sample holding technique. Based on this assumption, a Schmidt hammer was utilized in the field to determine the uniaxial compressive strength (UCS) of a fresh and nearly unweathered exposed rock surface and joint wall. The Uniaxial compressive strength of the rocks along the road critical slope section was determined using the empirical equation (Barton & Choubey, 1977).

$$\log_{10} (\sigma c) = 0.00088 * \gamma * R + 1.0 \qquad \text{Eq (3.1)}$$

Where; ‘σc’ is the uniaxial compressive strength (UCS) in Mpa, γ is the dry rock densities in kN/m^3, and R is the average Schmidt hammer rebound value.

3.4.1.3. Soils and Rocks Sampling for Laboratory Tests

3.4.1.3.1 Soil Sampling

The disturbed soil samples, which are representative of failed slopes, were collected from a critical section as indicated in (Fig.3.2). Soil samples were collected for index and strength testing in this investigation. Disturbed soil samples weighing 25 Kg are from pits each dug to a depth of 1–1.5 m. To retain the natural moisture content of the soil samples, they were collected and placed in a plastic bag. Soil sampling was done to collect samples for later testing in the lab. These soil investigations were carried out to characterize the materials and to determine related parameters for slope stability analysis.

Figure 3. 2: Soil sampling at A) SS1 and B)SS2

3.4.1.3.2. Rock sampling

Representative samples of rock units along road sections were collected for laboratory testing to characterize the engineering properties of rocks in the research area. Fresh rock samples were collected from a specific slope portion for point load strength and unit weight tests..

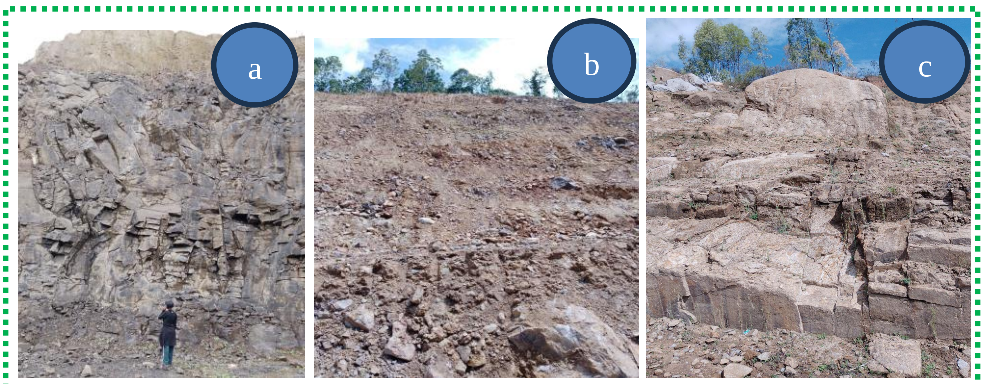

Figure 3. 3: (a),(b),(c) Rock sampling at critical slope sections

3.5 Laboratory analysis

A laboratory test was done on rock and soil samples gathered in the field. Several laboratory tests were carried out to identify and define the problematic slope material, As well as to discover the material properties that were important for slope stability study.

3.5.1 Soil Laboratory Tests

In the laboratory, soil samples were examined to evaluate the strength and index properties of the soil in the research area.

In the laboratory, soil samples were subjected to grain size analysis (sieve and hydrometer studies), specific gravity tests, natural moisture contents, the Atterberg limit (liquid and plastic limit), and shear strength tests (cohesion and angle of internal friction).

3.5.1.1 Grain Sizes Analysis

Grain size analysis determines if soil particles are categorized based on their diameter. Large and small particles were discovered in soil samples taken from the critical slope of the study area. The samples were examined using sieves and hydrometers.

- ✓ **Sieve Analysis**

Sieve analysis is used to determine the distribution of coarser grain sizes with diameters higher than 75 µm. The test was carried out by ASTM D422. First, the dry soil samples were prepared and crushed into appropriate small sizes using a hammer and pestle grinder. After cleaning the sieve stack with a brush, a set of sieves with progressively smaller openings from top to bottom was put, and the pan was placed at the bottom of the finest sieve. The soil retained on each sieve and pan was measured with a digital balance after 15 minutes. The dry mass of soil grains from individual sieving was used to calculate the percentage of soil grains passing and, consequently, the percentage retained in each sieve size. Finally, the outcomes were analyzed on a Microsoft Excel datasheet, and the grain size distribution curve was drawn from the diameter versus percent finer using the sieve analysis result (Fig. 5.1).

- ✓ **Hydrometer Test**

The hydrometer analysis is used to determine the distribution of fine particles with diameters less than (75µm). The test was carried out following ASTM D422. The test was performed initially. The fine-grain soil retained on the pan was weighed at 50 g and placed in a beaker with water and a 125 ml mixture of dispersion agent (sodium hexametaphosphate). After adding 125 ml of the dispersing agent, the soaking soil fills the control cylinder with distilled water. Then, transfer the soil slurry into the empty sedimentation cylinder and top it over with distilled water. Then, for one minute, turn the open cylinder upside down while covering it with your hand. Set the cylinder down and take the reading for 24 hours by examining the top of the meniscus-formed suspension hydrometer (Huluka & Miller,2014). The cylinder was placed in a constant-temperature water bath for this testing. Finally, the grain diameter was determined using the calibrated curves and the grain size distribution curve was produced using the diameter versus percent finer analysis result.

3.5.1.2 Atterberg limit

The Atterberg limit also known as fine soil consistency, is the physical state in which soil can remain or the water content at which soil transitions from one state to another. The Atterberg limit test is used to assess the liquid limit (LL) and plastic limit (PL) of soil. The percentage of moisture (%) at which the soil transforms from liquid to plastic, and the percentage of moisture (%) at which the soil changes from plastic to semi-solid(Sharma & Bora,2015). The test was performed according to the ASTM D4318 standard. The Atterberg limit tests were carried out on soil samples that passed sieve number 40 (0.425 mm), while the Casagrande test was carried out using distilled water. The laboratory test was performed following the following liquid and plastic limit test procedures:

- ✓ **Liquid Limit Test**

The liquid limit (LL) of soil is the point at which it transforms from a plastic to a liquid state. For this examination, part of the soil samples that passed through sieve #40 (0.425mm) opening size were placed in an evaporating dish. The soil sample was mixed with water and stirred with a spatula to create a smooth surface paste of soil. The soil mixture was split into two parts by using a grooving tool and turning the handle at 2 revolutions per second until it came into contact with the bottom of the groove at a distance of 13 mm. The number of blows needed to close the two halves of a soil specimen by 13mm was counted. A representative sample was collected from the flow section and placed in moisture cans, which were oven-dried for 24 hours at 105°C. Moisture cans are then used to determine the moisture content. Finally, the moisture content of each soil sample was recorded and evaluated.

- ✓ **Plastic limit**

The plastic limit (PL) of soil is the moisture content (%) at which it transitions from semisolid to plastic. In preparation for the liquid limit test, this test was performed on the sample. The soil sample was placed on the glass plate and rolled with a finger to generate a consistent diameter thread. Before disintegrating, the thread was rolled until it was 3mm in diameter. The crumbled soil sample was collected in containers, weighed using a mass digital scale, and placed in the oven for 24 hours. The oven temperature was set up at 105°C.

Finally, the moisture cans were taken out of the oven to dry, and the findings of each sample were recorded and examined. Finally, the plasticity index (PI) of the soil was calculated using the following equation based on the liquid limit and plastic limit tests:

PI = LL-PL……………………..Eq (3.2)

Figure 3. 4: (a) hydromter (b) Sieve (c) Plastic limit (d) casagrandae apparatus tests of soils

3.5.1.3 Natural Moisture Contents Tests

The natural moisture content of the soil in the field shows its condition. Moisture content has an impact on soil engineering behavior, especially in cohesive soil (Rasti et al., 2020). The test was performed on fresh soil samples according to ASTMD2216 standards using the oven drying technique. Furthermore, representative soil samples from the two critical slope portions have been gathered and preserved in plastic bags to retain their in-situ natural moisture content. A digital balance was used to calculate the wet mass (Mw) of the soil samples.

To obtain the dry mass of the weighted samples, they were oven-dried for 24 hours at 105°C (Md). Finally, the natural moisture content was calculated using an equation.

$$W = Mw - Md\ /Md \times 100\% \qquad \text{Eq (3.3)}$$

Where: w is the natural moisture content in (%), Mw is the mass of wet soil samples in (g), and Md is the mass of oven-dried soil samples in (g).

3.5.1.4 Specific Gravity of Soil

The purpose of the test is to determine the specific gravity of the soil. The specific gravity of the soil was determined using a pycnometer filled with distilled water at a certain temperature(Rashid et al., 2017). The soil-specific gravity was determined using oven-dry techniques according to ASTM D854 standard procedures. Before beginning the test, weigh the empty, clean, and dry pycnometer (W1) with a digital balance, then add 10g of an oven-dried soil sample that passed sieve #10 to the pycnometer and record the weight as (M2). Fill the pycnometer to a level slightly above the soil sample, immerse it for 10 minutes, and then use the boiling procedure to release the trapped air. Then, fill the pycnometer with distilled water to the mark, and weigh the pycnometer containing the soil and water (W3). The pycnometer was then drained, cleaned, and refilled with distilled water to mark and weigh the distilled water (W4). Finally, eq. can be used to compute specific gravity.

$$Gs = W2 - w1\ W4 - w1 - (W3 - W2) \qquad \text{Eq(3.4)}$$

Where: W1 is the weight of a clean and dry pycnometer, W2 is the weight of oven-dried soil and pycnometer, $W3$ is the weight of the pycnometer filled with water and $W4$ is the weight of a pycnometer filled with water and soil.

Figure 3. 5: specific gravity of soil

3.5.1.5 Shear Strength Tests

Shear strength is the soil's maximum resistance to shear force just before failure. Shear strength is one of the most essential engineering properties of soil. In this study, the direct shear strength test was utilized to evaluate shear strength features such as cohesion and angle of internal friction in failed slope sections. The apparatus consists of a square brass box divided horizontally at the level of the soil sample and held in place by metal grilles and porous stone. The vertical load is applied to the sample in the manner seen in the image and is held constant during the test during the test, constant vertical load is applied to the sample. The sample is subjected to an increasing horizontal load at the box's bottom until it fails in shear. The horizontal and vertical shear displacements were recorded at regular intervals for each normal load applied. Shear and normal stresses were computed and displayed in the graph based on the test findings.

Finally, the Mohr-Coulomb failure criterion describes the. The relationship between a soil shear strength at a point on a particular plane and its normal stress is as follows in equation 4.0

$$\tau = c + \partial \tan\phi \ (4.0) \qquad \text{Eq (3.5)}$$

Where: C is the cohesion and ϕ is the internal angle friction of the soil particle

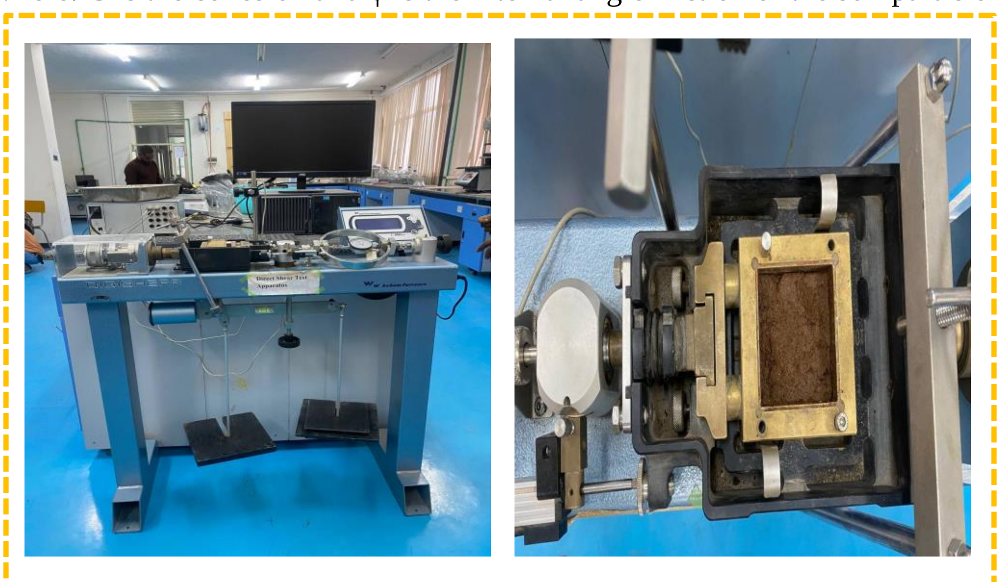

Figure 3. 6: Equipment used for direct shear strength test

3.5.1.6 Unit Weight of Soils

Soil unit weight is one of the input parameters used in soil slope stability assessments. The outcomes of the laboratory tests on the soil sample from the research area were utilized to compute the saturated and dry unit weights of the soil.

The product of density and gravity acceleration (g) was used to compute the in-situ unit weights of soils both bulk (y) and dry (d). For this investigation, representative soil samples were collected from critical slope sections, and the associated unit weight was calculated. Based on the bulk and dry density data, the unit weight of the soil sample was estimated as follows:

Bulk unit weight = bulk density*g .Eq (3.6)

Dry unit weight = dry density*g Eq (3.7)

3.5.1.7 Compaction Test

The maximum density and optimum moisture content of the soil used in the shear strength test are determined by compaction. Proctor tests are performed to see how soil compaction varies when moisture content changes. Two soil samples were tested following ASTM D698 on a critical slope section of the study area.As a result, the laboratory test was carried out as follows: To begin, collect 5kg of soil sample that has been processed through a No. # 4 sieve. Add the measured amount of water to the soil and thoroughly mix it in. Calculate the weight of the compaction molds in the base (M1). The soil sample was then filled into the cylinder molds in three layers, 25 blows for each layer. Remove the collar and level any extra compacted soil beyond the mold rim. The weight of the compacted soil within the mold and base was then measured (M2).Using a mechanical extruder, remove the compacted earth from the molds. The soil sample was then split using a knife, and a sample was taken from the bottom and top of the moisture cans, which were then placed in an oven at 105 °C for 24 hours. After that, the bulk density and dry density of the soil are determined by the following equations 3.8 and 3.9, respectively.

$\gamma b = M2 - M1\ V$ (3.8) .Eq (3.8)

Where: γb - the bulk density of the soil

M2- the mass soil after being compacted with mold, M1- is the mass of the mold and V is the volume of the mold.

The dry density of the soil is also calculated as the following equation.

$$\gamma d = \gamma b\ (1 + w\ 100) \qquad \text{Eq (3.9)}$$

Where: γd is the dry unit weight, γb is the bulk unit weight, and W is the moisture contents of soils. Finally, the results of the recorded data were analyzed on a Microsoft Excel datasheet and the graph of the dry density versus moisture contents for analysis results (Fig.5).

Figure 3. 7: Equipment used for compaction test

3.5.2 Laboratory Testing on Rocks Sample

To characterize the engineering properties of the rock found in the research area, a point load strength test was performed on a representative fresh sample of the rock obtained from the field. The buoyancy method was also employed to calculate the rock's unit weight.

3.5.2.1 Point load test

The unconfined compressive strength of intact rock was determined using a point load strength test. The tests were conducted according to ASTM D 2938. The test was performed on a minimum of two to four irregular rock samples collected at each critical slope section. The rock sample is placed in the point load tester model PIL-7 with a diameter to average width ratio greater than 0.3mm and half of the diameter less than the length of the rock sample, and the load is applied continuously until failures appear and the peak values of the failure load (P) are recorded.

Later, the corrected point load strength average was converted to the rock uniaxial compressive strength using the empirical equation proposed by (Broch & Franklin, 1972) which showed the relationship between the corrected point load strength and the rock uniaxial compressive strength (Eq. 3.1).

3.5.2.2 Unit Weight Rock

A rock weight and stress are calculated using the unit weight. The unit weight of the rock was one of the input elements used in calculating the safety factor for rock slope stability calculations. As a result, in this study, the test to determine the unit weight of the rock was done on a minimum of three irregular rock samples acquired from each critical rock slope, as stated by ISRM (1981), as follows:

The rock was first weighed at its natural moisture content (M1) before being oven-dried for 24 hours at 105°C. M2 was the weight of the oven-dried rock samples.The initial water volume (V1 in ml) was measured after filling the cylinder with water. In a water-filled cylinder, the volume change (V2 in ml) of oven-dried samples was measured. Then immerse an oven-dried irregular rock in a water-filled cylinder and compute the sample volume change as follows:

$$\Delta V = V2 - V1 \qquad \text{Eq (3.10)}$$

weighed (M1) under their natural moisture content and oven-dried for 24 hours at 105°C, then the weight of the oven-dried rock samples was recorded (M2).Finally, the dry density (γd) and unit weight (γ) of each rock sample were determined using Equations

$$\text{pd} = M2\ \Delta V \qquad \text{Eq(3.11)}$$

$$\gamma = \text{Pd} \times \text{g} \ldots \qquad \text{Eq (3.12)}$$

Where γd is the dry density of the rock samples in g/cm3, M2 is the mass of the rock samples after oven drying in (g), and V is the difference between the water volume after and before the rock sample is placed in the cylinder. g is the gravitational acceleration (in m/s2) and is the unit weight of rock in KN/m^3.

3.6 Data processing and analysis

The information gathered from secondary and primary sources through desk research, reconnaissance and comprehensive field surveys, laboratory testing, and literature studies was organized and processed so that it could be easily accessed during subsequent stability assessments. Slope stability was assessed using Rocsciences software after gathering and processing all of the data required for stability assessments.

3.6.1 Rock Mass Classifications Method

3.6.1.1 RQD

Rock mass classification is one of the most extensively used empirical classifications in rock engineering (Salmanfarsi et al., 2020). The classification of rock quality is an important factor in identifying rock masses. A variety of parameters influence the RQD index, including joint orientation, joint spacing, fracture frequency, and joint roughness(Azimian, 2016).RQD is defined as the percentage of intact drill core pieces longer than 10cm recovered during a single core run(Abzalov, 2016).

The general equation is represented by the symbol.

$$RQD = \sum \frac{\text{Core pieces>10cm}}{\text{The total length of the core run}} \times 100\% \qquad \text{Eq (3.13)}$$

The volumetric joint count (Jv) is a measure of jointing degree or inter-block size that can be used to define rock mass jointing (Palmström et al., 2001). Joint spacing (S), as described by the Jv, is the distance between two successive discontinuities measured along a line on the rock surface. The number of joints that cross a one-m3 volume is represented by the JV count Palmstrom (1974)claims that the connection between RQD and volumetric discontinuity joints Jv can also be used to determine RQD.

$$\text{RQD} = 115 - 3.3\text{J} \qquad \text{Eq (3.14)}$$

Where the volumetric discontinuity joints Jv are the sum of the number of discontinuities per unit length for all discontinuity sets, which can be determined from the discontinuity set spacings within a volume of the rock mass (Palmstrom, 1982)as follows:

$$\text{JV} = \frac{1}{s1}+\frac{1}{s2}+\frac{1}{s3}\cdots + \frac{1}{sn} \qquad \text{Eq (3.15)}$$

Where s1, s2, and s3 are the mean discontinuity set spacings. (Palmstrom, 2005)suggests that r= 5 m be assumed. As a result, the volumetric discontinuity frequency Jv can be generalized as

$$\text{Jv} = + \frac{1}{s1}+\frac{1}{s2}+\frac{1}{s3}\cdots+ \frac{Nr}{5}. \qquad \text{Eq (3.16)}$$

Where Nr is the number of random discontinuities.

3.6.2 Shear strength parameters

3.6.2.1 Shear strength parameters of soil

The shear strength properties of the soil were evaluated using a laboratory direct shear test. To compute soil cohesion and friction angle, the measured horizontal displacement, shear box area, shear load, and shear stress were entered into Excel as input parameters.

3.6.2.2 Shear Strength Parameters of Rock mass

When assessing the stability of a rock slope, cohesion and the angle of internal friction are critical shear strength elements to consider. RocData software was used in this work to forecast the shear strength characteristics of the rocks (cohesion and friction angle) along the discontinuity plane based on an empirically derived correlation indicated by Barton Bandies.

$$\tau = \partial * \tan \{\text{JRC} * \log 10 \left(\frac{jcs}{\sigma n}\right) + \phi b\} \qquad \text{Eq (3.17)}$$

Where: τ = Peak shear strength, ∂n = Effective normal stress, JRC = Joint roughness coefficient, JCS = Joint wall compressive strength, ϕb = basic friction angle.

The primary input parameters of Rocdata software, according to Barton and Bandis shear strength requirements, are:-

- ✓ basic friction angle (ϕb)
- ✓ joint roughness coefficient profile (JRC
- ✓ joint wall compressive strength (JCS)
- ✓ slope height
- ✓ unit weight of the rock

During fieldwork, the joint roughness coefficient was visually determined by comparing discontinuity surfaces to joint roughness profiles developed by Barton and Choubey(1977). The value of the basic friction angle (ϕb) is between 25 and 35 for most smooth and unweathered rock surfaces Barton and Choubey(1977).Furthermore, the Heok-Brown failure criterion was utilized to calculate the shear strength and deformation parameters of the rock mass (Hoek et al., 2002) using Rocdata software and generalized Hoek-Brown failure criteria to calculate the cohesiveness (C) and internal friction angle (ϕ) of rock masses.

Rocdata software allows users to easily estimate rock mass properties according to (Hoek et al.,2002), using generalized Hoek-Brown failure criteria and shear strength parameters requirements are:-

- ✓ The Geological Strength Index (GSI),
- ✓ Uniaxial compressive strength of intact rocks (UCS),
- ✓ The material constant of intact rock (mi)
- ✓ Disturbance factor (D)
- ✓ unit weight of a rock
- ✓ slope height (H) for slope application (ROCSCIENCE, 2004).

The point load strength index was used to calculate the uniaxial compressive strength of intact rock in the laboratory. The GSI was determined in the field by taking into account the weathering conditions of the discontinuity surface rock mass structure and the interlocking of rock blocks, (Marinos & Hoek, 2000). The material constant of intact rock (mi) was derived from the standard table of the Rocdata software (Hoek et al., 2002).

Wyllie and Mah's (2004) criteria were used to determine the disturbance factor, which was based on the degree of disturbance of the rock mass subjected to mechanical excavation. In addition, the rock unit weight was calculated in the lab using buoyancy techniques(ISRM, 1978), and the slope height was measured in the field with a tap meter. Finally, the Rocdata software output parameters were employed as input parameters in the slope stability analyses.

3.7 Slope Stability Analysis Method

Kinematics, limit equilibrium, and finite element approaches were used in the current slope stability investigation. Geotechnical data from field surveys and laboratory experiments were combined to create the slope models. This section provides a brief overview of each slope stability analysis approach.

3.7.1 Kinematic Analysis Methods

To analyze the various failure mechanisms, such as planar, wedge, and toppling failure, kinematic analysis was performed using Dips software(Khanna & Dubey, 2021).

The identification of the type of rock slope mode of failure induced by a discontinuity plane is usually the initial stage in rock slope stability investigations based on field manifestations and kinematic analysis (Park & West,2001). Kinematic analyses determine the mode of rock slope failure based on slope geometry and discontinuity orientations(Park et al.,2005).

Rock slope failure most typically happens around structural discontinuities or weak planes such as joints, faults, and so on. The orientations of exposed slope and structural discontinuities across selected critical rock slope faces were measured on the field with a Brunton compass in this study. Dips software(ROCSCIENCE, 2004) was used in this study to examine the kinematics of a rock slope for structurally controlled failure. A rock slope's stability was estimated using plotted structural data and daylight envelopes.

The data plotted can be utilized to determine the active failure mechanism and the potential of a failure zone on a slope.

Dips Software requires input parameters are:-

- ✓ slope orientations,
- ✓ major joint set dip and dip directions
- ✓ friction angle (Khanna & Dubey, 2021)

The orientation of slopes and structural discontinuities (dip and dip direction) in critical rock slope sections were measured in the field with a Brunton compass. Rocdata software used nonlinear failure criteria to calculate the angle of friction along the failure plane (Barton and Bandis, 1990). Finally, the Dips software (Rocscience, 2004; Dips7) was used to perform a kinematic analysis of the main plane to determine the mode of slope failure in the critical rock slope sections of the research area.

3.7.2. Deterministic Slope Stability Modelling Method

For the mechanism of rock slope failure, the deterministic technique was utilized to determine the safety factor and evaluate the stability analysis(Park& West,2001). The software Rocplane, Swedge, and Roctopple were used to assess stability. The Rocplane software(ROCSCIENCE, 2004) was used to perform a planar rock slope failure analysis, which was designed based on stability analyses of the planar rock slope failure (Park & West, 2001).

The Swedge software (Swedge 4.0, Rocscience, 2004) was used to analyze the stability analyses of rock slopes with wedge modes of failure, which were developed based on(Park & West,2001).Stability analyses of wedge modes of rock slope failure. Furthermore, the Roctopple software (Rocscience, 2004; Roctopple 2), was developed based on the stability analysis of rock toppling failure(Hoek & Bray,1981).was used to do the stability analysis for rock slopes with toppling failure.The input parameters used for the stability analyses of the mode of three types of rock slope failures were:-

- ✓ Slope geometry and orientations of discontinuities,
- ✓ Shear strength parameter (cohesion and angle of internal friction),
- ✓ Unit weight of the rock.

The slope geometry and discontinuity set orientation were obtained in the fields, whereas the shear strength parameter of the discontinuity sets (cohesion and angle of internal friction) was evaluated using Rocdata software (Rocdata, 3, Rocscience, 2004) following the non-linear failure criteria proposed by Barton and Bandis (1990). The laboratory test findings were used to calculate the unit weight of rock. Finally, the safety factor was calculated for a variety of anticipated situations, including static and dynamic dry, as well as static and dynamic saturated.

3.7.3 Limit Equilibrium Method

The safety factor is calculated using the limited equilibrium approach, which compares the shear strength adjacent to the sliding surface to the force required to keep the slope in equilibrium(Ullah et al.,2020). The limit equilibrium technique assumes that all points along failure surfaces are on the verge of failure. The sliding mass is divided into slices for static equilibrium conditions, the shear and normal inter-slice forces are computed, and the appropriate force and/or moment equilibrium equations are satisfied. Limit equilibrium (LE) approaches use the Mohr-Coulomb failure criterion to calculate shear strength along the slip surface.

3.7.3.1 Slide software

For this investigation, the slide software's limit equilibrium approach was used to model and compute the factor safety (Slide 6, Rocscience, 2004) for rock and soil-selected slope sections**.**

The input parameters for slide software include:

- ✓ Shear strength parameters of rock and soil (cohesion and angle of internal frictions)
- ✓ The unit weight of rock and soil
- ✓ Slope geometry
- ✓ External force (seismic load).

Rocdata software was used to calculate the shear strength of a rock mass-selected slope section based on the Hoek-Brown failure criterion. Soil shear strength (cohesion and friction angle) was determined by direct shear testing the rock's unit weight was determined in the laboratory using buoyancy techniques developed by(ISRM, 1978). A tap meter was used to measure the slope geometry in the field. The horizontal seismic acceleration was calculated using data from a seismic risk map. (ISRM,1978).

3.7.4 Finite element method

The finite element approach was used to evaluate the stability of the natural slope. Finite element analysis can be performed using Phase2 software. In the finite element slope stability study, a shear strength reduction technique is applied. To measure slope stability, the Phase2 software (ROCSCIENCE, 2004) is employed in this work.

3.7.4.1 Phase 2

To measure slope stability, the Phase2 software(ROCSCIENCE, 2004) is employed in this study. The Phase2 software is a strong finite element tool that can be used to analyze engineering slope stability in a variety of conditions (You et al.,2018). The uniaxial compressive strength of intact rocks and the unit weight of rocks, which are derived from laboratory testing, are determined during data preparation and phase 2 software analyses. In the field, the geological strength index and slope height were determined. The material constant of intact rock (mi) was taken from the Rocdata software's standard table (Hoek et al.,2002).

Rocdata software(RocData, 2004). Was used to calculate the shear strength parameters (cohesion and angle of friction) along the plane of failure of the rocks. A direct shear test was used to assess the shear strength characteristics (cohesion and angle of friction) of soil materials along the plane of failure. The Rocdata software was also used to obtain the Hoek Brown parameters(RocData, 2004). The disturbance factor was calculated using Wyllie and Mah, 2004) recommendations based on the degree of disturbance of the rock mass.

The Poisson's ratio of the rock mass can be computed for this study utilizing the relationship suggested by Balazs(2009)between the material constant (mi) and the geological strength index Equation (4.3), as shown in Equation 3.18 below.

$$\nu rm = -0.002GSI - 0.003mi + 0.457 \qquad \text{Eq (3.18)}$$

Where: Vrm is the Poisson's ratio of the rock mass; mi is the material constant of intact rock (mi) taken from the Rocdata software; and GSI is the geological strength index of rocks that can be estimated in the field. The deformation modulus of the rock mass was calculated for this investigation using the General Hoek Brown failure criterion from Rocdata software (RocData, 2004).

Hoek and Brown(1997) calculated the deformation modulus of rock mass using equations 3.19 and 3.20 below.

For UCS ≤ 100 Mpa $$Em = (1 - \frac{D}{2})\sqrt{\frac{Ucs}{100}}\, 10^{\frac{(GSI-10)}{40}} \qquad \text{Eq(3.19)}$$

For USC >100 Mpa $$Em = (1 - \frac{D}{2})10^{\frac{(GSI-10)}{40}} \qquad \text{Eq(3.20)}$$

Where Em is the modulus of deformation of the rock mass, UCS is the uniaxial compressive strength of intact rocks, D is the disturbance factor, and GSI is the geological strength index established in the field. Finally, by importing the input parameter into the software, the safety factor was calculated for several expected situations such as dynamic dry, dynamic saturated, static dry, and static saturated conditions. Furthermore, the soil's elasticity modulus (E) and Poisson's ratio (v) are utilized in numerical modeling to examine deformation. As a result of numerical correlations and a review of the literature, appropriate values for these parameters were determined. The standard penetration test (SPT) has been used to correlate different soil parameters such as:-

- ✓ unit weight (γ),
- ✓ the angle of internal friction (φ) and
- ✓ Undrained compressive strength (qu) for estimating the stress-strain modulus elasticity of soils.

For this study, SPT N values were linked to saturated unit weights of soils Bowles' (1996) equation 4.6 can be used to compute the drained poison ratio of granular soils. This study calculated the corrected standard penetration test N value from an average energy ratio of N60 using the equation published by (Terzaghi et al.,1996). According to Ameratunga et al.(2016).the modulus of elasticity of the soil was determined using an equation from the SPT N60 value.

$$V = 0.1 + 0.3\ (\phi - 25)\ 20\ for\ \phi < 45° \ (4.6) \qquad \text{Eq (3.20)}$$

$$\gamma sat = 16.8 + 0.15N60\ (KN/m3)\ (4.7) \qquad \text{Eq (3.21)}$$

$$Es = 1200\ (N+6)\ KN/m2 \text{ for } N < 15 \qquad \text{Eq (3,22)}$$

$$Es = 4000 + 1200(N-6)\ KN/m2 \text{ for } N > 15 \qquad \text{Eq (3.23)}$$

Where V is the poisons of soils, γsat is the saturated unit weight of soil and Es is the elasticity deformation modulus of soil.

3.8 Materials used for study

The materials and equipment used in this study include both laboratory and field equipment. For field data collection, measurement, and testing, the following equipment and materials are used: in-situ rock strength tests and laboratory analysis.

3.8.1Material used in filed

- ✓ The critical slope sections in the field were located using the global positioning system (GPS)
- ✓ The discontinuity orientation of rocks (dip/dip direction) and slope orientation in the field were measured using a Burton compass.
- ✓ The Schmidt hammer was used to determine the uniaxial compressive strength of representative rocks.
- ✓ In the field, slope height and discontinuity spacing were measured with a tape meter.

3.8.2 Material used in the laboratory

- ✓ Soil mechanics laboratory equipment such as the direct shear test, sieve, hydrometer, pyrometer, and atterberg have been used to determine the index and engineering properties of soils.
- ✓ The rock mechanics laboratory was used to measure the strength of the intact rock, such as point load, and the unit weight of the rock was determined using a cylinder with a defined volume.

3.8.3 Software Used for Analysis

- ✓ Maps and diagrams were created using Arc GIS 10.8, Sulfur , and Global Mapper.
- ✓ For various slope stability evaluations, Rocscience software such as Dips, Rocdata, Slide, Rocplane, and Phase 2 is utilized.

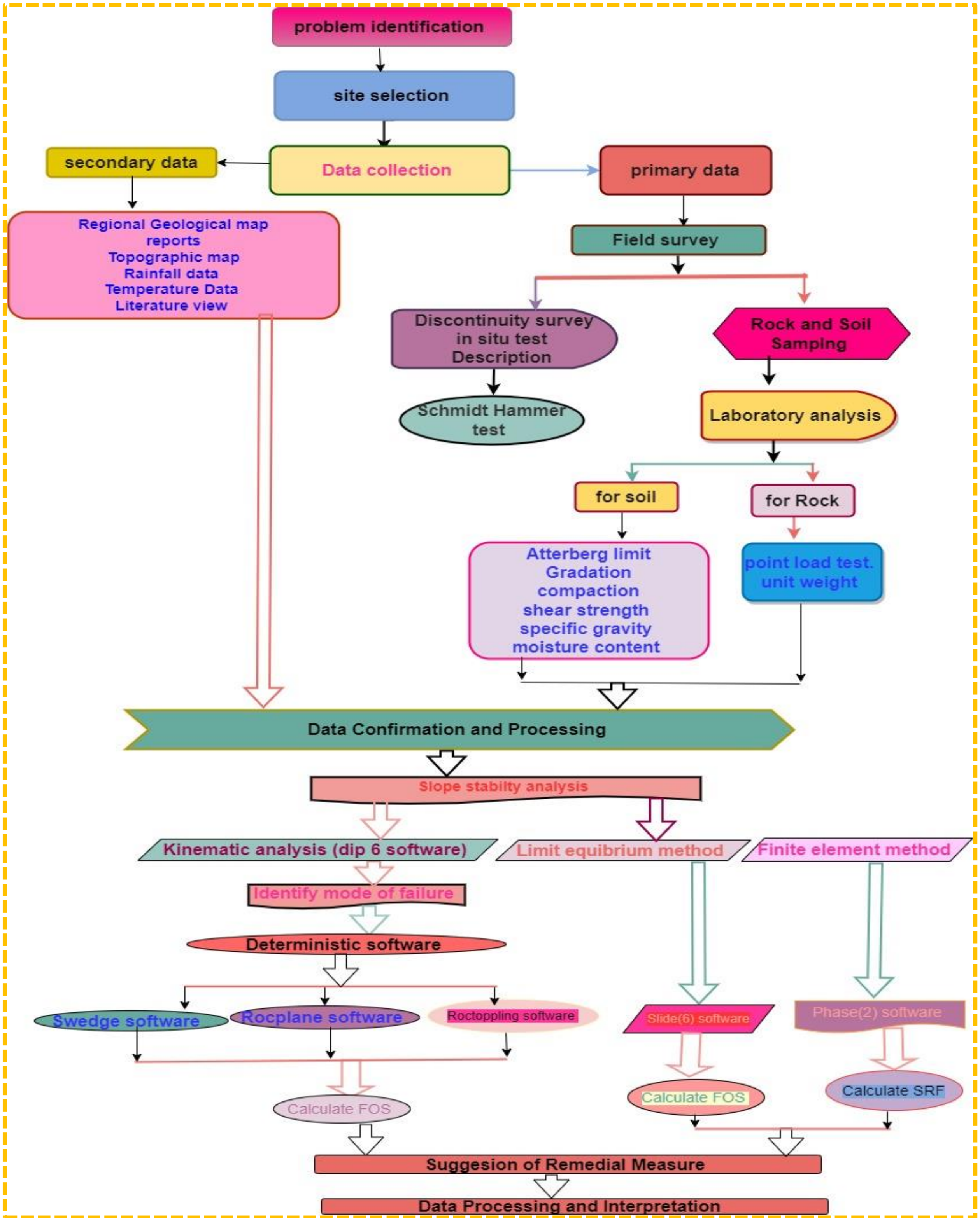

Figure 3. 8: General Methodological flow chart of research

CHAPTER FOUR

4. GEOLOGY OF THE STUDY AREA

4.1 Regional Geology and Structural Setting

The study area geology is conveniently divided into four major age groups of rock units: Neoproterozoic to early Paleozoic crystalline basement and intrusive rocks; Tertiary sediments; Early-Mid Tertiary volcanic rocks (Eocene to Miocene pre-rift volcanic rocks); and Upper Tertiary-Quaternary sediments (late Miocene to Holocene syn- and post-rift sediments). Ethiopia's physiographic features include extensive north-western and south-eastern regions, the Main Ethiopian Rift Valley (MER), and the Afar Depression (Tefera et al.,1996). The south-western Ethiopian plateau is characterized by a Precambrian basement, Tertiary volcanic rocks, and Quaternary sediments(Tefera et al.,1996). The Ethiopian plateau is underlain at depth by Afro-Arabian Shield Precambrian rocks.

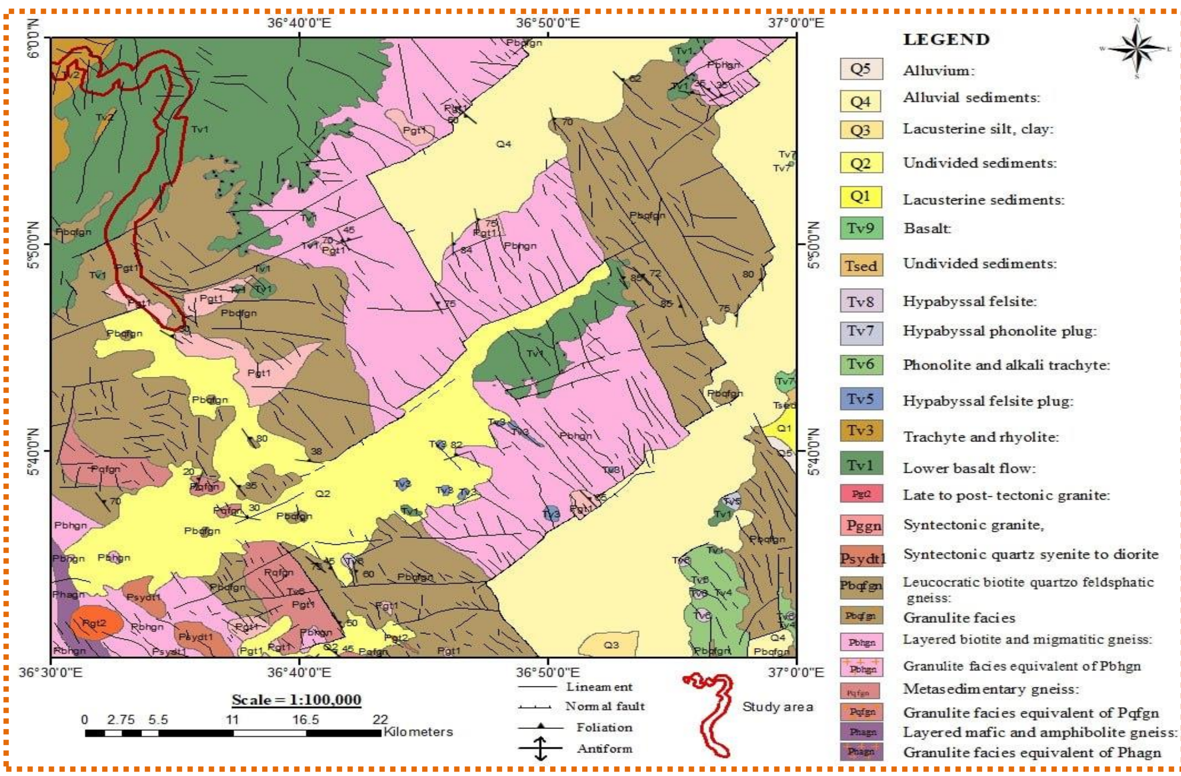

Figure 4. 1: Regional Geological map of the area (source:Tarkegn Dure,Temegen Demissie and other reserchers work).

4.2 Stratigraphy

Based on geochronology, the study area's stratigraphy is divided into three major groups of rock units.

The oldest rock unit is the crystalline basement, which formed between the Neoproterozoic and early Paleozoic ages. This rock unit includes high-grade gneiss, as well as pre-, synth-, and post-tectonic plutonic rocks. The Neoproterozoic basement rocks are overlain by pre-rift volcanic layers, which are one of the three major rock units in the area. The pre-rift volcanic rocks were formed during the Eocene age. A thin, red, residual sandstone unit that covers much of the crystalline basement beneath the early Tertiary flood basalt cover is unknown age. The last major section is the late Miocene to Holocene post-rift deposits. With the exception that unconformable relationships are only manifesting, and future erosion of the older rocks on blocks between zones of faults may be indicated by a hiatus without appreciable unconformity, these groupings are separated from one another by major unconformities.

4.3 Local Geology of the Study Area

The study area is divided into two major rock groups of three local geological formations as presented below.

- ✓ Moderately weathered Basalts
- ✓ Highly weathered Rhyolites
- ✓ Slightly weathered Granite

4.3.1 Moderately weathered Basalt unit

This rock unit is also characterized by moderate to steep terrain. Basalt rocks are massive and weathered, with aphanitic textures, dark grey tints, fine-grained textures, and large columnar joints. Decomposed basalts can be found on steep and mountainous terrain. Texture and compositional variation are frequent in basalt flows. Predominantly fine-grained, aphanitic to porphyritic in texture, and sometimes vesicular; fresh to decayed; massive to fissile; thinly to widely jointed; and moderately to strongly fractured.

Figure 4. 2 (a) and (b) Basalt unit observed in the study area

4.3.2 Highly weathered Rhyolite

These rocks were characteristically gray to light brown, dense, and poorly to non-vesicular. These rocks show primary fabrics.It forms topographic highs and steep slopes. The rock is light in color, fine to medium-grained, acidic lava composed essentially of quartz and plagioclase feldspar with flow banding, anisotropic character, and poor shape. In the present study area, rhyolite rocks are highly weathered.

Figure 4. 3 highly weathered Rhyolite

4.3.3 Slightly weathered Granite

The granular texture of the granitic material is medium to coarse. This granite is massive, medium-grained, and equigranular. It contains quartz, hornblende, and gray feldspar. Granite rocks are slightly weathered in the current study area.

Figure 4. 4: Slightly weathered granite

4.4 Unconsolidated unit

4.4.1 Residual soil

Residual soils are the product of in-situ weathering of parent rocks that have not been transported and are still in their original location. They are typically found in tropical climates with relatively high temperatures and rainfall, and they frequently grade into decomposed (with weak relict structures and the parent materials fabric still maintained) and weathered rocks with depth. At side cuts, stream or river banks, and hillside slopes, residual soils are commonly varied in color, ranging from light grey to reddish brown to dark brown silty clays.

Figure 4. 5: (a) and (b) Residual soil in the study area

4.4.2Colluvial soil

Colluvial soils are primarily coarse-grained soils with fine-grained soil matrixes that are weathering products of rocks that are transported primarily by gravity and deposited along foot slopes. Colluvium is sediment that has moved downhill without the assistance of moving water in streams. Colluvium can be unstable on steep slopes and is frequently prone to subsequent instability.

Figure 4. 6: Colluvial soil observed in the study area

4.4.3 The alluvial soils

Alluvial soils are commonly those that have been transported by rainwater from hill slopes and deposited over the lower ground. This type of soil mainly exists in the mountainous terrain approach to the major rivers or at the banks of the river channel in the road.

4.5 Geological Structures

The study area has a variety of geological structures, including joints, and fractures, along the lithological units of the road section that were identified during the fieldwork.

4.5.1 Exfoliation and Spheroidal Structures

Lower basalt flows are the oldest and most extensive of the volcanic units. This basalt is characterized by thick and widespread lava flows. Lower basalt flows are mostly aphyric, fine-grained, and plagioclase-phyric basalts with secondary mineral vesicles and amygdules. The rock is heavily weathered, with spheroidal and onion skin weathering being common**.**

Figure 4.7 (a)Onion (exfoliation) weathering and (b) burst (spheroidal) weathering

4.5.2 Joints

One of the most essential parameters for detecting slope rock mass stability conditions is fracture set conditions (Hack et al., 2003). A joint is a brittle fracture surface in rocks that has experienced little or no displacement. On the field, the dip and dip direction of the joints were measured to determine their effect on slope stability. The joint spacing conditions were classified as close to wide space.

Figure 4. 8: (a) and (B) Joints observed in the study

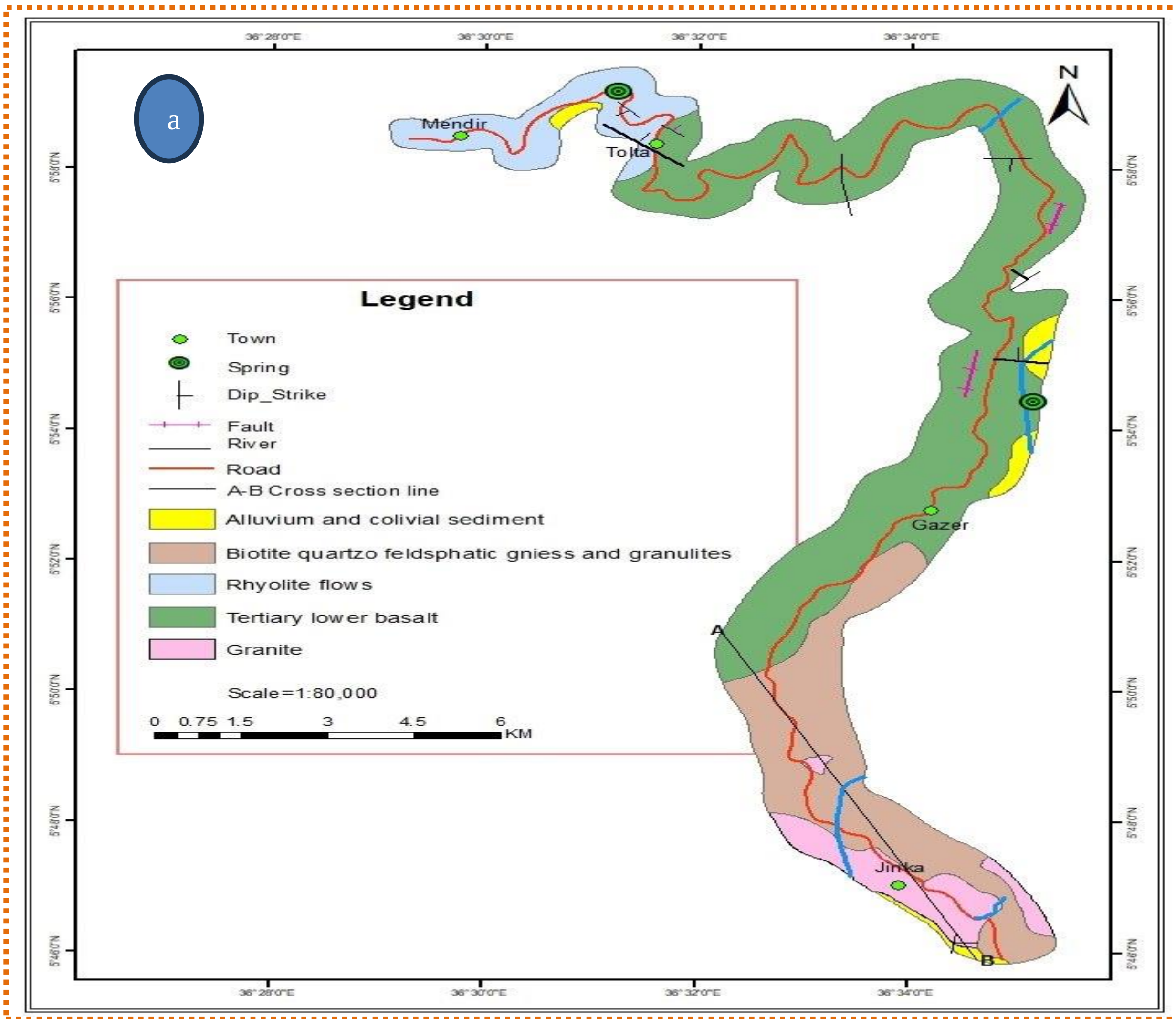

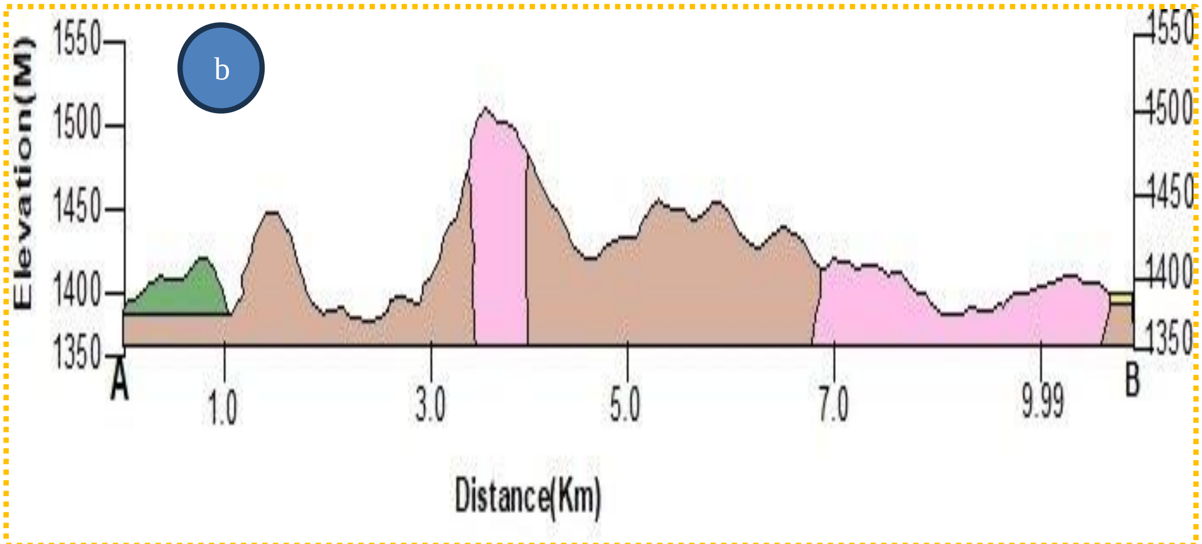

Figure 4. 9(a) Geological map of the study area and (b) cross-section along A-B.

CHAPTER- FIVE

5. RESULT and DISCUSSION

5.1. Engineering Geological Characterization of the Rock Mass

A comprehensive field study was conducted to identify critical slope stability along the section of the road and to detail the geological components of the soils and rocks. To identify the types of rocks, weathering, and fractures in the research area, a comprehensive field survey was conducted. Even though three critical rock slope sections and two soil slope sections were detected during the field investigation.

5.1.1. In-Situ Rock Strength Test

The Schmidt hammer strength test (Barton & Choubey, 1977) was used in the field to assess the uniaxial compressive strength (UCS) of the intact rock at the critical slope sections. This test was performed following ASTM D5873 (2001) to get rebound values. The empirical formulas (Eq.3.1) proposed by Barton and Choubey (1977) were used to convert the representative average rebound value of rocks into UCS. The rock's lowest and greatest strengths were determined using the Schmidt hammer (L-type), which ranged from 68.3 Mpa to 95 MPa for slope sections RSS4 and RSS5, respectively, as shown in Table 5.1.

Table 5. 1 Schmidt Rebound and UCS values from different critical slope section

Slope sections	Schmidt hammer rebound value from each critical slope section	Average of Rebound value	Ave (R)	UCS (Mpa)	According to ISRM (1979)
RSS3	40,45,54,53,47.5,60,61,59.5,44,45	50.9	41.9	72.8	Medium strength
	33,32,43,31.5,25,21,19.5,39.5,41,42.5	32.8			
RSS4	40,53.5,55,39,51.5,57.5,55,56,48.5,47	50.3	38.7	68.3	Medium strength
	36,20,21,29,26.5,27.5,11,32,31.5,37	27.15			
RSS5	50,55,49,50,42.5,41,58,50,59,49	50.35	47.7	95	Medium strength
	42.5,49,35,40,43,45,50,49,47,50	45.5			

5.1.2 Rock Quality Designation (RQD)

According to Palmstrom (1982) in the current study, the volumetric joint count (JV) for rock mass exposed at important slope sections along the road in the study area was utilized to assess rock quality classification. As a result, volumetric joint account measurements on exposed rock surfaces along the road's critical slope sections in the research area were collected. After gathering measurements from each important slope section, the volumetric joint account was calculated from the average spacing of joints using equation 3.14. Table 5.2 summarises the rock quality designation index (RQD) derived by the joint count approach. The minimum and highest RQD values obtained using the combined volumetric count technique are 66% and 82%, respectively (Table 5.2). The rock mass exposed to the road section of the research area was evaluated as good and very good by (Deere, 1988).

Table 5. 2 The Rock quality designation index determined from the volumetric joint count.

Slope section	JV (av)/1m*1m	RQD %	According to Deree (1988)
RSS3	10	82	Good
RSS4	15	66	Fair
RSS = Rock slope section and Jv, = volumetric joint account			

5.1.3 Rock Mass Rating (RMR)

The quality of the rock which composes the critical rock slope in the study area was determined according to the (Bieniawski, 1989) basic rock mass rating system. The five basic parameters such as uniaxial compressive strength, rock quality designation index, spacing of discontinuity, condition of discontinuity, and groundwater condition were determined and used as input parameters for RMR determination (Table.5.3) below. According to ISRM (1978), the determined spacing of the discontinuities ranges from 0.2m to 3m which is classified as moderately spacing to wide spacing.

Table 5.3: Input parameter used to classify rock at critical slope section.

parameter		Location of critical rock slope section	
		RSS3	RSS4
UCS (Mpa)		72.8	68.3
RQD (%)		82	66
Joint spacing (cm)		2.5 m	20 cm
Condition of discontinuity	Persistence(m)	>50	>50
	Aperture(mm/cm)	7.5 cm	16.5 mm
	Filling	Partially Open	Partially field with soil
	Roughness	rough	Slightly rough
	Degree of weathering	Slightly weathered	Moderately Weathered
Ground water condition		Damp	Damp

To classify the rocks of critical slope sections according to (Bieniawski, 1989) rating value given for each parameter was added together to calculate RMR describe the rocks based on the value. According to (Bieniawski, 1989) in this study area, the quality of rock at the critical slope section (RSS3) was described as Good rock the rock at the critical slope section (RSS4) was described as Fair rock.

Table 5.4: classification of rock of critical slope sections based on Rock Mass Rating Method

Slope sections	The five basic RMR parameters rating value					RMR	Class	Descript ion
	UCS	RQD	J. SPC	C. DSC	GWC			
RSS3	7	17	20	6	10	60	III	Fair rock
RSS4	7	13	10	6	10	46	III	Fair rock

5.1.4 Slope Mass Rating (SMR)

Slope mass rating (SMR) was proposed by (Romana, 1985) which was the extension of RMR after Beniawski (1979), It was only used for a planar and toppling mode of failure before (Anbalagal et al., 1992) and modified to account for wedge mode of failure.Finally, stability class and probability of failure of rock slope can be indicated by using the following equation.

$$SMR = RMRbasic + (F1 * F2 * F3) + F4$$

Table 5.5: classification of rock of critical slope sections based on Slope Mass Rating Method

Slope sections	The five basic RMR parameters rating value					SMR	Class	
	F1	F2	F3	F4	RMR			Description
RSS3	0.925	0.275	-3	15	60	74	II	Good
RSS4	0.70	0.40	0	15	46	61	II	Good

5.2. Laboratory Test results from the Rock sample

The laboratory tests that are used for the engineering characterization of rocks were normally conducted for classification purposes at each critical slope section of rock along the road. This study used laboratory investigation of rocks to identify engineering characteristics of rocks such as point load testing, unit weight, and density. The following is a summary of the tests used in this study:

5.2.1 Point Load Tests

Point load strength tests were used to measure the uniaxial compressive strength of the intact rock. The research area's rock strength classification and point load strength test were carried out on samples acquired from each selected critical rock slope section by ASTM D 2938. From the study area's critical rock slope sections 11 irregular rock samples were calculated. Using equation 2.12, the average corrected point load strength was converted to the appropriate uniaxial compressive strength (UCS). According to the corrected point load strength test findings for each critical rock slope section (Table 5.3), the rock point load strength index ranges from 3.95 MPa to 6.16 MPa, with corresponding uniaxial compressive strengths ranging from 95 MPa to 148 MPa. The results of the point load strength tests on the rock samples revealed that the rock in the critical slope sections of the research area had strengths ranging from medium to high(Deere & Miller, 1966).

Table 5. 6 Point load and uniaxial compressive strength test results of intact rocks

Slope sections	Sample ID	IS (50) Mpa	Ave, I S (50)	UCS (Mpa)	According to Deree and Miller 1966
RSS-3	RSS3-01	5.36	5.80	139.2	High strength
	RSS3-02	4.68			
	RSS3-03	5.65			
	RSS3-04	7.53			
RSS-4	RSS4-01	2.94	3.95	95	Medium strength
	RSS4-02	4.94			
	RSS4-03	3.57			
	RSS4-04	4.36			
RSS-5	RSS5-01	5.82	6.16	148	High strength
	RSS5-02	6.93			
	RSS5-03	5.75			
	RSS = Rock Slope section, Ave- average, IS (50) corrected point load test, UCS- Uniaxial compressive strength of intact rocks				

5.2.2 Density and Unit Weight of the Rocks

In slope stability studies, one of the input parameters is the unit weight of the rock. In this work, the density of rock was evaluated utilizing buoyancy techniques for irregular rock samples following an ISRM (1978) standard using equation 3.11. As a result, representative rock samples were obtained from the three critical rock slope sections of the study area, and their corresponding unit weight was calculated. Dry unit weights range from 23.51 to 25.13 KN/m^3, whereas saturated unit weights range from 25.5 to 26.88 KN/m^3.

Table 5. 7 Dry and saturated unit weights of rocks from laboratory tests

Sample ID	Rock units	γd (KN/m^3)	γsat (kN/m^3)
RSS3	Granite	24.27	26.35
RSS4	Basalt	25.13	26.88
RSS5	Rhyolite	23.51.	25.5
RSS=Rock slope section γd=Dry unit weight γsat=Saturated unit weight			

5.3. Rock Mass Strength and Deformation Parameters

5.3.1 Determination of Rock mass Shear Strength Parameters

The shear strength of a rock mass is calculated using the Rocdata software's generalized Hoek-Brown strength criterion in terms of major and minor principal stresses.

Based on the Hoek Browen, the equivalent Mohr-Coulomb shear strength parameters(c and ϕ)were calculated using the Rocdata program (RocData, 2004).

The input parameters of Rocdata software

- ✓ Geological Strength Index (GSI),
- ✓ Uniaxial Compressive Strength of Intact Rocks (UCS)
- ✓ The material constant of intact rock (mi),
- ✓ Unit weight of rocks (γ),
- ✓ Slope height, and
- ✓ Disturbance factor (D).

The field value of GSI was estimated in this study. The UCS can be calculated by measuring the point load strength index on irregular samples from the laboratory experiments listed in Table 5.3. The material constant of unbroken rock (mi) was extracted from the supplied data and was already pre-programmed into the rock data software Rocscience (2004). The unit weight of rocks (γ) was utilized in the analysis, which was obtained in the laboratory using buoyancy techniques as shown in Table 5.6. In the field, The slope height can be estimated by measuring the tape meter and the disturbance factor (D) is a factor that depends on how much the rock mass has been disturbed by blast damage and stress reduction. It varies from zero for undisturbed in situ rock masses to highly disturbed rock masses. Furthermore, the disturbance factor (D) for blasted rock slopes is in the range of 0.7 to 1.0. The D value used in this study ranged from 0.7 to 1, which is already provided in the Rocdata software.

Table 5. 8 Input parameters for determining the shear strength of rock for determining the shear strength of rock

Input for Rocdata	RSS3	RSS4	RSS5
UCS, (Mpa)	139.2	95	148
GSI	65	55	20
Mi	32	25	25
D	0.7	1	1
γ (KN/m3)	24.27	25.13	23.5
H (m)	15	20	22
Rock type	Granite	Basalt	Rhyolite
RSS = Slope sections, UCS, = Uniaxial compressive strength of intact rocks, GSI = Geological strength index, mi = Rock material constant, D = disturbance factor, γ = is the unit weight of rocks, and H = height of the slope.			

5.3.2. Determination of Rock Mass Deformation Parameters

The deformation modulus and strength of the rock mass are needed inputs for numerical models in this study to evaluate the rock slope stability analysis. Furthermore, Poisson's ratio (vrm) and intact modulus (Ei) are two of the most important rock characteristics used in the numerical modeling of rock slopes. Rocdata software was used to calculate the modulus of deformation of rocks (Rocscience,2004 rocdata,3).According to (Balázs & Takács,2018) the Poisson's ratio of the rock mass (vrm) was determined from equation 4.2 using the relationship between the Poisson's ratio, the geological strength index (GSI), and the material constant (mi). Table 5.6 provides detailed information on the deformation parameters of the nonstructural controlled rock mass at important rock slope sections in the study area.

Table 5. 9 Summary of the deformation parameters of the rock mass in the study area

Slope sections	Rock units	Cohesion (Mpa)	Friction angle (ϕ)	Deformation modulus, Em (Mpa)	Poisson's ratio(V)
Slope section	Rhyolite	0.097	36.89	889.14	0.3

5.4. Engineering Properties of Soils

Soil engineering properties are used to correlate, categorize, and characterize the soil, as well as provide input parameters for slope stability analysis at important slope sections of the study area. Grain size analyses, Atterberg limit tests, natural moisture contents, specific gravity tests, density and unit weight, compaction tests, and shear strength tests were performed on soil samples obtained during the field study. These tests were carried out on a representative soil sample taken from the research area along the road section. Each parameter will be discussed as follows:

5.4.1 Grain Size Analysis

The percentage of different particle sizes in the soil that composes the critical soil slope located along the road was determined using grain size analysis. The laboratory test was performed on two disturbed soil samples obtained from the field test pits.Depending on the particle size of the soil, this test was conducted using mechanical sieve analysis and hydrometer analysis. For particle sizes higher than 0.075mm diameter (No. 200 Sieve), mechanical sieve analysis was utilized, and hydrometer analyses were used for particle sizes smaller than 0.075mm diameter (No. 200 Sieve). The particle size diameter vs. % finer (particle size distribution curve) was plotted for each soil sample based on the particle size analysis results, as illustrated in Fig. 5.1. The soil in the study area's critical slope sections was classified as low and high plasticity silt, respectively, based on grain size analysis results at SS1 and SS2. Table 5.7 shows a summary of the percentage of soil particles in each sample.

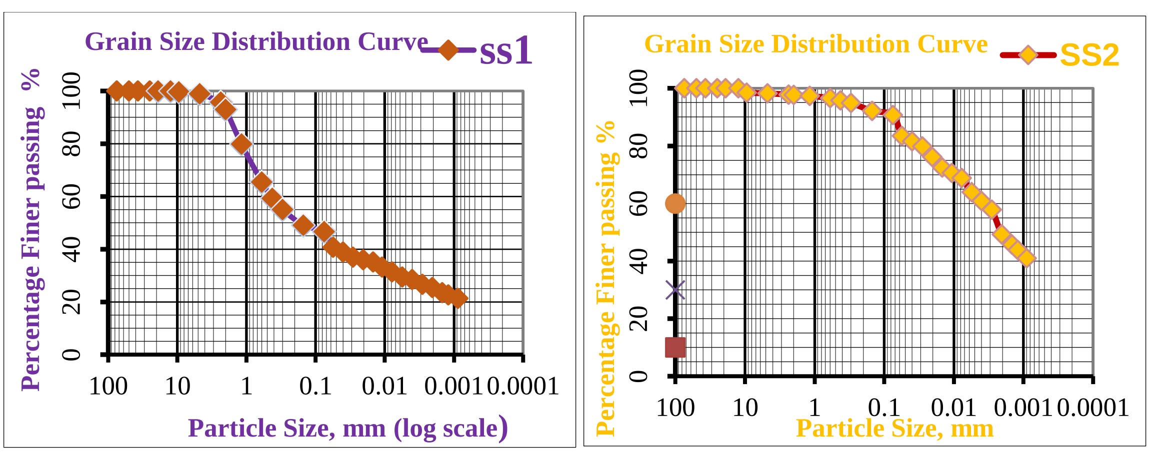

Figure 5. 1: Particle size distribution curve from sieve and Hydrometer test at SS1 and SS2

5.4.2 Atterberg Limit Test

The ASTM D 4318 (1998) standard procedure and the Casagrande technique were used to perform the Atterberg limit test on soil samples from the critical slope sections. This test is used to determine fine-grained soil liquid limit, plastic limit, and plasticity index, as well as to categorize soil using the Unified Soil Classification System (Ramana, 1993). The liquid limit test was used to assess how much water was necessary for the soils to lose their cohesiveness and flow like liquid. Figure 5.3 is from the liquid limit determination chart. This test consists of 25 blows. A plastic limit test was performed to assess how much water was necessary for the soil to crumble. Furthermore, the plasticity index was calculated using liquid and plastic limits (Table 5.10) to establish the range of the soils in the research area.

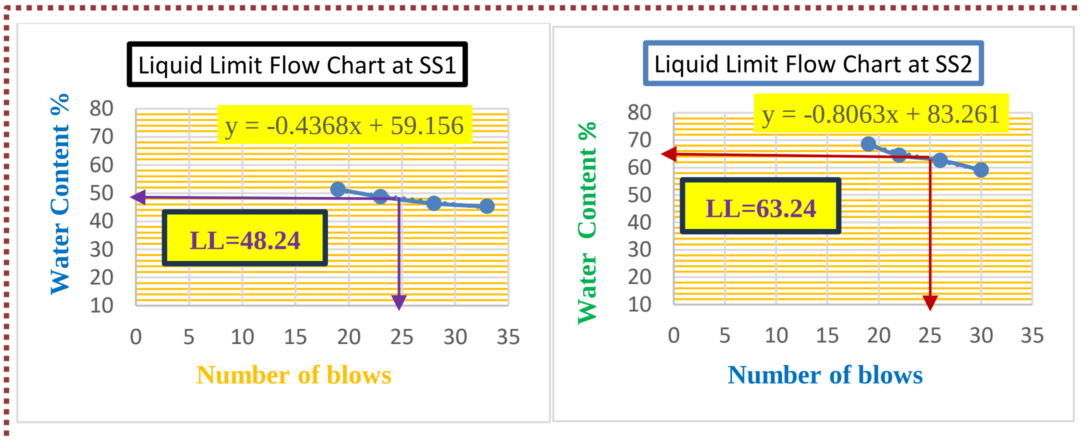

Figure 5. 2 Liquid limit chart of the critical soil slopes at SS1 and SS2

Table 5. 10 Atterberg limit tests and plasticity index result of soil at critical slope sections

Slope sections	Depth (m)	Sample type	Atterberg limit tests			Plasticity Class according to Das, (2002)
			LL%	PL%	PI%	
SS1	1	Disturbed	48.24	39.49	8.74	Low plasticity
SS2	1.5	Disturbed	63.24	43.2	19.9	High plasticity
SS = Soil slope section, LL = Liquid limit, PL = plastic limits, PI= Plasticity index						

5.4.3 Natural Moisture Contents

The in-situ water content of soils determined using freshly excavated soil samples before exposing them to air is known as natural moisture content (w). According to ASTM D 2216 (1998), samples were taken from two critical slope sections.

5.4.4 Specific Gravity of Soils

A pycnometer and distilled water at a certain temperature were used to determine the specific gravity of soils in a designated slope section of the study area. The specific gravity of the soil can be determined for each sample using the ASTM D 854 (1998) standard.

Soil specific gravity ranged from 2.62 to 2.70 at selected slope sections in the research area (Table 5.8).ranged from 2.6 to 2.7 at selected slope sections in the research area (Table 5.8).

Table 5. 11 Specific gravity and Natural moisture content of the soil slope sections

Slope section	Depth of sample (m)	Natural Moisture Content	Specific Gravity (Gs)
SS1	1	13.7	2.7
SS2	1.5	32.6	2.6

5.4.5 Unit Weight of Soils

The saturated and dry unit weights of the soil at the critical slope section were calculated using laboratory test results from field soil samples. This test is carried out on two soil samples taken at various depth intervals in the study area. The unit weight was used as an input parameter in the slope stability analysis of the soil slope sections for this investigation.

5.4.6 Standard Compaction Tests

The Standard Proctor Compaction Test is used to assess the relationship between a specific soil sample's moisture content and dry density at a certain compaction effort. Using a standard proctor test, two soil samples were taken from the study area's critical slope areas. Based on the compaction test findings, the maximum dry density (MDD) and optimum moisture content (OMC) of the soil utilized to remold the soil for the shear strength test were calculated.

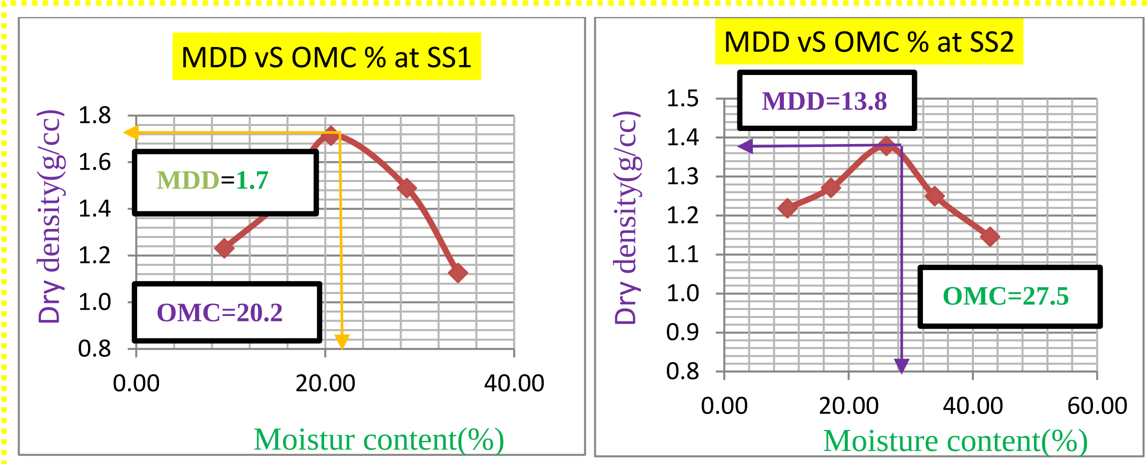

Figure 5. 3: Compaction curves of the soil critical soil slope section of the study area at SS1and SS2

5.4.7 Direct Shear Strength Tests

The direct shear test is one of the most common soil strength tests used to establish shear strength parameters for slope stability analysis. The shear strength characteristics, such as cohesion and angle of internal friction, of the selected critical soil slope section were obtained using direct shear testing in this study, as shown in Table 5.9 The direct shear test results that the internal friction angles of soil slope sections one (SS1) and two (SS2) are 10.07 ^{o} and 15.6 ^{o}, respectively.While the soil cohesiveness in slope sections one (SS1) and two (SS2) was found to be 17 KN/m^2 and 21 KN/m^2, respectively (Fig. 5.5),

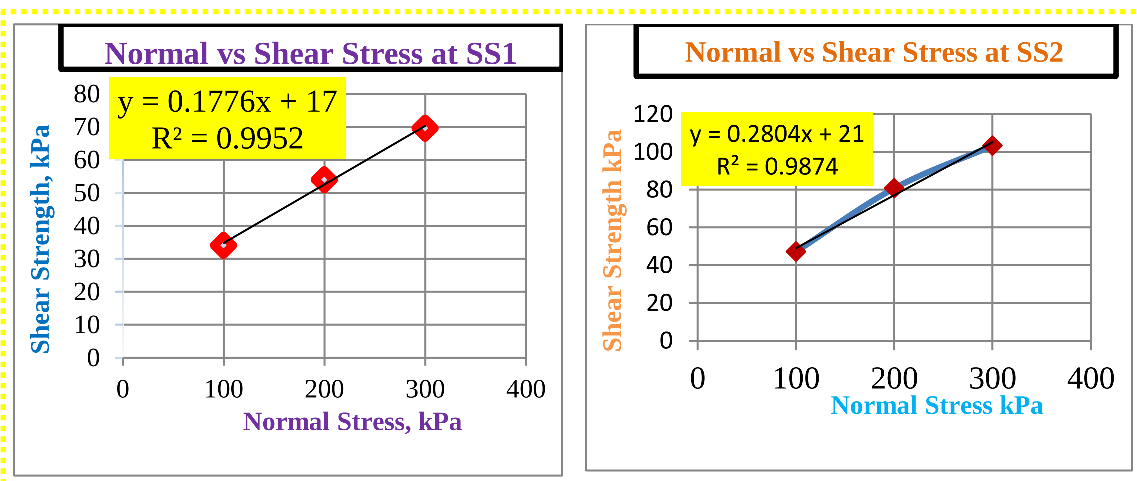

Figure 5.4 Shear stress vs Normal stress of soil at SS1 and SS2

Table 5. 12 Shear strength parameters of soils for the soil slope section at SS1 and SS2

Slope sections	Soil description	Shear strength parameter	
		Cohesion, (C) Kpa	The angle of internal friction (ϕ)
SS1	Low plasticity silt	17	10.07
SS2	High plasticity silt	21	15.66

5.5 Classification of Soils based on the Unified Soil Classification (USC) System and AASHTO classification system

The detailed result and the UCS and AASHTO classification of the soils for the study area are presented in (Table 5.10).

Table 5. 13: Classifications of Soils based on the USC and AASHTO Classification System

Slope sections	Atterberg limit			USC soil section	AASHTO		
	LL %	PL %	PI %		Classification	Group classification	Plasticity chart
SS1	48	40	9	Low plasticity silt	Silt-clay materials	A-5	High plasticity silt
SS2	63	43	20	High plasticity silt	Silt-clay materials	A-7-5	High plasticity silt

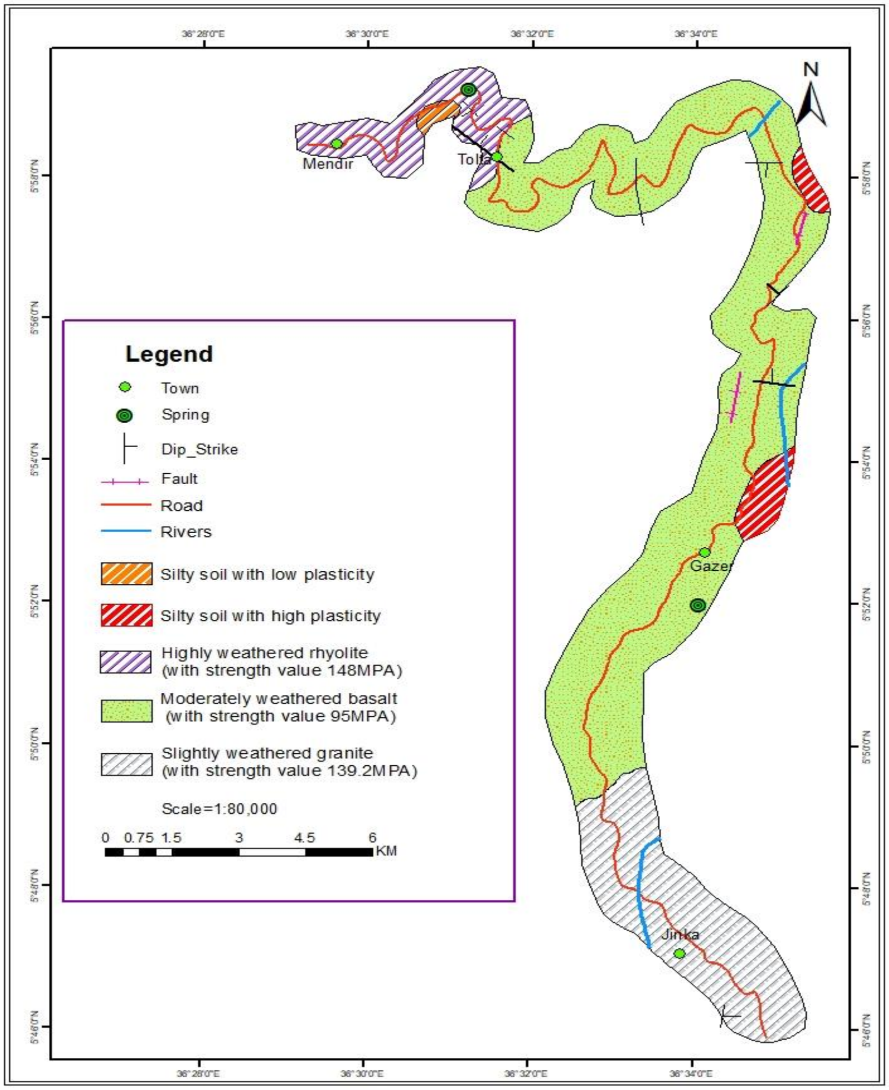

Figure 5. 5: Engineering geological map along the road section of the study area

5.6. Stability Analysis of Rock Slopes (Structural Control)

The stability of rock slopes in the study area was analyzed using kinematic, limit equilibrium, deterministic, and finite element methods.

5.6.1 Kinematic Slope Stability Analysis

The kinematic analysis for this study was performed using Dips 6 software (Rocscience, 2004). to examine several slope failure mechanisms such as planar, wedge, and toppling (Fig. 5.6). The data for the rock slope discontinuity was processed using Dip's software, which needed the orientation of the discontinuities (dip and dip direction of joints), the slope face orientation (dip and dip direction of slope), and the friction angle (Khanna & Dubey, 2021).

The dip and dip direction of joints, as well as the slope face orientation, were measured in the field, but the friction angle along the failure plane was calculated using Rocdata software.

Table 5.14 Input parameters used in Dips software for kinematic analysis.

Slope sections	Slope face orientation	Joint set orientations (Dip and Dip direction)			
	Slope D/DD, (º)	JS1,(º)	JS2,(º)	JS3,(º)	Friction cone (º)
RSS-3	75/173	68/173	50 /167	77/232	36
RSS-4	85/332	76/250	61/320	70/230	40

During the field survey, the orientations of various joint sets were projected on a lower hemisphere net using a contoured stereographic projection to identify the various pole concentrations (Fig. 5.8). The incline of the planar mode of failure occurred at the critical rock slope area of RSS3 and RSS4. The research found that planar failure, which may be situated at the RSS3, was vulnerable to planar failure due to discontinuity sets JS1 and JS2, in which the pole of the joint set fails inside the critical zone of planar failure.

In the same way, the pole of joint set two (PJS2) was plotted within the critical zone of the planar mode of failure at slope section RSS4 (Fig. 5.7). This demonstrated that the planar failure at slope section RSS4 was caused by joint set JS2. Table 5.16 provides a detailed summary of the possible modes of failure at the critical slope section, as well as the joint set accountable for mode failure. Finally, the stability analysis of one type of failure was performed using a deterministic method to calculate the factor of safety.

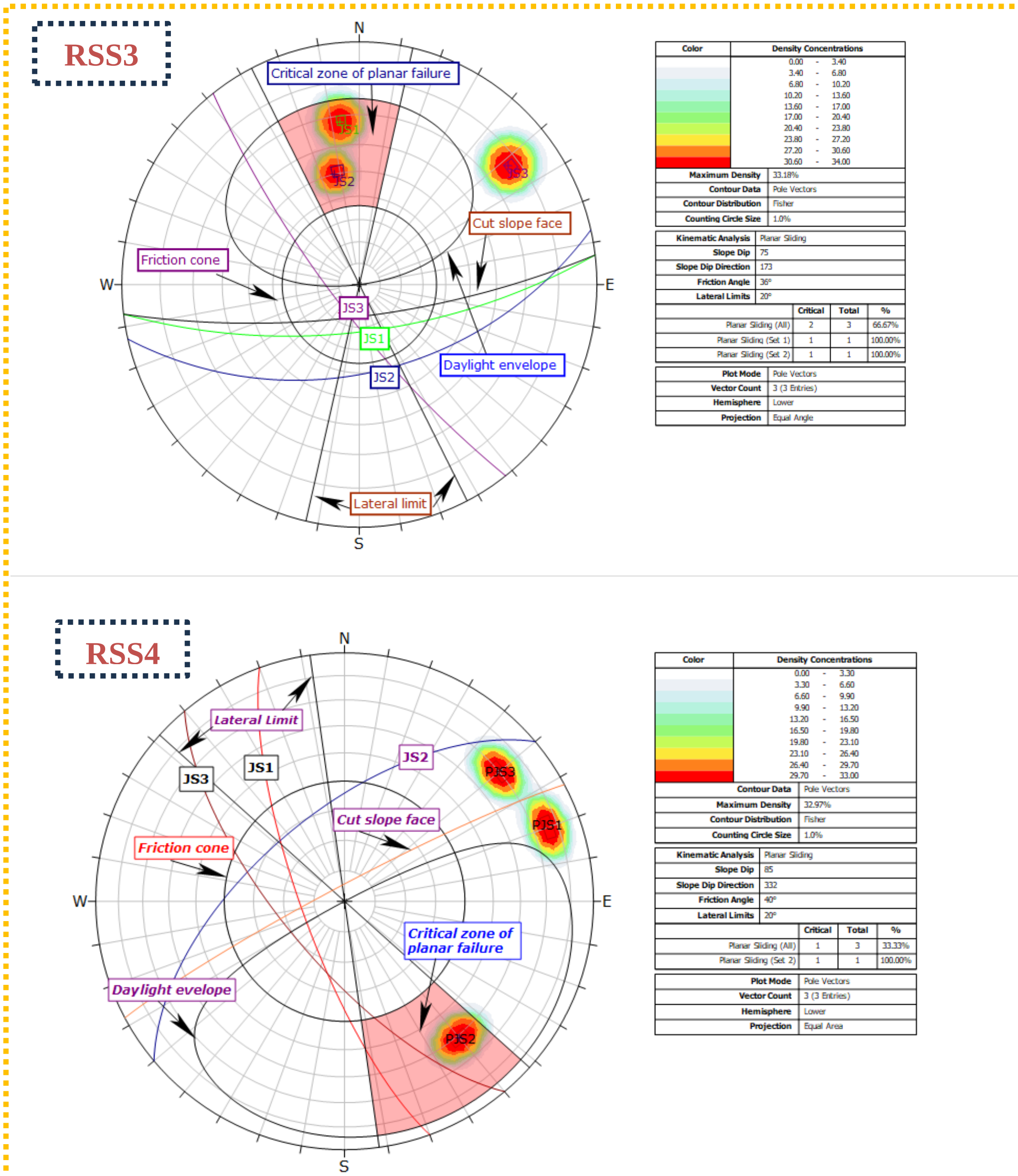

Figure 5.6: Kinematic analyses for planar modes of rock slope failure

Table 5. 15 Mode of failures from kinematic analysis of rock slope sections

Slope sections	Mode of failure from kinematic analysis rock slope sections
RSS3	Planar failure due to joint set JS1 and JS2
RSS4	Planar failure due to joint set JS2

5.6.2 Rock Slope Stability Analysis Using LEM

According to the results of the kinematic study (Fig.5.6), probable planar rock slope failure occurs at slope sections RSS3 and RSS4.

Rocplane was used to analyze the factory safety The software was used to examine and interpret the factor of safety for the structurally controlled critical rock slope when it was static dry, static saturated, dynamic dry, and dynamic saturated. Shear strength parameters (cohesion and friction angle) of rock mass were obtained from Barton-Bandis failure criteria for the two structurally controlled critical selected rock slope sections using Rocdata software (Rocscience 2004, Rocdata, 3), and the unit weight of rock was obtained from laboratory tests and summarised in Table 5.6. External loads such as horizontal seismic acceleration and groundwater conditions were also taken into account during the stability analysis.

The kinematic analysis results in Fig. 5.6 revealed that planar modes of failure occurred at rock slope sections RSS3 and RSS4 due to joint sets JS1 (PJ1) and JS2 (PJ2) and JS2, respectively. Deterministic analysis was used to construct the three-dimensional and side-view graphs of the rock slope using the RocPlane software(Sadagah, 2014). As a result, the factor of safety (FOS) for the planar mode of failure was calculated with the RocPlane software (Rocscience, 2004). The Rocplane software uses slope geometry, discontinuity set orientation, shear strength parameters (cohesion and angle of internal friction), and rock unit weight to calculate the factor of safety. Table 5.13 summarises the input parameters used in RocPlane software to determine FOS for critical rock slope sections with a planar mode of failure

Table 5. 16 input parameters used in Rocplnae software for the planar mode of failure

Slope section	Input parameters for RocPlane V. 2.0										
	JS	Slope geometry						Strength		Force	
		Sa $(^0)$	Sh (m)	γ (t/m^3) d/s	Fpa $(^0)$	W $(^0)$	USA $(^0)$	C (t/m^2)	$\Phi(^0)$	γw (t/m^3)	αs
RSS3	JS1	75	15	2.47/2.69	68	15	8	1.6	36.37	1	0.07
	JS2	75	15	2.47/2.69	50	15	8	2.1	38.16	1	0.07
RSS4	JS2	85	20	2.56/2.74	61	8	10	5.4	43.02	1	0.07

JS= Joint set, Sa= slope angle, Sh= slope height, γ= unit weight, Fpa= failure plane angle, W= waviness, USA=upper face angle, c= cohesion, Φ= friction angle, γw= unit weight of water,s=saturated, d=dry αs = seismic coefficient.

Planar failure modeling in Figs. 5.7, 5.8, and 5.9 indicated that due to the existence of JS1 and JS2, planar failures are possible at the rock slope section RSS3. The RocPlane software (Rocscience, 2004) was used to perform a factor of safety analysis on both JS1 and JS2 on rock slope section RSS3 (Figs. 5.8 and 5.9).As a result of the investigation, the FOS at the static and dynamic saturated condition rock slope section RSS3 for both joint set 1 (JS1) and joint set 2 (JS2) is less than one. A slope that had a factor of safety of less than one was unstable, according to a slope stability study(Christian, 2004);(Shariati & Fereidooni, 2021). As a result of the investigation, the FOS at the static and dynamic saturated condition rock slope section RSS4 for joint set 2 (JS2) is less than one. As demonstrated in Figs. 5.9 slope section RSS4 was stable under static dry, dynamic dry, and unstable in static saturated, and dynamic saturated circumstances.

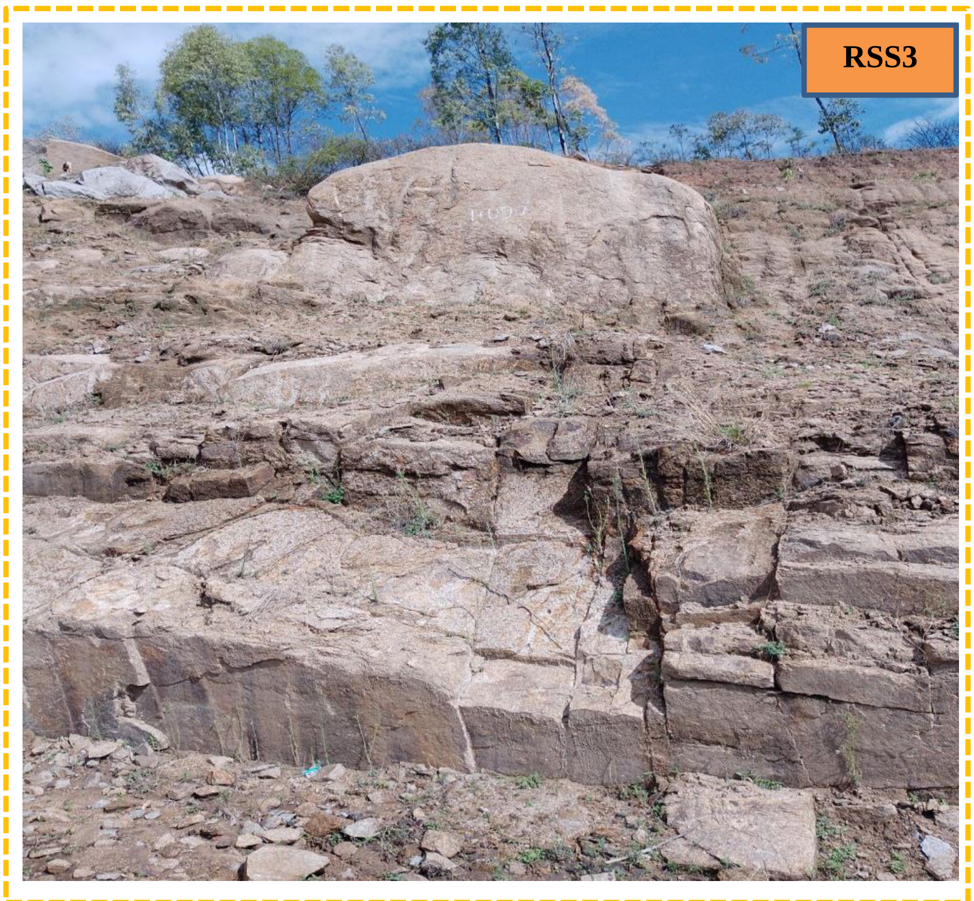

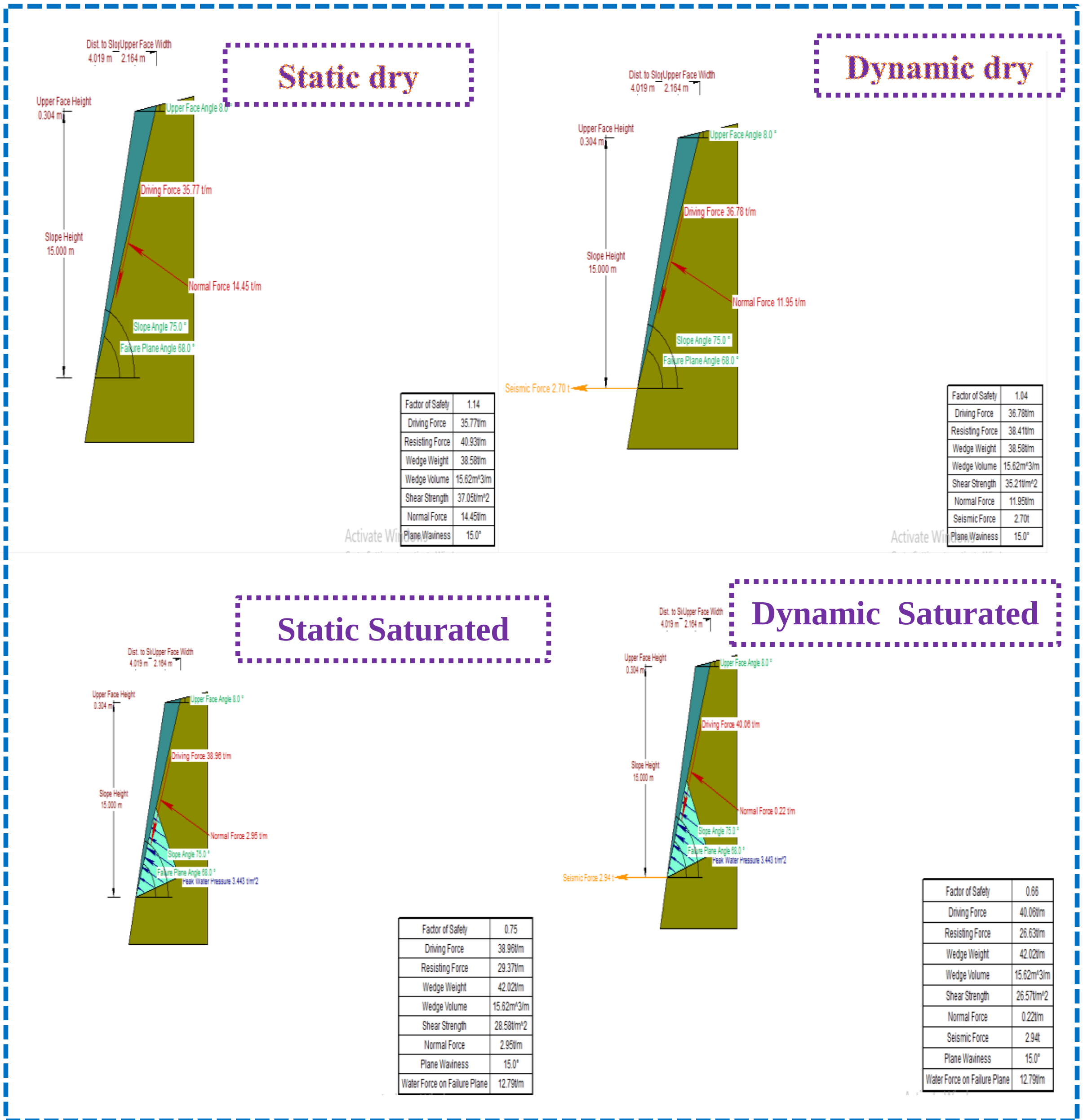

Figure 5.7: Slope stability analysis RocPlane software the planar failure rock slope section three (RSS3) forces acting on failure plane JS1 at different conditions.

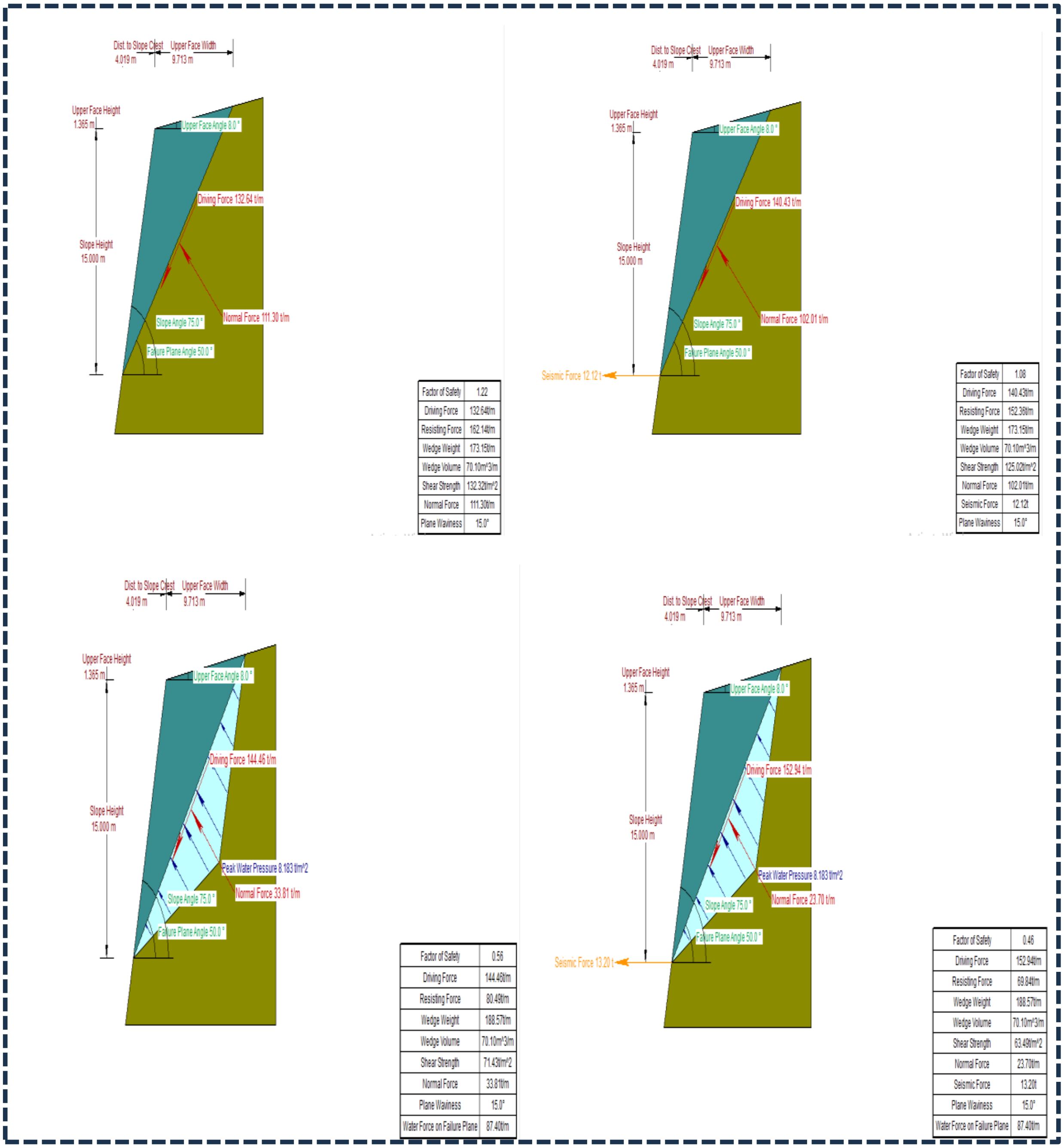

Figure 5. 8: Slope stability analysis RocPlane software the planar failure rock slope section RSS3, forces acting on failure plane JS2 at different conditions.

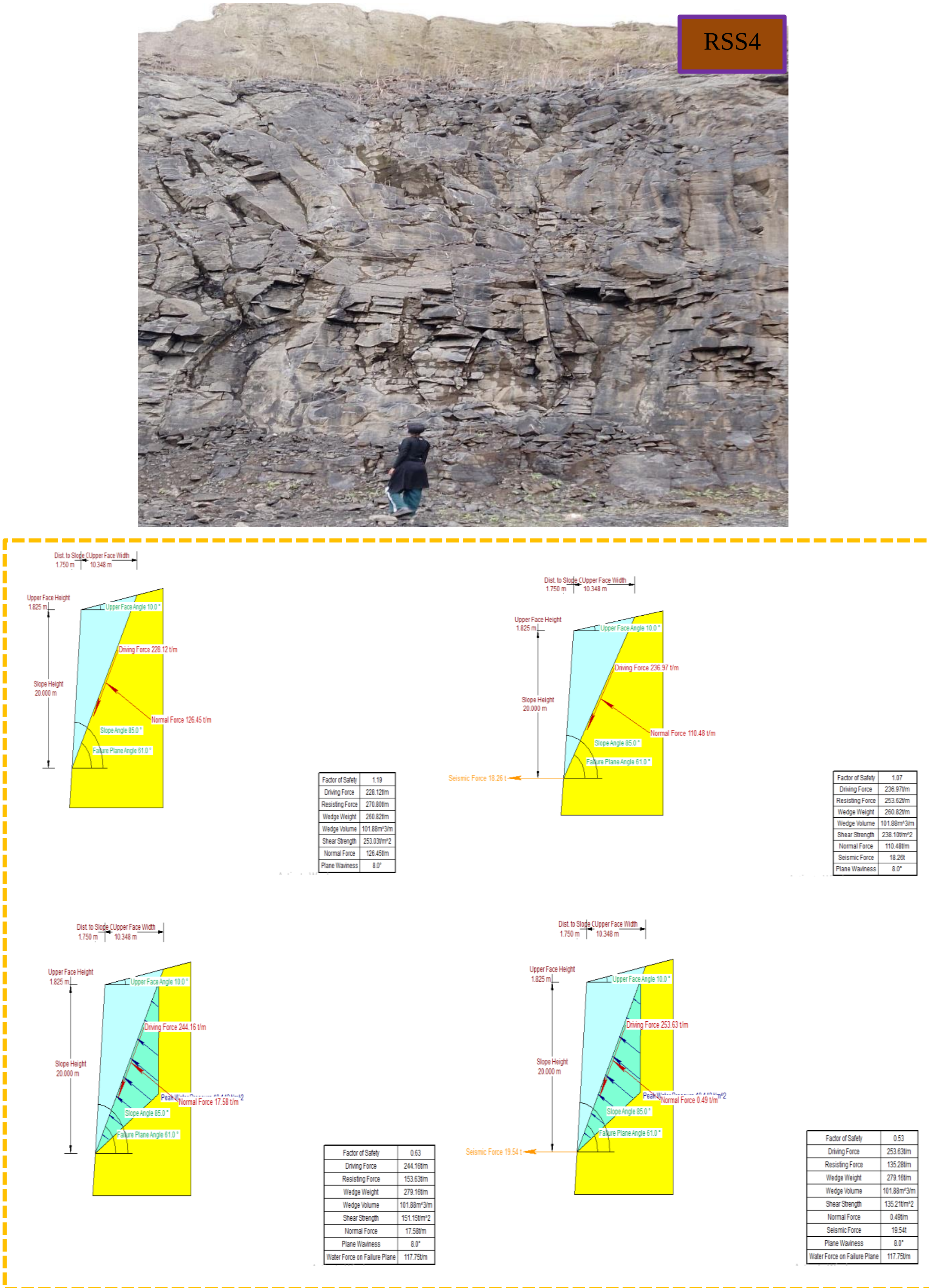

Figure 5.9: Slope stability analysis RocPlane software the planar failure rock slope section RSS4, forces acting on failure plane JS2 at different conditions

Table 5. 17 Factors of safety and slope status under different conditions for planar rock failurr failure.

Slope sections	Joint set	The factor of safety planar formed in rock slope section RSS3 and RSS4 at different conditions			
		Static dry (FOS)	Static saturated (FOS)	Dynamic dry (FOS)	Dynamic saturated (FOS)
RSS3	JS1	1.14	0.75	1.04	0.66
	JS2	1.22	0.56	1.08	0.46
	Stability condition	Stable	Unstable	Stable	Unstable
RSS4	JS2	1.19	0.63	1.07	0.53
	Stability condition	Stable	Unstable	Stable	Unstable

5.7 Stability analysis of Soil and Highly weathered Rock (Non-Structural Controlled)

5.7.1 Rock Slope Stability Analysis Using Limit Equilibrium Method

Slope stability analysis of one critical slope section was undertaken for this study utilizing the limit equilibrium approach in terms of the factor of safety (FOS) using the General Limit Equilibrium (GLEM) or Morgenstern-Price method. The stability of a single critical slope section was assessed by calculating the factor of safety under various scenarios. The investigation was carried out with the use of slide software((Rocscience 2004, slide 6) and the Mohr-Coulomb model.

Material characteristics such as cohesiveness, angle of internal friction, and rock unit weight are employed as input parameters in this software. For this study, shear strength parameters (cohesion and friction angle) of rock mass were obtained from Hoek-Brown failure criteria using Rocdata software (Rocscience 2004, Rocdata3), and the unit weight of rock was obtained from laboratory tests, as shown in Table 5.6. Furthermore, during the stability analysis, external loads such as horizontal seismic acceleration and groundwater conditions were included. The study location is located in a high seismic zone, and for dynamic dry and dynamic saturated conditions, the horizontal acceleration from seismic loading with a magnitude average (α) of 0.07g (Asfaw, 1986) was employed.

Table 5. 18 Input parameters for limit equilibrium slope stability analysis of rocks

Slope sections	Material	Strength model	Input parameters				Seismic horizontal acceleration (α) g
			Cohesion (Mpa)	friction angle, (º)	Unit weight (KN/m3)		
					Γdry	Γsat	
RSS5	Rhyolite	Mohr-coulomb	0.097	36.89	23.51	25.5	0.07

The slope stability Analysis factor safety for non-Structurally Controlled critical selected one rock Slope Sections were determined using slide software through the Mohr-Coulomb model evaluated as follows

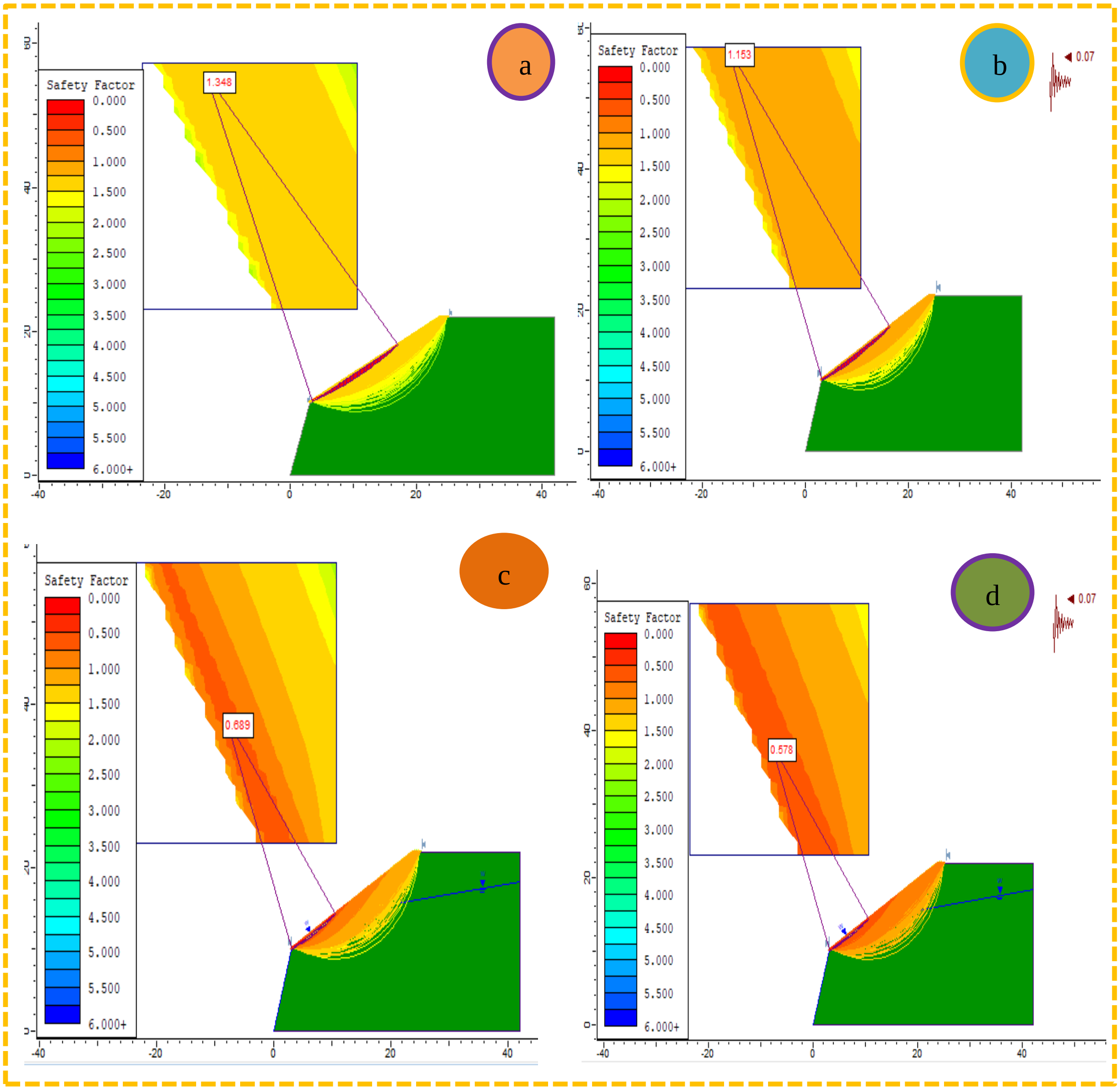

Figure 5.10: Slope stability analysis result using Limit equilibrium method for rock slope section RSS5 under a) static dry condition, b) Dynamic dry condition, c) Static saturated condition, and d) dynamic saturated conditions.

Based on the results of the previous study, the minimum factor of safety and critical slip surface of the rock at critical slope section RSS5 are estimated using general limit equilibrium methods while taking into account various variables, as shown in Figure 5.10. As a consequence of the analytical results at the critical rock slope section RSS5, the factor of safety under static dry and dynamic dry conditions is 1.348 and 1.153, respectively, as illustrated in Figs. 5.10 (a) and (b).

As demonstrated in (c) and (d), the factory of safety in static saturated and dynamic saturated situations is 0.689 and 0.578, respectively. This suggested that the rocks at the RSS5 critical slope section were unstable under static and dynamic saturated conditions.

Table 5. 19 Summary of the minimum factor of safety and slope status for the RSS5 section

Slope sections	Method	Loading condition	Factor of safety	Slope stability condition
RSS5	GLEM/ Morgenstern-price method	Static dry	1.348	Stable
		Static saturated	0.689	Unstable
		Dynamic dry	1.153	Stable
		Dynamic saturated	0.578	Unstable

5.7.2 Rock Slope Stability Analysis Using Finite Element Method

The finite element approach was used to analyze the rock slope stability of critical selected slope sections for this investigation. The Phase2 software (Rocscience 2004, Phase2) was used for the finite element analysis, and the slope stability condition can be represented in terms of the Strength Reduction Factor (SRF) value. The critical shear strength reduction factor (SRF), which is equivalent to the factor of safety (FOS), was determined in the Phase2 software program using a finite-element-based numerical simulation (Bushira et al., 2018). Limit equilibrium and finite element methods were used to determine the critical rock-selected slope section, the factory of safety, for this investigation, utilizing the same material parameters, slope angle, slope geometry, and boundary condition. Furthermore, except for Young's modulus (Erm), Poisson's ratio (v), and the dilatancy angle of the rocks, the input parameters utilized in this approach are the same as those used in the limit equilibrium method.

The Young's modulus (Erm) of rock mass was computed in this work using Rocdata software according to Hoek (2006), and the Poisson ratio (v) of rock slope materials was determined using appropriate literature(Balázs,2018). This study used a finite element slope stability analysis to estimate the critical strength reduction factor, or FOS, of the rock slope's static dry, static saturated, dynamic dry, and dynamic saturated conditions. The critical strength reduction factor (SRF) of a non-structurally controlled one critical rock slope section was computed using phase 2 software and the Mohr-Coulomb model, as illustrated in Fig. 5.11.

Table 5. 20 Input parameters for finite element stability analysis to compute critical strength reduction factor

Slope section	Material	Strength model	C (Mpa)	ϕ,(º)	Erm (Mpa)	Ψ(º)	Unit weight (KN/m^3)		V	α (g)
							γdry	γsat		
RSS5	Rhyolite	Mohr-coulomb	0.097 MPA	36.89	889.14 MPA	6.89	23.51	25.5	0.3	0.07

RSS = Rock slope section, C = cohesion, ϕ = angle of internal friction, Erm= deformation modulus, γ = Unit weight of rocks, V = Poisson ratio and α = seismic horizontal acceleration, Ψ = Dilatancy angle of rocks

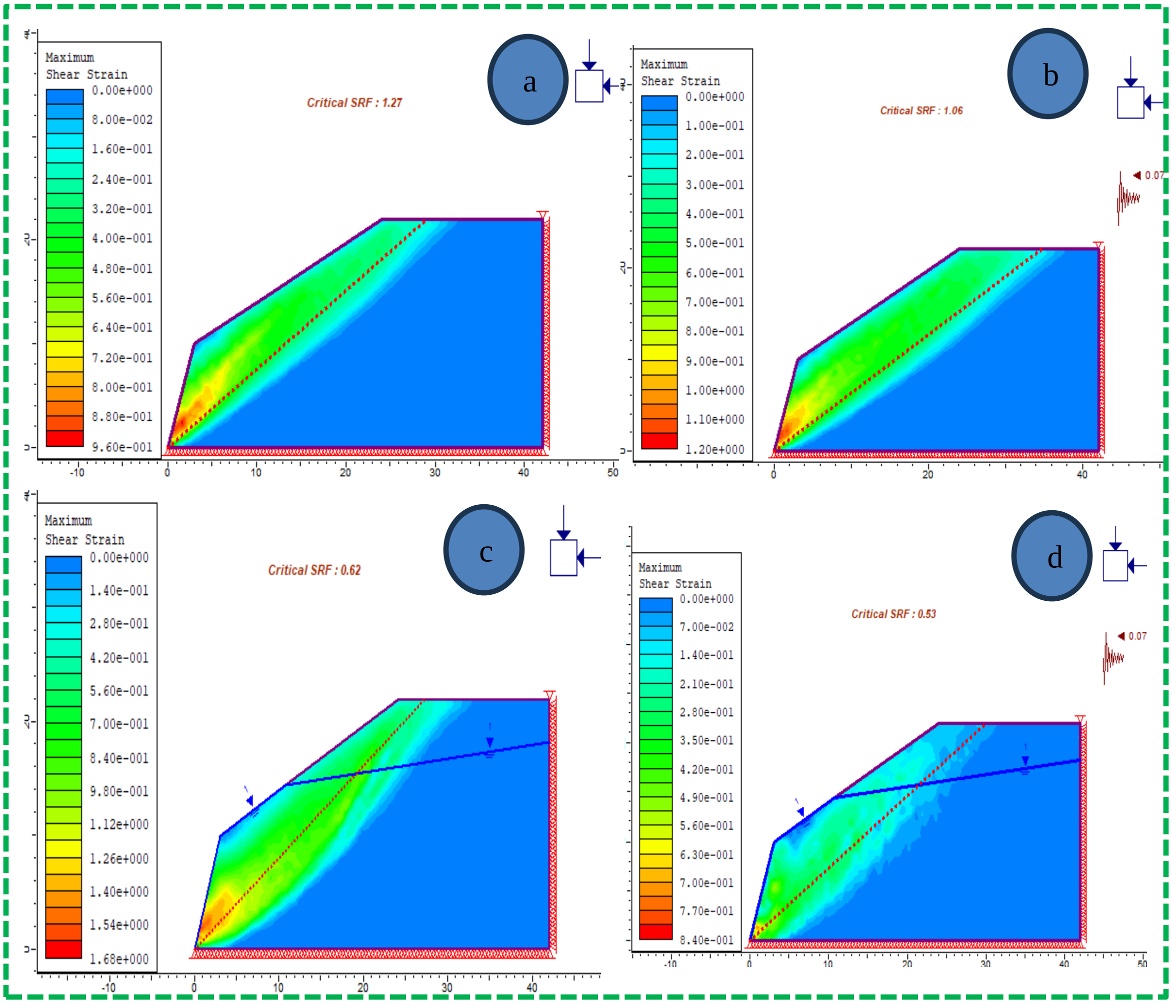

Figure 5. 11: Slope stability analysis finite element method for rock slope section RSS5 under a) static dry condition b) Dynamic dry condition c) Static saturated condition and d) dynamic saturated condition.

The strength reduction factor of the rock slope section RSS5 is 1.27 and 1.06 under static dry and dynamic dry circumstances, respectively, as illustrated in Figs. 5.11 (a) and (b). However, as demonstrated in (c) and (d), the rock slope section (RSS5) strength reduction factor is 0.62 under static saturated conditions and 0.53 under dynamic saturated conditions. According to the findings, the critical SRF or FOS at static dry, and dynamic dry will be stable, and under static,dynamic saturated will be unstable(Christian, 2004; Shariati & Fereidooni, 2021).According to the result, There is a chance that the slope will collapse due to triggering events such as heavy rain and seismic activity.

Table 5. 21 Critical SRF and slope stability under different conditions of rock slope section

Slope sections	Method	Loading condition	Strength reduction factor (SRF)	Slope stability condition
RSS5	GLEM/ Morgenstern-price method	Static dry	1.27	Satble
		Static saturated	0.62	Unstable
		Dynamic dry	1.06	Stable
		Dynamic saturated	0.53	Unstable
	GLEM = General Limit Equilibrium Method			

5.7.3 Slope Stability Analysis of Soils Using Limit Equilibrium Method

The general limit equilibrium (GLE) or Morgenstern-Price approach was used to examine the slope stability of two soil slope sections. Determining the critical potential slip surface in slope stability analysis using General Limit Equilibrium (GLE) or the Morgenstern-Price method using Rocscience slide software is an essential measure for obtaining a minimum factor of safety in each slope section(Abramson et al., 2001; Singh et al., 2016). Furthermore, the general limit equilibrium approaches in the Rocscience Slide software satisfy all of the equilibrium conditions. The finite element approach and limit equilibrium were used in this work to assess the stability of two important selected soil slope sections along the road that were identified and observed in the field. According to the results of the soil slope laboratory test, SS1 is low plasticity silt and SS2 is high plasticity silt. Soil slope stability analysis requires the measurement of slope geometry, shear strength parameters (angle of internal friction and cohesion), and soil unit weight. Laboratory experiments are used to establish the internal friction angle, cohesiveness, and unit weight of the soils on slopes SS1 and SS2, which are summarised in Table 5.19.

The General Limit Equilibrium Methods (GLEM) were employed in this study to calculate the factor of safety for two distinct slope sections with different geometry and material properties under static dry, static saturated, dynamic dry, and dynamic saturated slope situations.

Table 5. 22 The input parameter for soil slope stability analysis

Slope sections	Material	Unit weight (KN/m3)		Cohesions (KN/m^2)	The angle of internal friction (degree)
		γdry	γsat		
SS1	Low plasticity silt	11.01	14.56	17 kpa	10.07
SS2	High plasticity silt	15.36	17.30	21 kpa	15.66
SS = soil slope section, γdry = dry unit weight, and γsat = saturated unit weight of soils.					

For this study, the factor of safety (FOS) and slip surface were determined and interpreted using the General Limit Equilibrium or Morgenstern-Price LEM methods for static dry, static saturated, dynamic dry, and dynamic saturated conditions using the above input parameters in Table 5.19. The safety factor evaluation was carried out in static dry conditions, representing the stability state without taking a seismic load into account.Furthermore, the safety factor evaluation was carried out under dynamic saturated conditions, which implies that the slope was subjected to seismic horizontal acceleration (= 0.07 g) in the study area and was assumed to be saturated under heavy rains (Lamessa & Meten, 2021b).

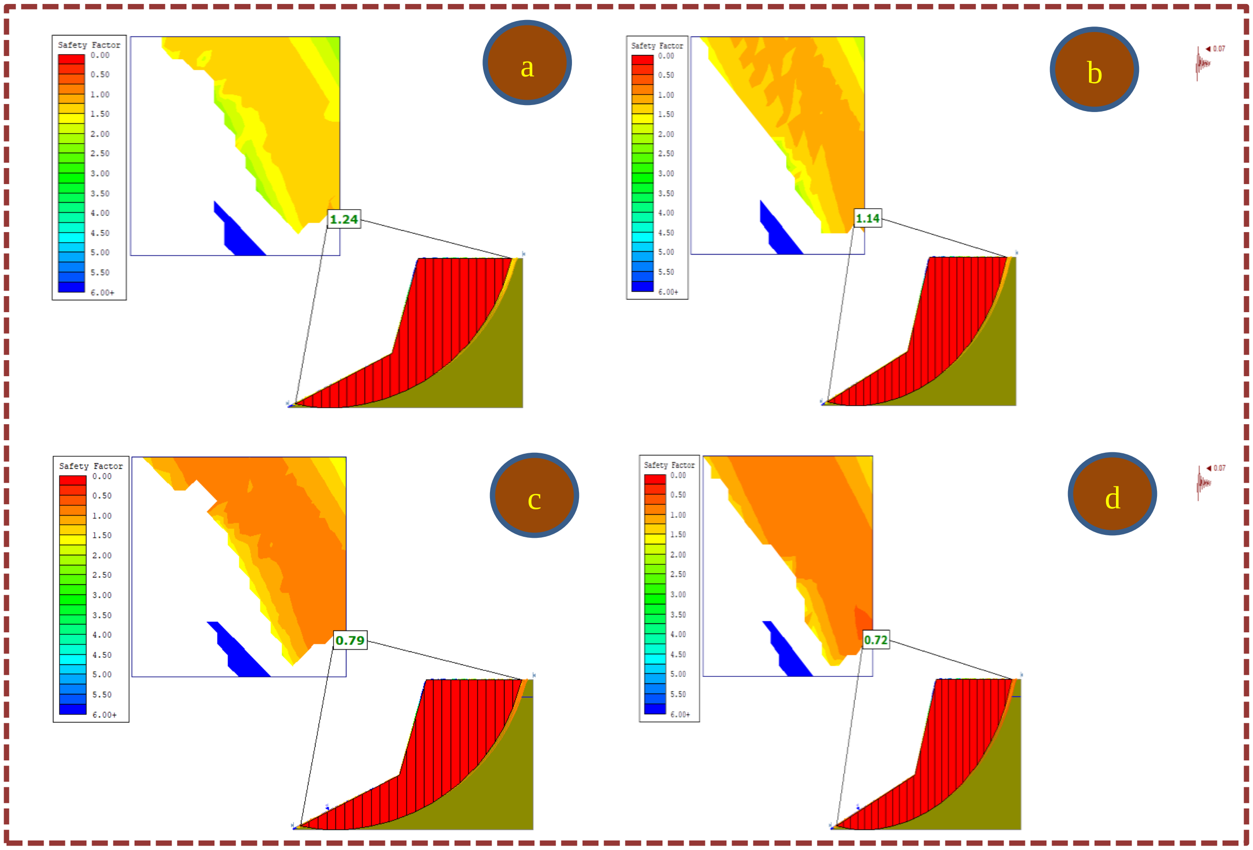

Figure 5.12 Slope stability analysis Limit equilibrium method for soil slope section SS1 at a) static dry, b) dynamic dry, c) static saturated, and d) dynamic saturated conditions

According to the above analysis, slope section SS1 has a factor of safety of 1.24 and 1.14 in static and dynamic dry conditions, respectively (Fig. 5.12 a and b). The findings revealed that the soil slope section SS1 is stable under both static and dynamic drying conditions. However, the factor of safety found for the slope section SS1 under static saturated and dynamic saturated circumstances is 0.79 and 0.72 (Fig. 5.12 c and d, respectively). The slope will be unstable under static and dynamic saturated conditions this implies that slope stability can be influenced by groundwater by raising pore water pressure, increasing weight on a slope when the soil mass is fully saturated, decreasing effective stress, and losing shear.

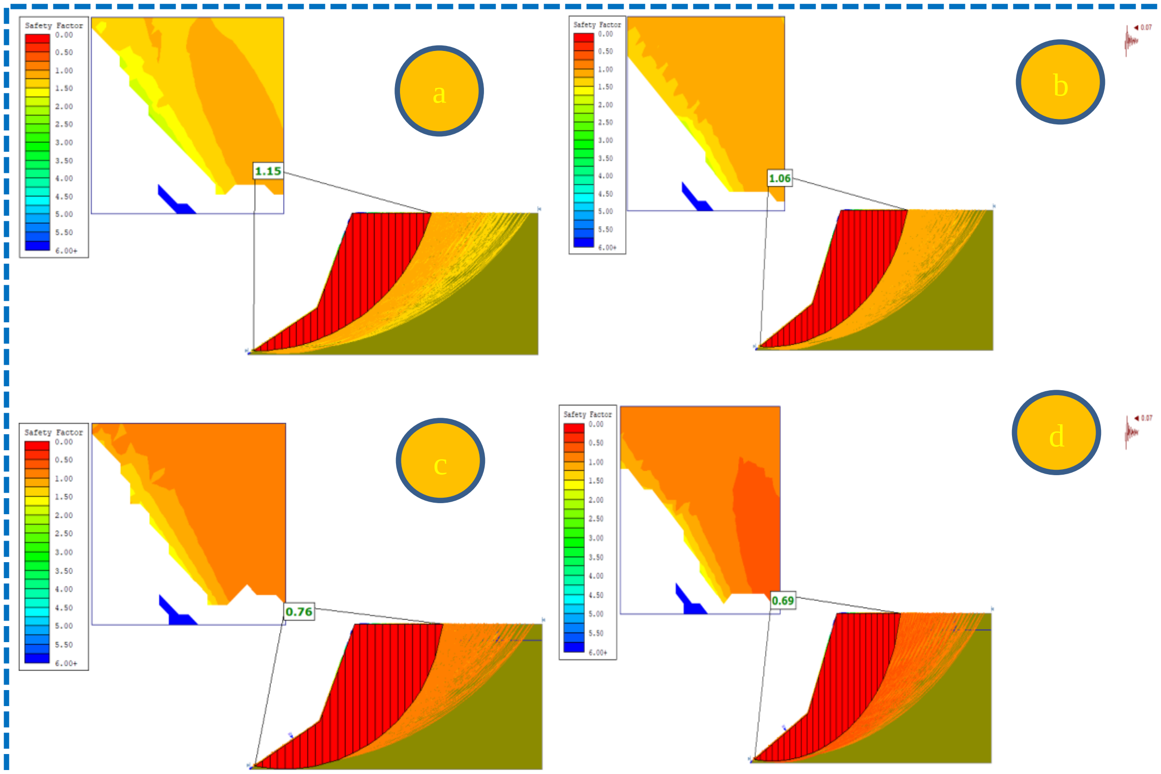

Figure 5.13: Slope stability analysis Limit equilibrium method for soil slope section SS2 under a) static dry condition b) Dynamic dry condition c) Static saturated condition and d) dynamic saturated conditions

Under static and dynamic dry conditions, the factor of safety for a soil slope section SS2 is 1.15 and 1.06, respectively (Figs.5.13 a and b). This demonstrates that soil slope section SS2 remained stable in both static and dynamic dry circumstances. However, the factor of safety found for the slope section SS2 under static saturated and dynamic saturated circumstances is 0.76 and 0.69, respectively (Figs. 5.13 c and d). based on the result slope will be unstable under static and dynamic saturated conditions this implies that slope stability can be influenced by groundwater by raising pore water pressure, increasing weight on a slope when the soil mass is fully saturated, decreasing effective stress, and losing shear.

From dynamic dry to dynamic saturated conditions, the effect of seismic activity on slope stability changes considerably. Furthermore, when compared to static dry slope conditions, the factor of safety derived for slope section SS2 under saturated slope conditions is quite minimal. This suggests that the rise in the groundwater table during the rainy season has a substantial impact on slope instability. Using slide software, the factor of safety for the two specified soil slope sections was calculated. The slope condition, material qualities, and slope angle all influence the factor of safety, which is the ratio of resistance force to driving force. The slope will be stable if the factor of safety is larger than one, but unstable if the factor of safety is less than one(Christian, 2004; Shariati & Fereidooni, 2021). Table 5.20 summarises the factors of safety derived using the general limit equilibrium method (GLEM) under static dry, static saturated, dynamic dry, and dynamic saturated slope circumstances.

Table 5. 23 Factors of safety and slope status under different anticipated conditions of soil slope sections SS1 and SS2.

Slope sections	Method	Loading condition	The factor of safety (FOS)	Slope stability condition
SS1	GLEM/ Morgenstern-price method	Static dry	1.24	Stable
		Static saturated	0.79	Unstable
		Dynamic dry	1.14	Stable
		Dynamic saturated	0.72	Unstable
SS2	GLEM/ Morgenstern-price method	Static dry	1.15	Stable
		Static saturated	0.76	Unstable
		Dynamic dry	1.06	Stable
		Dynamic saturated	0.69	Unstable

5.7.4 Slope Stability Analysis of Soil using Finite Element method

The factory of safety for the two soil critical slope sections is evaluated using limit equilibrium and finite element methods with the same material parameters, slope angle, and slope geometry as in the previous study. The analysis was performed to determine whether the slope was stable or unstable. The factor of safety (FOS) was calculated and interpreted for failure surfaces in soil slopes under static dry, static saturated, dynamic dry, and dynamic saturated circumstances using the finite element method. Cohesion, internal friction angle, soil unit weight, Poisson's ratio (v), dilatancy angles (ψ), and Young's modulus are the input parameters for the two soil slope sections utilized in finite element modeling. Laboratory experiments are used to establish the internal friction angle, cohesiveness, and unit weight of the two soil slope sections (SS1 and SS2). The correlation and suggestions of the literature were used to establish the deformation modulus of soil (Es) and Poisson's ration (v) that are used for numerical modeling (Terzaghi et al., 1996).

The Poisson's ration (v) was computed using eq. 4.5 (Bowles, 1996), and the deformation modulus was computed using eq. 4.7 based on the correlation and recommendations of Das (1995) and Ameratuga et al. (2016). The safety factors for the selected two critical soil slope sections (SS1and SS2) were determined in Phase2 software (Rocscience, 2004) using the Mohr-Coulomb model discussed as stated bellows

Table 5.24 : Input parameters for soil slope stability analysis using finite element method

Slope sections	Material	Unit weight (KN/m^2)		C MPA	ϕ(º)	Ψ (º)	v	Es (KN/m^2)
		γdry	Γsat					
SS1	Low plasticity silt	11.01	14.56	17 kpa	10.07	0	0.3	10716
SS2	High plasticity silt	15.36	17.30	21kpa	15.66	0	0.3	11160
γdry = dry unit weight of soil, γsat = the saturated unit weight of soil, C = cohesion, ϕ = angle of internal friction, ψ = dilatancy angle, v = Poisson’s ratio, and Es = young modulus.								

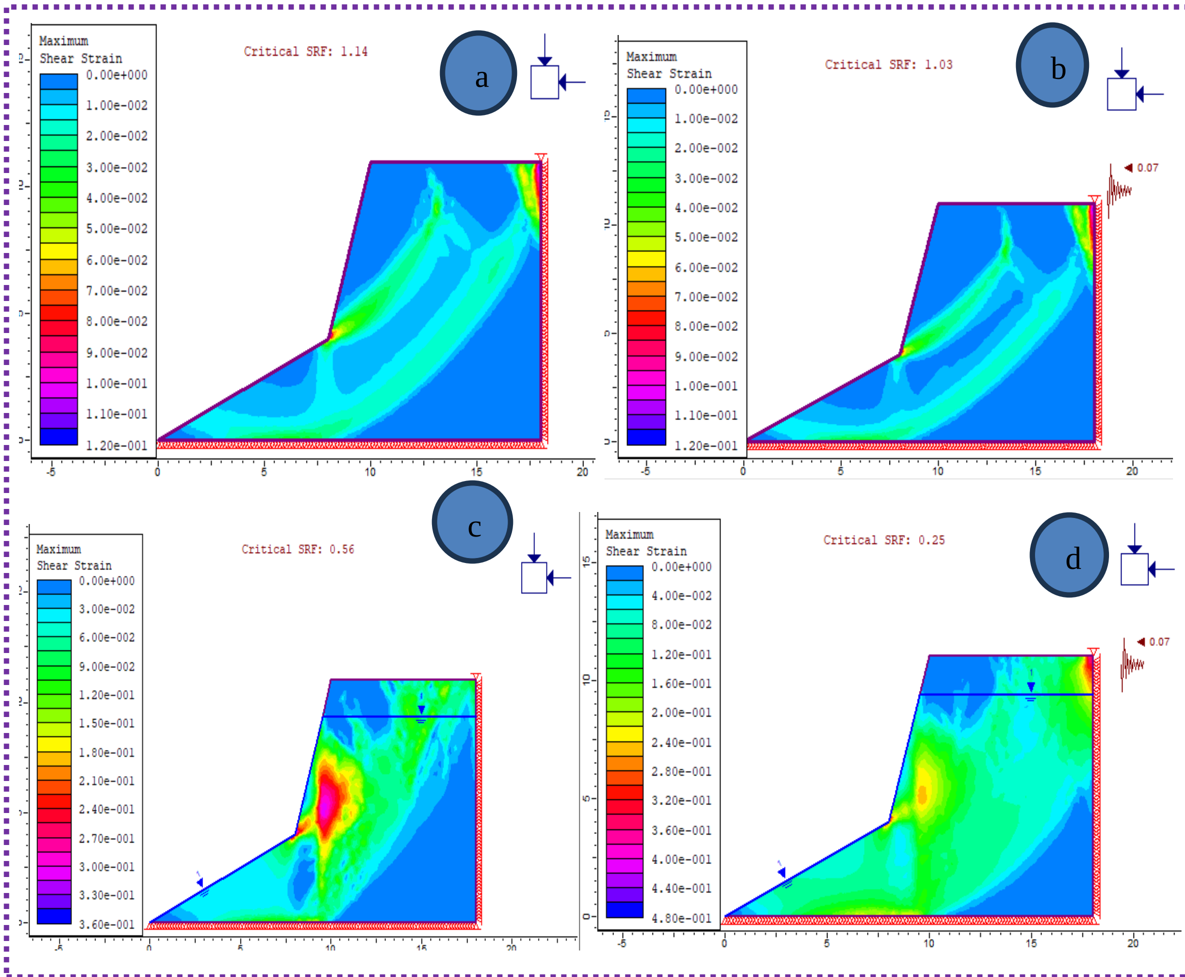

Figure 5.14: Strength Reduction Factor for slope soil section SS1 using phase2 software under a) static dry, b) dynamic dry, c) static saturated, and d) dynamic saturated conditions.

According to the above analytical results, the soil factor of safety at slope section SS1 is 1.14 and 1.03 under static and dynamic dry circumstances, respectively Figs. 5.14 (a) and (b). This demonstrates that soil slope section SS1 remained steady in both situations. However, the factor of safety determined for the soil slope section SS1 under static saturated and dynamic saturated circumstances is 0.56 and 0.25 less than one, respectively Figs. 5.15 (c) and (d). This implies that the soil is unstable at critical slope section SS1.

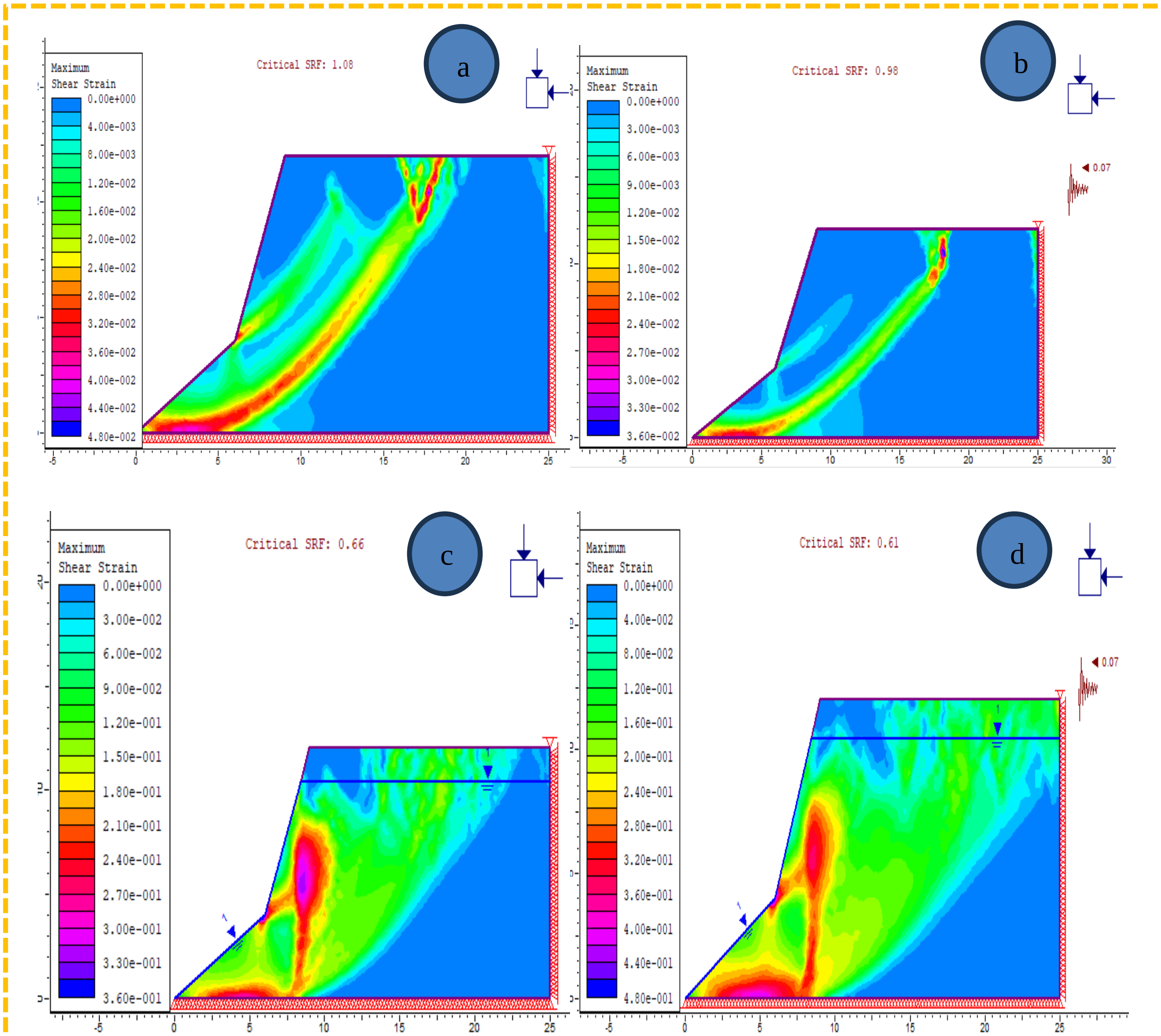

Figure 5. 15: Strength Reduction Factor for slope soil section SS2 using phase2 software under a) static dry, b) dynamic dry, c) static saturated, and d) dynamic saturated conditions

As illustrated in Figs. 5.15 (a) the minimal factors of safety or strength reduction factor calculated from the FEM studies of the soil slope section SS2 are 1.08 for static dry this shows that the soil slope section (SS2) remained stable in static dry circumstances. However, the strength reduction factor found for the soil slope section SS2 under static saturated and dynamic saturated conditions, dynamic dry is 0.66,0.61,0.98 respectively, as illustrated in Figs. 5.15 (b),(c) and (d). Because pore water pressure and seismic force affect shear strength, the decreasing factor of safety shows that they have a major impact on slope stability.

5.8 Comparison of FEM and LEM Results

The FEM strength reduction approach and factor safety were compared in this study. The results were achieved utilizing general limit equilibrium methods and the FEM method (FEM). As a result, the factor of safety results obtained using FEM was very close to those obtained utilizing limit equilibrium approaches. factor of safety derived via LEM, on the other hand, is slightly higher than that obtained from FEM. FEM results have been shown to provide additional information about the failure surface, such as stress, strain, deformation, and displacements, at any position along the slope section. Furthermore, when the slope angle increases, the values of the factor of safety in both LEM and FEM decrease. (Cheng,2008) conducted slope stability research of homogeneous and non-homogeneous material parameters and compared the FEM and LEM results.

The study revealed that for homogeneous slopes, the results of FEM and LEM were generally in good agreement. According to(Vinod, 2017), the factor of safety differences between the results of the finite element approach and the limit equilibrium method are minor. Under various predicted conditions, the results of both the FEM and LEM techniques were in good agreement in this research. When simple slope geometry, material properties, and external loads were taken into account, the results in both methods were comparable. Table 5.22 depicts the factor safety (FOS) and strength reduction factor (SRF) results from FEM and LEM calculations.

Table 5. 25 Comparison of LEM with FEM

Section		Static dry	Dynamic dry	Static saturated	Dynamic saturated
RSS5	FOS(LEM)	1.348	1.153	0.689	0.578
	SRF(FEM)	1.27	1.06	0.62	0.53
SS1	FOS(LEM)	1.24	1.14	0.79	0.72
	SRF(FEM)	1.14	1.03	0.56	0.25
SS2	FOS(LEM)	1.15	1.06	0.76	0.69
	FEM(FEM)	1.08	0.98	0.66	0.61

5.9 Remedial Measures

Based on the actual stability condition of the slope as established by numerical evaluation and field investigation, appropriate remedial methods were advised in this study.

According to (Popescu, 2002), slope failure remedial measures are broadly classified into four categories: slope geometry alteration, drainage, engineering retaining structures, and internal soil reinforcement. To ensure the stability of the study area's critical slope sections, it is advised that slope geometry be modified, drainage and engineered retaining structures be installed, and internal soil reinforcements be installed. on the actual stability condition of the slope, as established by numerical evaluation and field investigation, appropriate remedial methods were advised in this study.

5.9.1 Possible Remedial Measures for Structural Controlled Slope Sections

As stated in section fig 5.7,5.8,5.9, the Rocplane 2.0 software (Rocplane 2.0 Rocscience, 2004) analysis of structurally controlled slope sections showed that slope section RSS3 is unstable for JS1 and JS2 under for planar mode of failure under static and dynamic saturated conditions. Similarly, the analysis also revealed that RSS4 is unstable for JS2 under the planar mode of failure under static and dynamic saturated conditions. Hence, appropriate remedial measures are very crucial for these slope sections so that they can withstand failure even if they are subjected to the worst-case scenario (i.e. dynamic saturated condition). Accordingly, the stabilization analysis of the planar mode of failure was carried out by adopting Rocplane 2.0 software (Rocplane 2.0 Rocscience, 2004) through the application of Rock Bolts which were implanted across the failure plane to relatively strength rock. The designed bolt length was considered to pass the failure plane to increase the factor of safety. Since the slope sections are found to be unstable considering the worst condition (dynamic saturated condition), the rock slope sections must be stabilized. The failure to do so could potentially compromise the structural integrity.

Therefore, rock bolts are required for the planar mode of failure. The correct implementation of rock bolts could result in the increase of resisting force and shear strength which arise from the cohesion and frictional strength of sliding planes and a decrease in the driving force (which includes the mass of accelerated through gravity, seismic force, and water pressure). The change in the resisting and driving forces increases the factor of safety consequently. In this research work, the stabilization of planar mode of failure was done by employing RocPlane 2.0 software (RocPlane 2.0 Rocscience 2004) through the implementation of rock bolts that were installed across the failure plane to the relatively sound rock. All the stabilization design was carried out by considering the worst condition of the slope sections (i.e. dynamic saturated condition).

5.9.1.1 Rock bolt applied to RSS3 for planar mode of failure due to JSS1 and JSS2

about 2 rock bolts with lengths of 4m each were applied to the unstable slope section RSS3 with planar mode failure due to JS1 at an angle of 55º each, bolt capacity of 70t/m each, and resultant active bolt force of 140t/m. After the rock bolts with these properties are applied to the slope section, the factor of safety has increased from 0.66 to 1.24 with the resisting force to 144.57 t/m and driving force to 116.31 t/m as shown in Figure 5.16.

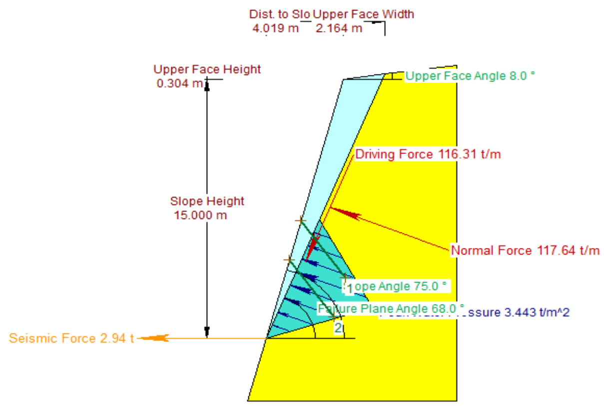

Factor of Safety	1.24
Driving Force	116.31t/m
Resisting Force	144.57t/m
Wedge Weight	42.02t/m
Wedge Volume	15.62m^3/m
Shear Strength	113.04t/m^2
Normal Force	117.64t/m
Seismic Force	2.94t
Plane Waviness	15.0°
Active Bolt Force	140.00t
Active Bolt Angle	305.0°
Passive Bolt Force	0.00t
Passive Bolt Angle	0.0°
Water Force on Failure Plane	12.79t/m

Bolt Properties:

#	Angle	Capacity	Length	AnchLength
1	55.0 °	70.00t/m	4.000 m	2.979 m
2	55.0 °	70.00t/m	4.000 m	3.320 m

Figure 5. 16: A designed and installed rock bolt for JS1 of RSS3

Similarly, about 2 rock bolts with lengths of 7m each were applied to the unstable slope section RSS3 with planar mode failure due to JS2 at an angle of 52º each, bolt capacity of 75t/m each, and resultant active bolt force of 150t/m. After the rock bolts with these properties are applied to the slope section, the factor of safety has increased from 0.46 to 1.22 with the resisting force to 224.44 t/m and driving force to 184.13 t/m as shown in Figure 5.17.

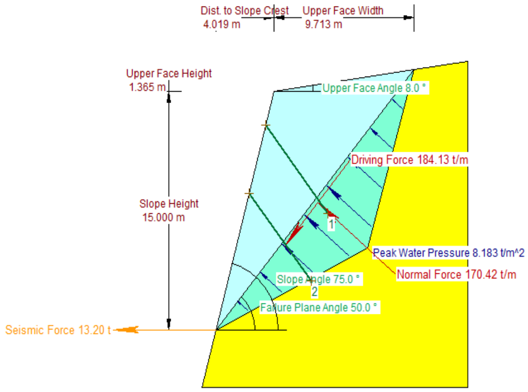

Factor of Safety	1.22
Driving Force	184.13t/m
Resisting Force	224.44t/m
Wedge Weight	188.57t/m
Wedge Volume	70.10m^3/m
Shear Strength	178.78t/m^2
Normal Force	170.42t/m
Seismic Force	13.20t
Plane Waviness	15.0°
Active Bolt Force	150.00t
Active Bolt Angle	308.0°
Passive Bolt Force	0.00t
Passive Bolt Angle	0.0°
Water Force on Failure Plane	87.40t/m

Bolt Properties:

#	Angle	Capacity	Length	AnchLength
1	52.0 °	75.00t/m	7.000 m	1.245 m
2	52.0 °	75.00t/m	7.000 m	3.153 m

Figure 5.17 A designed and installed rock bolt for JS2 of RSS3

5.9.1.2 Rock bolt applied to RSS4 for planar mode of failure due to JSS2

about 2 rock bolts with lengths of 9m each were applied to the unstable slope section RSS4 with planar mode failure due to JS1 at the angle of 37° each, bolt capacity of 99t/m each, and resultant active bolt force of 323t/m. After the rock bolts with these properties are applied to the slope section, the factor of safety has increased from 0.53 to 1.23 with the resisting force to 345.80 t/m and driving force to 281.19 t/m as shown in Figure 5.18.

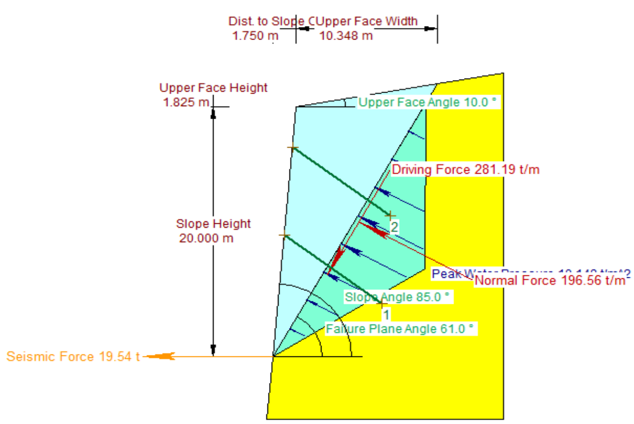

Factor of Safety	1.23
Driving Force	281.19t/m
Resisting Force	345.80t/m
Wedge Weight	279.16t/m
Wedge Volume	101.88m^3/m
Shear Strength	318.18t/m^2
Normal Force	196.56t/m
Seismic Force	19.54t
Plane Waviness	8.0°
Active Bolt Force	198.00t
Active Bolt Angle	323.0°
Passive Bolt Force	0.00t
Passive Bolt Angle	0.0°
Water Force on Failure Plane	117.75t/m

Bolt Properties:

#	Angle	Capacity	Length	AnchLength
1	37.0 °	99.00t/m	9.000 m	5.007 m
2	37.0 °	99.00t/m	9.000 m	2.117 m

Figure 5.18 A designed and installed rock bolt for JS2 of RSS4

5.9.2 Possible Remedial Measures for Non-Structural Controlled Slope Sections

The slope of the research area is moderate to very steep, which increases tangential gravity force due to the maximum value of shear stress and so encourages slope instability. One of the most important characteristics influencing slope stability is its shape (Popescu, 2002). By reducing the slope angle and slope height and removing material from the landslip in the study area, the slope geometry can be modified (Anbalagan & Singh, 1996; Raghuvanshi et al., 2014). According to the results of the analysis, the slope height and slope angle are significant elements impacting the stability conditions of the analyzed slopes in this study.Mitigation techniques that reduce their volatility were proposed in light of these issues. The LEM method using the application slide software was used to analyze slope stability for restorative operations (Slide 6 Rocscience 2004). The slope's stability was evaluated using the factor of safety (FOS). The influence of slope height and slope angle on slope modification geometry was presented and analyzed using slide software (Slide 6, Rocscience, 2004).

5.9.2.1 Reducing of Slope Angle and Slope Height

Slope angle and height impact slope stability because raising these parameters increases shear stress while decreasing shear strength on the possible failure plane. The effect of these characteristics was quantitatively modeled for various slope heights and slope angles. The influence of slope angle was investigated under various scenarios utilizing the worst condition of unstable rock slope section five (RSS5). To investigate the influence of slope angle on the factor of safety and slope stability, the critical slope section RSS5 was modeled at 30º,28 º,25º, and 22º,18º.To demonstrate the effect of slope angle on slope stability, the value of the factor of safety was calculated in slide software (Rocscience, 2004, slide 6) using the General limit equilibrium method. The safety factors were computed by lowering the slope angle from the original condition 30º to 28º,25º and 22º,18º). Figure 5.19 indicates that decreasing the slope angle enhances the factor of safety on a slope (Chatterjee and Krishna, 2019).

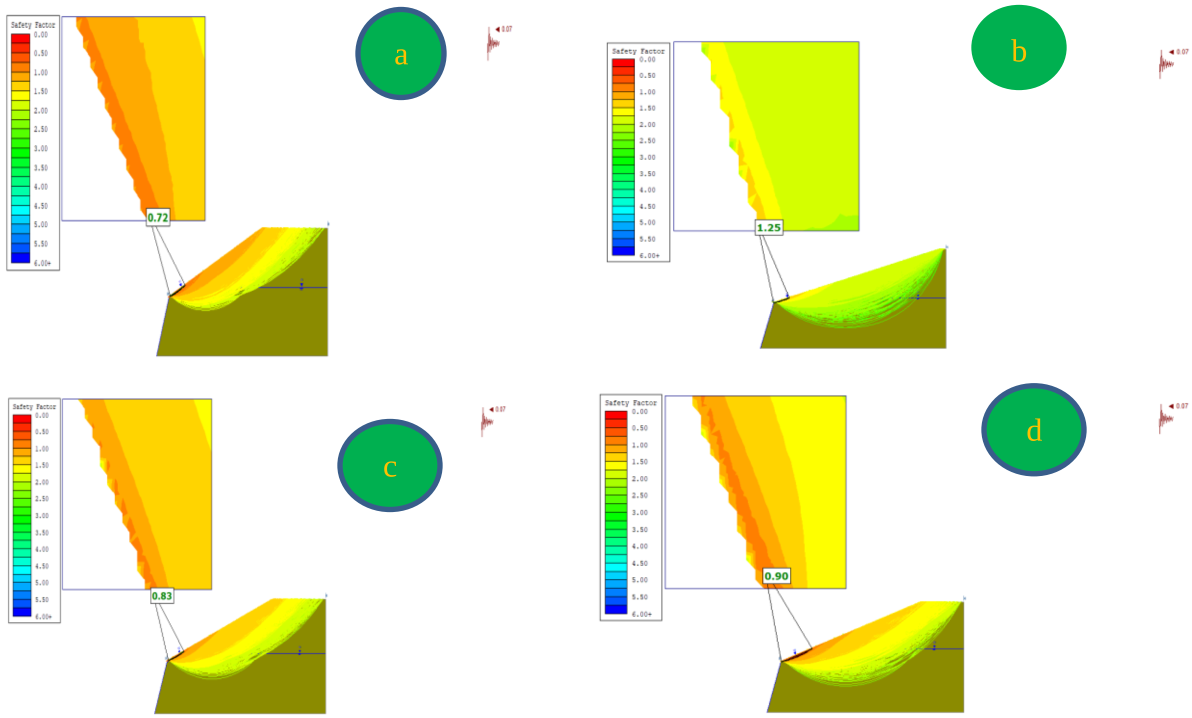

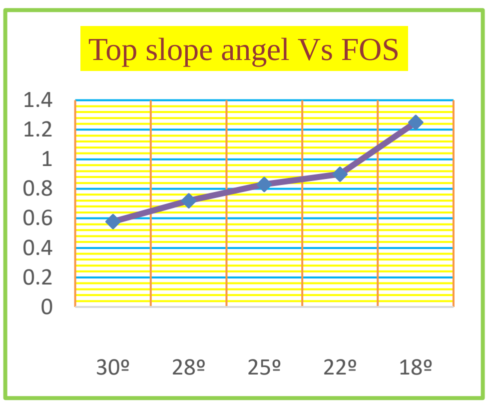

Top slope angel(º)	FOS
30º	0.578
28º	0.72
25º	0.83
22º	0.90
18º	1.25

Figure 5. 19: Effect of slope angle on the factor of safety slope analysis using slide software, a) at 28º, b) at 25º and c) at 22º,d) at 18º

The above analysis results (Fig.5.19) indicate that when the slope angle decreases the factor safety increases (Kale et al., 2021). This indicates that the slope angle and factor of safety are inversely related.By examining the slope at various heights, the influence of slope height was also studied. The evaluation result was plotted and shown in Fig. 5.20 below using slide software (Rocscience, 2004).

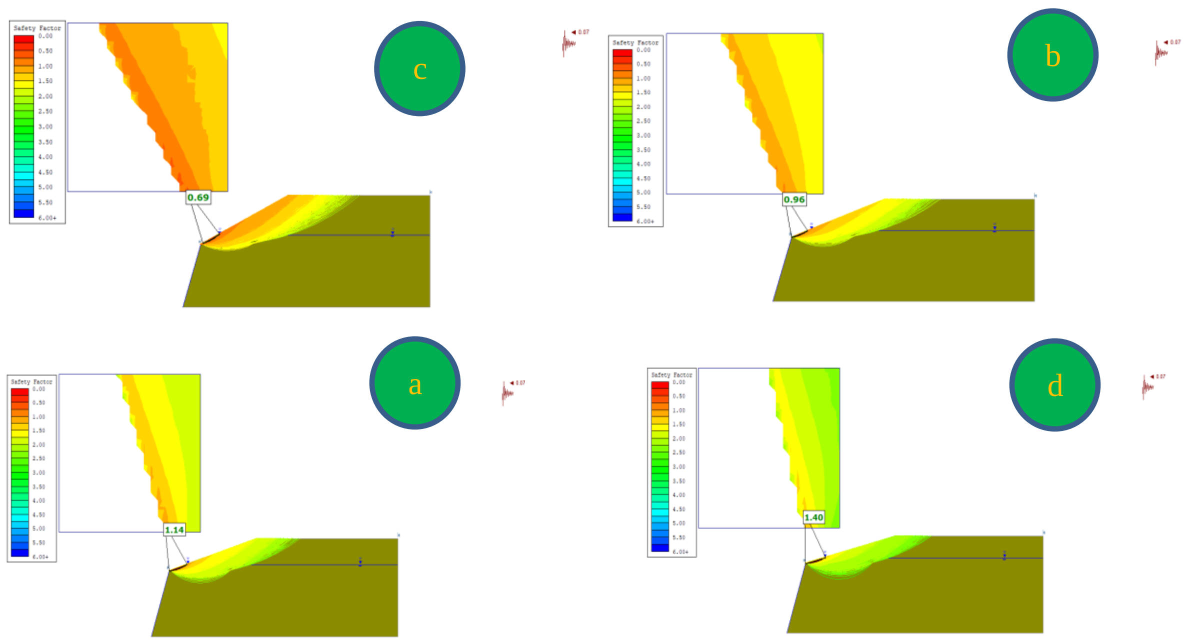

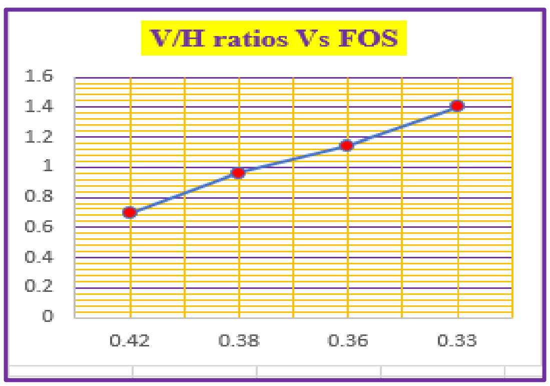

V/H Ratios	FOS
0.42	0.69
0.38	0.96
0.36	1.14
0.33	1.40

Figure 5.20 Effect of slope height on a factor of safety slope analysis using slide software, a) at 18m, b) at 16m and c) at 15m d) at 14m

The slope height correlation study, as shown in the figure above , demonstrates that there is an inverse link between slope height and factor safety. According to research, lowering the slope height at the start tends to increase the factor of safety at a lower rate (Anbalagan & Singh, 1996; Raghuvanshi et al., 2014).On the same premise, it is recognized that both increasing slope height and slope angle lower the factor of safety slope.

5.9.3 Possible Remedial Measures for Soil Slope Sections

The steep slope is highly susceptible to sliding due to the gravity effect when compared with the gentle slope section. The effect of slope angle was evaluated using the worst condition of the dynamic saturated soil slope sections.

The original slope angle was modeled as (1H: 1V) and the analysis was then carried out by subsequently reducing the slope angle from (1H:1V) to (1.5H:1V),(2H:1V) and (2.5H:1V),(3H:1V) by keeping the height (V) constant. This analysis was carried out using Slide 6.0 software (Slide 6.0 Rocscience, 2004) using the Morgersteren-price technique.

5.9.3.1 Flattening Slope Angle Using 2D Slide Software for SS1

According to the analysis shown below (fig 5.13), the factor of safety which was initially 0.72 at 75 and 28 at the top and bottom angel respectively made it unstable, with slope angles at 67 and 18 at the top and bottom angel respectively increased to 1.36 which made slope stable.

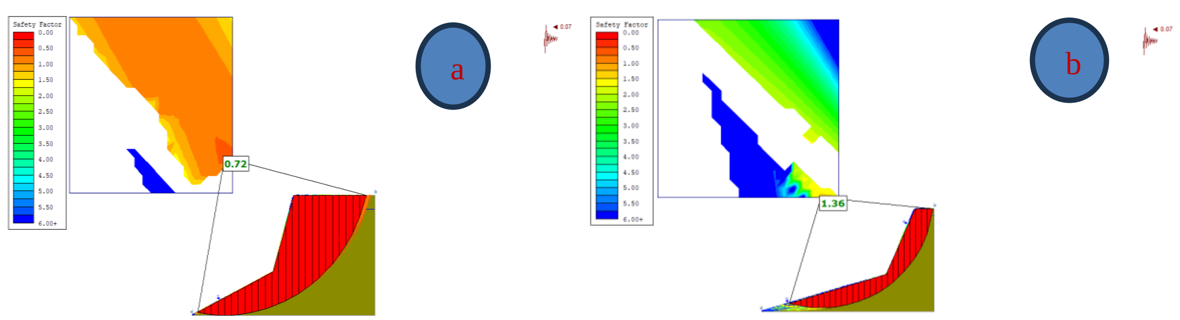

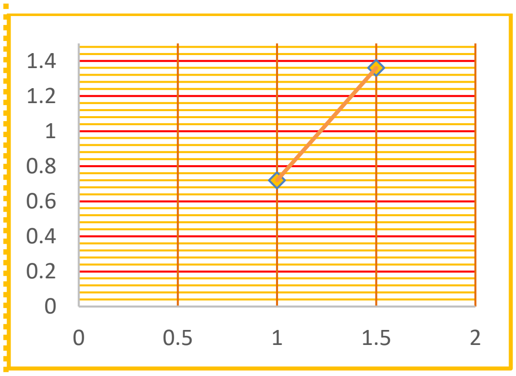

Slope angel		Slope ratio	H/V Ratio	FOS
Top	Tan(75)	1H:1V	1	0.72
Bottom	tan(28)			
Top	tan(67)	1.5H:1V	1.5	1.36
Bottom	Tan(18)			

Figure 5.21 Effect of slope flattening on the factor of safety at SS1 a) at 75 and 28 b) 67 and 18 at top and bottom angel respectively

5.9.3.2 Flattening Slope Angle Using 2D Slide Software for SS2

According to the analysis shown below (fig 5.14), the factor of safety which was initially 0.69 at 70 and 35 at the top and bottom angel respectively made it unstable, with slope angles at 58 and 24 at the top and bottom angel respectively increased to 0.79 which made slope unstable, with slope angels at 53 and 18 at top and bottom angel respectively increased to 0.92 which made again slope unstable.with slope angles at 45 and 15 at the top and bottom angle respectively increased to 1.17 which made the slope stable, with slope angles at 43 and 13 at the top and bottom angle stability increased to 1.50.

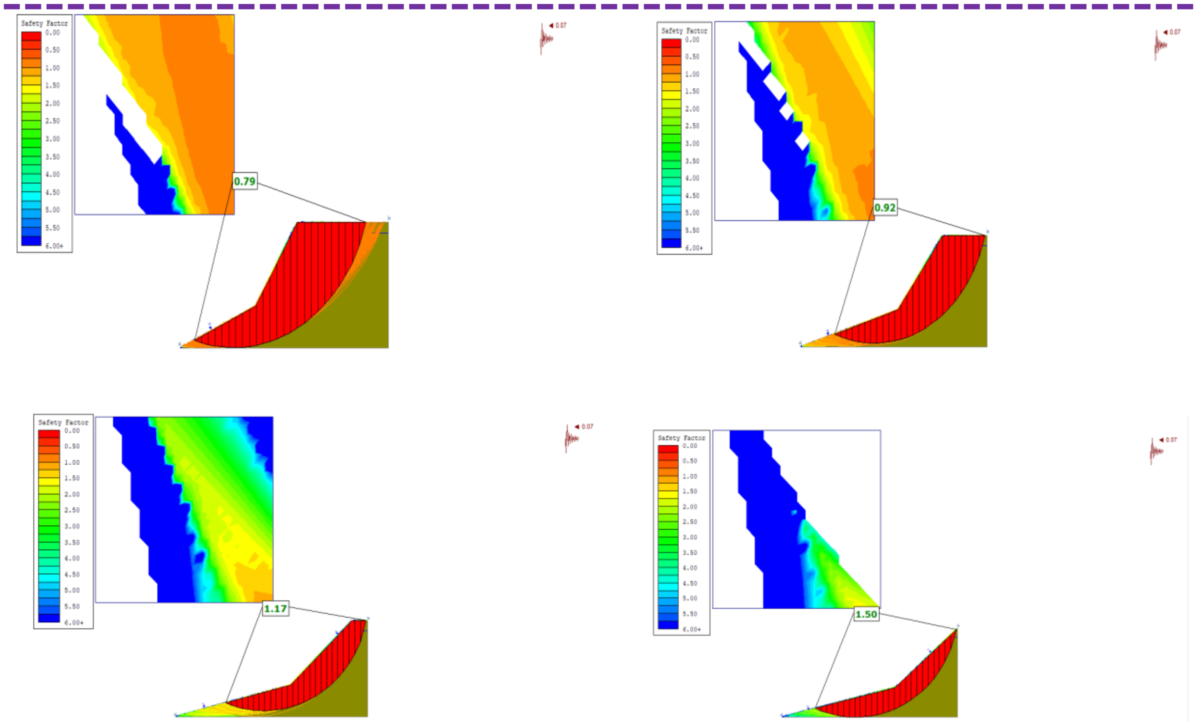

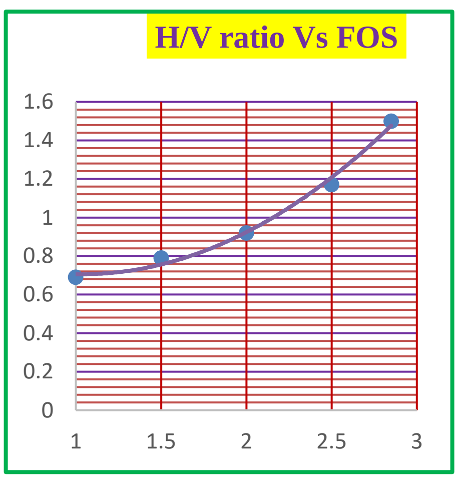

Slope angel		Slope ratio	H/V Ratio	FOS in slide 2
Top	Tan(70)	1H:1V	1	0.69
Bottom	tan(35)			
Top	tan(58)	1.5H:1V	1.5	0.79
Bottom	Tan(24)			
Top	tan(53)	2H:1V	2	0.92
Bottom	tan(18)			
Top	Tan(45)	2.5H:1V	2.5	1.17
Bottom	Tan (15)			
Top	Tan(43)	3H:1V	2.85	1.50
Bottom	Tan(13)			

Figure 5.22 Effect of slope flattening on the factor of safety at SS2 a) at 58 and 24 b) at 53 and 18 c) at 45 and 15 d) at 43 and 13 at top and bottom angel respectively

CHAPTER SIX

6. CONCLUSION AND RECOMMENDATION

6.1 Conclusion

This study evaluated the stability of the slope along the road section based on a detailed field survey followed by a laboratory test, rock quality designation, kinematic analysis, and LEM and FEM methods. Finally, the following concluding remarks were made

- Engineering geological evaluations of field manifestations indicated that the rock masses along the road sections showed a slightly to highly weathered, and 3 critical rock slopes and two critical soil slope sections were identified.
- The RQD values of the structural controlled slope sections classified range from fair to good rock according to Deer and Deere(1988) based on joint volumetric count (Jv).
- The UCS of rocks of the study area (for structurally controlled slope sections) ranges from 95 MPa to 139.2 Mpa and for non-structural controlled slope section 148 MPa.
- Most of the rocks along the road sections have medium to high strength, according to in-situ Schmidt hammer and laboratory point load testing on representative rock samples.
- Grain size analysis and Atterberg limit tests imply that the soils obtained from the critical slope section are dominantly composed of coarse-grained soil with a plasticity index ranging from 9 to 20 and a liquid limit varying from 48 to 63. Generally, according to the USCS system, the soils of the study area were classified as low-plastic to high-plastic silt.
- The kinematic analysis of structurally controlled slope sections revealed kinematic admissibility for planar failure due to JS1 and JS2 at RSS3. Similarly, this analysis also showed the occurrence of planar mode of failure due to JS2 at RSS4
- Further stability analysis of planar mode using Rocplane software showed that RSS3 is unstable (i.e. FOS < 1) under static and dynamic saturated conditions. Similarly, stability analysis of the planar mode of failure through Rocplane software revealed that slope section RSS4 is unstable under static and dynamic saturated conditions.
- One critical rock slope sections were analyzed under varying conditions using finite element and limit equilibrium stability analysis methods. The results of the analysis revealed that RSS5 is unstable under static and dynamic saturated conditions.

- The analysis of soil slope sections LEM results revealed that soil slope SS1 is stable in both static dry and dynamic dry conditions and unstable in both static saturated and dynamic saturated conditions. Similarly, Soil slope section SS2 is stable in both static dry and dynamic dry conditions and unstable in both static saturated and dynamic saturated conditions.
- A comparison of FOS obtained from LEM-based Slide 6.0 software and SRF obtained from FEM-based Phase 2.0 software is in very close agreement. However, a detailed examination showed that FEM yielded slightly lower SRF attributed to its consideration of stress and strain deformation.

6.2 Recommendation

For the most part, this study was concerned with slope stability analysis along the selected rock section from Jinka to Mendir Road. Different methods and approaches were used to analyze the slope section. Therefore, satisfactory and proper remedial measures are essential to stabilize the slope sections and are recommended based on the analysis result. Under static and dynamic saturated conditions the rock and soil slope sections were unstable. The structurally controlled rock slope sections can be stabilized and protected from future failure by installing rock bolts and the nonstructural slope section can be stabilized by reducing slope height and angle as well as the soil section can be stabilized by flattening slope angle.

- To control the effects of water saturation, surface drainage should be planned for non-structural controlled sections by redesigning the slope face to control water flow and runoff, providing a flow line to remove rainwater, constructing toe drains, and planting vegetation on the slope face. Also using subsurface drainage is recommended because the occurrence of springs along the slope surface indicates that the groundwater is shallow. Furthermore, a surface drainage system like covering the rock with an impervious material to control the water that enters into the joints is also recommended for structurally controlled slope sections
- Two rock bolts with a length of 4m each were applied to the unstable slope section with planar mode failure due to JS1 at the angle of 55º each, bolt capacity of 70t/m each, and resultant active bolt force of 140t/m.

- After the rock bolts with these properties are applied to the slope section, the factor of safety has increased from 0.66 to 1.24 with the resisting force 144.57 t/m and driving force to 116.31 t/m and Two rock bolts with length of 7m each were applied to the unstable slope section with planar mode failure due to JS2 at angle of 52º each, bolt capacity of 75t/m each and resultant active bolt force of 150t/m. After the rock bolts with these properties are applied to the slope section, the factor of safety has increased from 0.46 to 1.22 with the resisting force to 224.44 t/m and driving force to 184.13 t/m at RSS3
- Similarly, two rock bolts with a length of 9m each were applied to the unstable slope section with planar mode failure due to JS2 at the angle of 37º each, bolt capacity of 99t/m each, and resultant active bolt force of 198.00t/m. After the rock bolts with these properties are applied to the slope section, the factor of safety has increased from 0.53 to 1.23 with the resisting force 345.80 t/m and driving force 281.19 t/m at RSS4.
- For nonstractural sections reducing slope angle and height is recommended. To demonstrate the effect of slope angle on slope stability, the value of the factor of safety was calculated in slide software (Rocscience,2004, slide 6)using the General limit equilibrium method. The safety factors were computed by lowering the slope angle from the original condition 30º to 28º,25º and 22º,18º. indicates that decreasing the slope angle enhances the factor of safety on a slope By examining the slope at various heights, the influence of slope height was also studied. According to research, lowering the slope height at the start tends to increase the factor of safety at a lower rate.
- For soil sections Flattening Slope Angle Using 2D Slide Software is recommended. The original slope angle was modeled as (1H:1V) and the analysis was then carried out by subsequently reducing the slope angle from (1H:1V) to (1.5H:V), (2H:1V) and (2.5H: 1V),(3H:1V) by keeping the height (V) constant. This analysis was carried out using Slide 6.0 software using the Morgersteren-price technique. with reducing slope angle factor of safety will be increased.
- Retention measures such as designed ditches, broad shoulders, berms, steel barriers, and nets may be placed in addition to retaining walls to prevent further rock falling or sliding, particularly on slopes in basaltic rock units.

- Every effort should be taken in the future to conduct this type of assessment in the mountainous areas of the country where slope rock failure problems are major concerns. Furthermore, other researchers employ a variety of approaches to enhance the reliability of current research results.
- To further understand the impact of essential elements on slope instability, more extensive geotechnical investigations, geophysical surveys, and topographic surveys should be conducted.

REFERENCES

Abebe, B., Dramis, F., Fubelli, G., Umer, M., & Asrat, A. (2010). Landslides in the Ethiopian highlands and the Rift margins. Journal of African Earth Sciences, 56(4–5), 131–138.

Abramson, L. W., Lee, T. S., Sharma, S., & Boyce, G. M. (2001). Slope stability and stabilization methods. John Wiley & Sons.

Abzalov, M. (2016). Applied mining geology (Vol. 12). Springer.

Abzalov, M., & Abzalov, M. (2016). Geotechnical Logging and Mapping. Applied Mining Geology, 87–95.

Aleotti, P., & Chowdhury, R. (1999). Landslide hazard assessment: summary review and new perspectives. Bulletin of Engineering Geology and the Environment, 58(1), 21–44.

Alzo'ubi, A. K. (2016). Rock slopes processes and recommended methods for analysis. GEOMATE Journal, 11(25), 2520–2527.

Ameratunga, J., Sivakugan, N., Das, B. M., Ameratunga, J., Sivakugan, N., & Das, B. M. (2016). Correlations for Laboratory Test Parameters. Correlations of Soil and Rock Properties in Geotechnical Engineering, 51–86.

Anbalagan, R., & Singh, B. (1996). Landslide hazard and risk assessment mapping of mountainous terrains—a case study from Kumaun Himalaya, India. Engineering Geology, 43(4), 237–246.

Aryal, K. P. (2006). Slope stability evaluations by limit equilibrium and finite element methods.

Ayalew, L. (1999). The effect of seasonal rainfall on landslides in the highlands of Ethiopia. Bulletin of Engineering Geology and the Environment, 58(1), 9–19.

Ayalew, L., Yamagishi, H., & Ugawa, N. (2004). Landslide susceptibility mapping using GIS-based weighted linear combination, the case in Tsugawa area of Agano River, Niigata Prefecture, Japan. Landslides, 1, 73–81.

Azimian, A. (2016). A new method for improving the RQD determination of rock core in borehole. Rock Mechanics and Rock Engineering, 49, 1559–1566.

Balázs, B. Z., & Takács, M. (2018). Finite element modelling of thin chip removal process. IOP Conference Series: Materials Science and Engineering, 426(1), 12002.

Barton, N. (1973). Review of a new shear-strength criterion for rock joints. Engineering Geology, 7(4), 287–332.

Barton, N., & Choubey, V. (1977). The shear strength of rock joints in theory and practice. Rock Mechanics, 10, 1–54.

Berhe, S. M., Desta, B., Nicoletti, M., & Teferra, M. (1987). Geology, geochronology and geodynamic implications of the Cenozoic magmatic province in W and SE Ethiopia. Journal of the Geological Society, 144(2), 213–226.

Bieniawski, Z. T. (1973). Engineering classification of jointed rock masses. Civil Engineering Siviele Ingenieurswese, 1973(12), 335–343.

Bieniawski, Z. T. (1979). The geomechanics classification in rock engineering applications. 4th ISRM Congress.

Bieniawski, Z. T. (1989). Engineering rock mass classifications: a complete manual for engineers and geologists in mining, civil, and petroleum engineering. John Wiley & Sons.

Broch, E., & Franklin, J. A. (1972). The point-load strength test. International Journal of Rock Mechanics and Mining Sciences & Geomechanics Abstracts, 9(6), 669–676.

Burman, A., Acharya, S. P., Sahay, R. R., & Maity, D. (2015). A comparative study of slope stability analysis using traditional limit equilibrium method and finite element method.

Bushira, K. M., Gebregiorgis, Y. B., Verma, R. K., & Sheng, Z. (2018). Cut soil slope stability analysis along national Highway at wozeka–gidole road, Ethiopia. Modeling Earth Systems and Environment, 4, 591–600.

Chen, C. S. (2001). Stabilization of a failed slope with reinforced soil wall. Proceedings of the 14th Southeast Asia Goetechnical Conference, 1111–1114.

Cheng, Y. M., & Lau, C. K. (2008). Slope stability analysis and stabilization: new methods and insight. CRC press.

Cheng, Y. M., & Lau, C. K. (2014a). Slope stability analysis and stabilization: new methods and insight. CRC press.

Cheng, Y. M., & Lau, C. K. (2014b). Soil Slope stability analysis and stabilization–new methods and insights. Spon Press.

Christian, J. T. (2004). Geotechnical engineering reliability: How well do we know what we are doing? Journal of Geotechnical and Geoenvironmental Engineering, 130(10), 985–1003.

Dai, F. C., & Lee, C. F. (2002). Landslide characteristics and slope instability modeling using GIS, Lantau Island, Hong Kong. Geomorphology, 42(3–4), 213–228.

Davidson, A. (1983). The Omo River Project-Geology and Geochemistry'of parts of Ilubabor, Kefa, Gemu Gofa and Sidamo, Ethiopia. GSE.

Davidson, A., & Rex, D. C. (1980). Age of volcanism and rifting in southwestern Ethiopia. Nature, 283, 657–658.

Deere, D. U., & Miller, R. P. (1966). Engineering classification and index properties for intact rock. Illinois Univ At Urbana Dept Of Civil Engineering.

Duncan, J. M., Wright, S. G., & Brandon, T. L. (2014). Soil strength and slope stability. John Wiley & Sons.

George, R., Rogers, N., & Kelley, S. (1998). Earliest magmatism in Ethiopia: evidence for two mantle plumes in one flood basalt province. Geology, 26(10), 923–926.

Gischig, V., Amann, F., Moore, J. R., Loew, S., Eisenbeiss, H., & Stempfhuber, W. (2011). Composite rock slope kinematics at the current Randa instability, Switzerland, based on remote sensing and numerical modeling. Engineering Geology, 118(1–2), 37–53.

Goodman, R. E. (1991). Introduction to rock mechanics. John Wiley & Sons.

Griffiths, D. V, & Lane, P. A. (1999). Slope stability analysis by finite elements. Geotechnique, 49(3), 387–403.

Gurocak, Z., & Alemdag, S. (2012). Assessment of permeability and injection depth at the Atasu dam site (Turkey) based on experimental and numerical analyses. Bulletin of Engineering Geology and the Environment, 71, 221–229.

Gurocak, Z., Alemdag, S., & Zaman, M. M. (2008). Rock slope stability and excavatability assessment of rocks at the Kapikaya dam site, Turkey. Engineering Geology, 96(1–2), 17–27.

Hack, R., & Huisman, M. (2002). Estimating the intact rock strength of a rock mass by simple means. 9th Congr. of the Int. Ass. Engin. Geol. Env.

Hack, R., Price, D., & Rengers, N. (2003). A new approach to rock slope stability–a probability classification (SSPC). Bulletin of Engineering Geology and the Environment, 62, 167–184.

Hammah, R. E., Curran, J. H., Yacoub, T., & Corkum, B. (2004). Stability analysis of rock slopes using the finite element method. Proceedings of the ISRM Regional Symposium EUROCK.

Hamza, T., & Raghuvanshi, T. K. (2017). GIS based landslide hazard evaluation and zonation–A case from Jeldu District, Central Ethiopia. Journal of King Saud University-Science, 29(2), 151–165.

Hoek, E., & Bray, J. D. (1981). Rock slope engineering. CRC Press.

Hoek, E., & Brown, E. T. (1997). Practical estimates of rock mass strength. International Journal of Rock Mechanics and Mining Sciences, 34(8), 1165–1186.

Hoek, E., Carranza-Torres, C., & Corkum, B. (2002). Hoek-Brown failure criterion-2002 edition. Proceedings of NARMS-Tac, 1(1), 267–273.

Hoek, E., Carter, T. G., & Diederichs, M. S. (2013). Quantification of the geological strength index chart. 47th US Rock Mechanics. Geomechanics Symposium, 3, 1757–1764.

Hoek, E., Marinos, P., & Benissi, M. (1998). Applicability of the Geological Strength Index (GSI) classification for very weak and sheared rock masses. The case of the Athens Schist Formation. Bulletin of Engineering Geology and the Environment, 57, 151–160.

Huggel, C., Schneider, D., Miranda, P. J., Granados, H. D., & Kääb, A. (2008). Evaluation of ASTER and SRTM DEM data for lahar modeling: a case study on lahars from Popocatépetl Volcano, Mexico. Journal of Volcanology and Geothermal Research, 170(1–2), 99–110.

Huluka, G., & Miller, R. (2014). Particle size determination by hydrometer method. Southern Cooperative Series Bulletin, 419, 180–184.

Hunt, R. E. (2007). Geologic hazards: a field guide for geotechnical engineers. CRC press.

ISRM. (1978). International society for rock mechanics commission on standardization of laboratory and field tests: suggested methods for the quantitative description of discontinuities in rock masses. Int J Rock Mech Min Sci Geomech Abstr, 15(6), 319–368.

Janbu, N. (1973). Slope stability computations. Publication of: Wiley (John) and Sons, Incorporated.

Karaman, K., Kaya, A., & Kesimal, A. (2015). Use of the point load index in estimation of the strength rating for the RMR system. Journal of African Earth Sciences, 106, 40–49.

Kazmi, D., Qasim, S., Harahap, I. S. H., Baharom, S., Mehmood, M., Siddiqui, F. I., & Imran, M. (2017). Slope remediation techniques and overview of landslide risk management. Civil Engineering Journal, 3(3), 180–189.

Kazmin, V., Shifferaw, A., & Balcha, T. (1978). The Ethiopian basement: stratigraphy and possible manner of evolution. Geologische Rundschau, 67, 531–546.

Khandker, A. A., Anagnostou, J. T., & Deo, P. (2013). Geotechnical challenges in highway engineering in twenty first century: lessons from the past experiences and new technologies.

Khanna, R., & Dubey, R. K. (2021). Comparative assessment of slope stability along road-cuts through rock slope classification systems in Kullu Himalayas, Himachal Pradesh, India. Bulletin of Engineering Geology and the Environment, 80, 993–1017.

Komadja, G. C., Pradhan, S. P., Oluwasegun, A. D., Roul, A. R., Stanislas, T. T., Laïbi, R. A., Adebayo, B., & Onwualu, A. P. (2021). Geotechnical and geological investigation of slope stability of a section of road cut debris-slopes along NH-7, Uttarakhand, India. Results in Engineering, 10, 100227.

Kumar, A., Sharma, R. K., & Mehta, B. S. (2020). Slope stability analysis and mitigation measures for selected landslide sites along NH-205 in Himachal Pradesh, India. Journal of Earth System Science, 129, 1–14.

Lamessa, G., & Meten, M. (2021a). Stability analysis of rock slope along selected road sections from Gutane Migiru town to Fincha sugar factory, Oromiya, Ethiopia. SN Applied Sciences, 3(2), 151.

Lamessa, G., & Meten, M. (2021b). Stability analysis of rock slope along selected road sections from Gutane Migiru town to Fincha sugar factory , Oromiya , Ethiopia. SN Applied Sciences, 3(2), 1–16. https://doi.org/10.1007/s42452-020-04026-w

Liu, Y.-C., & Chen, C.-S. (2007). A new approach for application of rock mass classification

on rock slope stability assessment. Engineering Geology, 89(1–2), 129–143.

Marinos, P., & Hoek, E. (2000). GSI: a geologically friendly tool for rock mass strength estimation. ISRM International Symposium.

Matthews, C., Farook, Z., & Helm, P. (2014). Slope stability analysis – limit equilibrium or the finite element method ? Ground Engineering, May, 22–28.

Maula, B. H., & Zhang, L. (2011). Assessment of embankment factor safety using two commercially available programs in slope stability analysis. Procedia Engineering, 14, 559–566.

Mengesha, T., Tadiwos, C., & Werkneh, H. (1996). Explanation of the geological map of Ethiopia, Ethiopian institute of geological surveys. Addis Ababa, 3, 79.

Merla, G., Abbate, E., Azzaroli, A., Bruni, P., Canuti, P., Fazzuoli, M., Sagri, M., & Tacconi, P. (1979). A Geological Map of Ethiopia & Somalia (1973) 1: 2,000,000: And Comment with a Map of Major Landforms. University of Florence.

Morgenstern, N. R. u, & Price, V. E. (1965). The analysis of the stability of general slip surfaces. Geotechnique, 15(1), 79–93.

Naghadehi, M. Z., Jimenez, R., KhaloKakaie, R., & Jalali, S.-M. E. (2011). A probabilistic systems methodology to analyze the importance of factors affecting the stability of rock slopes. Engineering Geology, 118(3–4), 82–92.

Nazir, R., Momeni, E., Armaghani, D. J., & Amin, M. F. M. (2013). Prediction of unconfined compressive strength of limestone rock samples using L-type Schmidt hammer. Electronic Journal of Geotechnical Engineering, 18(I), 1767–1775.

Nelson, S. (2013). Slope Stability, triggering events, mass movement hazards. Nat. Disasters. EENS, 3050, 1–6.

Norrish, N. I., & Wyllie, D. C. (1996). Landslides: Investigation and Mitigation. Chapter 15-Rock slope stability analysis. Transportation Research Board Special Report, 247.

Palmstrom, A. (1974). Characterization of jointing density and the quality of rock masses. Intern. Rep. Norw. AB Berdal, 26(3).

Palmstrom, A. (1982). The volumetric joint count—a useful and simple measure of the degree of rock mass jointing. International Association of Engineering Geology. International Congress. 4, 221–228.

Palmstrom, A. (2005). Measurements of and correlations between block size and rock quality designation (RQD). Tunnelling and Underground Space Technology, 20(4), 362–377.

Palmström, A., Sharma, V. I., & Saxena, K. (2001). In-situ characterization of rocks. BALKEMA Publ, 1–40.

Pantelidis, L. (2009). Rock slope stability assessment through rock mass classification systems. International Journal of Rock Mechanics and Mining Sciences, 46(2), 315–325.

Pantelidis, L. (2010). An alternative rock mass classification system for rock slopes. Bulletin of Engineering Geology and the Environment, 69, 29–39.

Park, H.-J., Lee, J.-H., Kim, K.-M., & Um, J.-G. (2016). Assessment of rock slope stability using GIS-based probabilistic kinematic analysis. Engineering Geology, 203, 56–69.

Park, H.-J., West, T. R., & Woo, I. (2005). Probabilistic analysis of rock slope stability and random properties of discontinuity parameters, Interstate Highway 40, Western North Carolina, USA. Engineering Geology, 79(3–4), 230–250.

Park, H., & West, T. R. (2001). Development of a probabilistic approach for rock wedge failure. Engineering Geology, 59(3–4), 233–251.

Popescu, M. E. (2002). Landslide causal factors and landslide remediatial options. 3rd International Conference on Landslides, Slope Stability and Safety of Infra-Structures, 61–81.

Pradhan, S. P., & Siddique, T. (2020). Stability assessment of landslide-prone road cut rock slopes in Himalayan terrain: A finite element method based approach. J Rock Mech Geotech Eng 12 (1): 59–73.

Raghuvanshi, T. K. (2019). Plane failure in rock slopes–A review on stability analysis techniques. Journal of King Saud University-Science, 31(1), 101–109.

Raghuvanshi, T. K., Ibrahim, J., & Ayalew, D. (2014). Slope stability susceptibility evaluation parameter (SSEP) rating scheme–an approach for landslide hazard zonation. Journal of African Earth Sciences, 99, 595–612.

Rahim, A., Nasae, T. M., Hareyani, Z., Ngoroyemoto, T. F. K., Hasim, I., Sapawie, M. F., & Hussin, H. (2022). Evaluation of the effect of rock joints on the stability of underground tunnels. IOP Conference Series: Earth and Environmental Science, 1071(1), 12006.

Ramana, K. V. (1993). Humid tropical expansive soils of Trinidad: their geotechnical properties and areal distribution. Engineering Geology, 34(1–2), 27–44.

Rashid, A. S. A., Kalatehjari, R., Hashim, N. A., Yunus, N. M., & Noor, N. M. (2017). Determination of soil specific gravity by using partially vacuum and shaking methods. Journal of The Institution of Engineers (India): Series A, 98, 25–28.

Rasti, A., Pineda, M., & Razavi, M. (2020). Assessment of soil moisture content measurement methods: Conventional laboratory oven versus halogen moisture analyzer. Journal of Soil and Water Science, 4(1), 151–160.

Regmi, A. D., Yoshida, K., Nagata, H., Pradhan, A. M. S., Pradhan, B., & Pourghasemi, H. R. (2013). The relationship between geology and rock weathering on the rock instability along Mugling–Narayanghat road corridor, Central Nepal Himalaya. Natural Hazards, 66, 501–532.

Rocscience,2004. Dip 6.0, https://www.rocscience.com/software/dips

Rocscience,2004. Rocdata 3.0, https://www.rocscience.com/software/rocdata

Rocscience,2004. Slide 6.0 https://www.rocscience.com/software/slide

Rocscience,2004.Rocplane 2.0 https://www.rocscience.com/software/rocplane

Sadagah, B. (2014). Rock Slope Stability Problem Modeling and Remediation of the Arabian Shield Rocks: A Case Study From Werka Descent Road West of Saudi Arabia. The Open Geology Journal, 8(1).

Salmanfarsi, A. F., Awang, H., & Ali, M. I. (2020). Rock mass classification for rock slope stability assessment in Malaysia: a review. IOP Conference Series: Materials Science and Engineering, 712(1), 12035.

Searom, G. (2017). Landslide hazard evaluation and zonation in and Around Hagereselam Town. Addis Ababa University, Ethiopia.

Shariati, M., & Fereidooni, D. (2021). Rock slope stability evaluation using kinematic and kinetic methods along the Kamyaran-Marivan road, west of Iran. Journal of Mountain Science, 18(3), 779–793.

Sharma, B., & Bora, P. K. (2015). A study on correlation between liquid limit, plastic limit and consolidation properties of soils. Indian Geotechnical Journal, 45, 225–230.

Sharma, R. K., Mehta, B. S., & Jamwal, C. S. (2013). Cut slope stability evaluation of NH-21 along Nalayan-Gambhrola section, Bilaspur district, Himachal Pradesh, India. Natural Hazards, 66, 249–270.

Shepheard, C. J., Vardanega, P. J., Holcombe, E. A., Hen-Jones, R., & De Luca, F. (2019). Minding the geotechnical data gap: appraisal of the variability of key soil parameters for slope stability modelling in Saint Lucia. Bulletin of Engineering Geology and the Environment, 78, 4851–4864.

Sidle, R., & Ochiai, H. (2006). Processes, prediction, and land use. Water Resources Monograph. American Geophysical Union, Washington, 525.

Singh, T. N., Singh, R., Singh, B., Sharma, L. K., Singh, R., & Ansari, M. K. (2016). Investigations and stability analyses of Malin village landslide of Pune district, Maharashtra, India. Natural Hazards, 81, 2019–2030.

Spencer, E. (1967). A method of analysis of the stability of embankments assuming parallel inter-slice forces. Geotechnique, 17(1), 11–26.

Stark, T. D., Choi, H., & McCone, S. (2005). Drained shear strength parameters for analysis of landslides. Journal of Geotechnical and Geoenvironmental Engineering, 131(5), 575–588.

Stead, D., & Wolter, A. (2015). A critical review of rock slope failure mechanisms: the importance of structural geology. Journal of Structural Geology, 74, 1–23.

Taheri, A. (2013). Design of rock slopes using SSR classification system.

Tefera, M., Chernet, T., & Haro, W. (1996). Explanation of the geological map of Ethiopia. Geological Survey of Ethiopia.

Terzaghi, K., Peck, R. B., & Mesri, G. (1996). Soil mechanics in engineering practice. John wiley & sons.

Ullah, S., Khanb, M. U., & Rehmana, G. A. (2020). Brief review of the slope stability analysis methods. Geological Behavior (GBR), 4(2), 73–77.

Vásárhelyi, B. (2009). A possible method for estimating the Poisson's rate values of the rock masses. Acta Geodaetica et Geophysica Hungarica, 44, 313–322.

Vatanpour, N., Ghafoori, M., & Talouki, H. H. (2014). Probabilistic and sensitivity analyses of effective geotechnical parameters on rock slope stability: a case study of an urban area in northeast Iran. Natural Hazards, 71(3), 1659–1678.

Vinod, B., & Brislin, J. (2017). Finite Control Set based Optimized Model Predictive Current Control of Four-leg Shunt Active Power Filter. Journal of Control Engineering and Applied Informatics, 19(1), 67–76.

Woldearegay, K. (2013). Review of the occurrences and influencing factors of landslides in the highlands of Ethiopia: With implications for infrastructural development. Momona Ethiopian Journal of Science, 5(1), 3–31.

Wyllie, D. C., & Mah, C. (2004a). Rock slope engineering. CRC Press.

Wyllie, D. C., & Mah, C. (2004b). Rock slope engineering. CRC Press.

You, G., Mandalawi, M. Al, Soliman, A., Dowling, K., & Dahlhaus, P. (2018). Finite element analysis of rock slope stability using shear strength reduction method. Soil Testing, Soil Stability and Ground Improvement: Proceedings of the 1st GeoMEast International Congress and Exhibition, Egypt 2017 on Sustainable Civil Infrastructures 1, 227–235.

Zare, M., & Jimenez, R. (2015). On the development of a slope instability index for open-pit mines using an improved systems approach. ISRM Regional Symposium-EUROCK 2015.

Zhang, Q., Huang, X., Zhu, H., & Li, J. (2019). Quantitative assessments of the correlations between rock mass rating (RMR) and geological strength index (GSI). Tunnelling and Underground Space Technology, 83, 73–81.

Zhu, H.-H., Shi, B., Yan, J.-F., Zhang, J., & Wang, J. (2015). Investigation of the evolutionary process of a reinforced model slope using a fiber-optic monitoring network. Engineering Geology, 186, 34–43.

APPENDICES

Appendix A: Estimated shear strength parameters of rock mass using RocData software for the critical slope sections of rocks

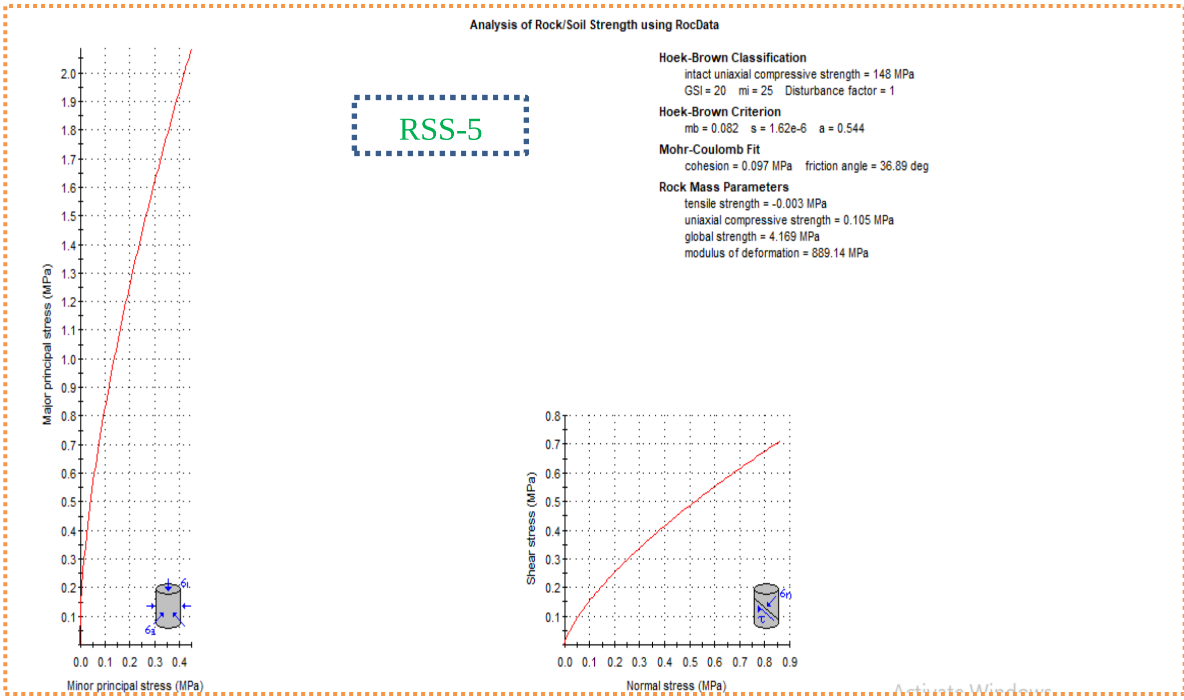

Appendix B: The evaluated shear strength parameters critical failure planes (joints) using Barton Bandis

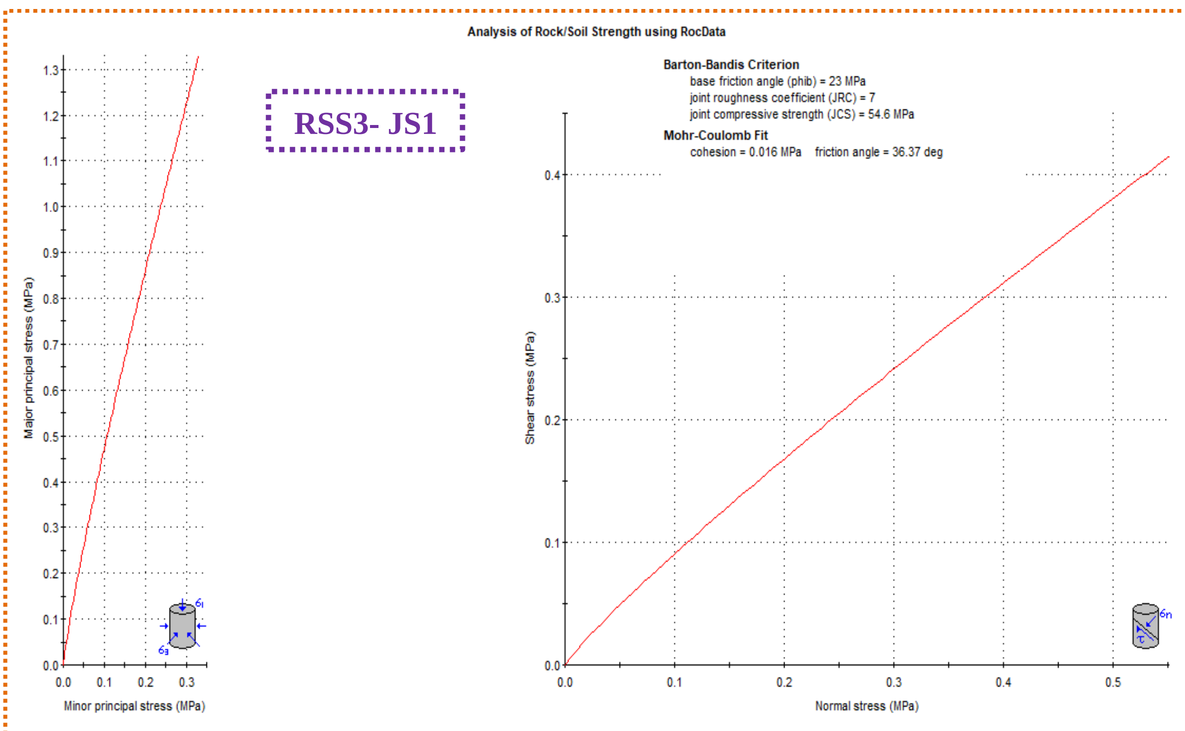

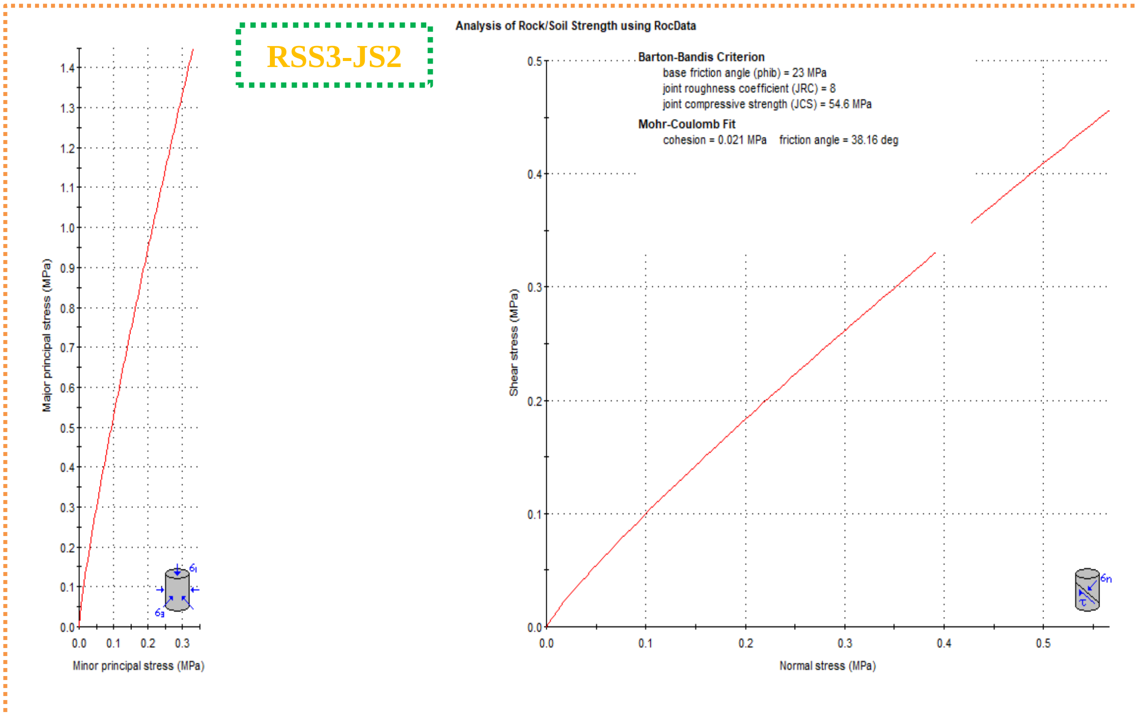
RSS3-JS2
Analysis of Rock/Soil Strength using RocData
Barton-Bandis Criterion
base friction angle (phib) = 23 MPa
joint roughness coefficient (JRC) = 8
joint compressive strength (JCS) = 54.6 MPa
Mohr-Coulomb Fit
cohesion = 0.021 MPa friction angle = 38.16 deg
Major principal stress (MPa)
Minor principal stress (MPa)
Shear stress (MPa)
Normal stress (MPa)

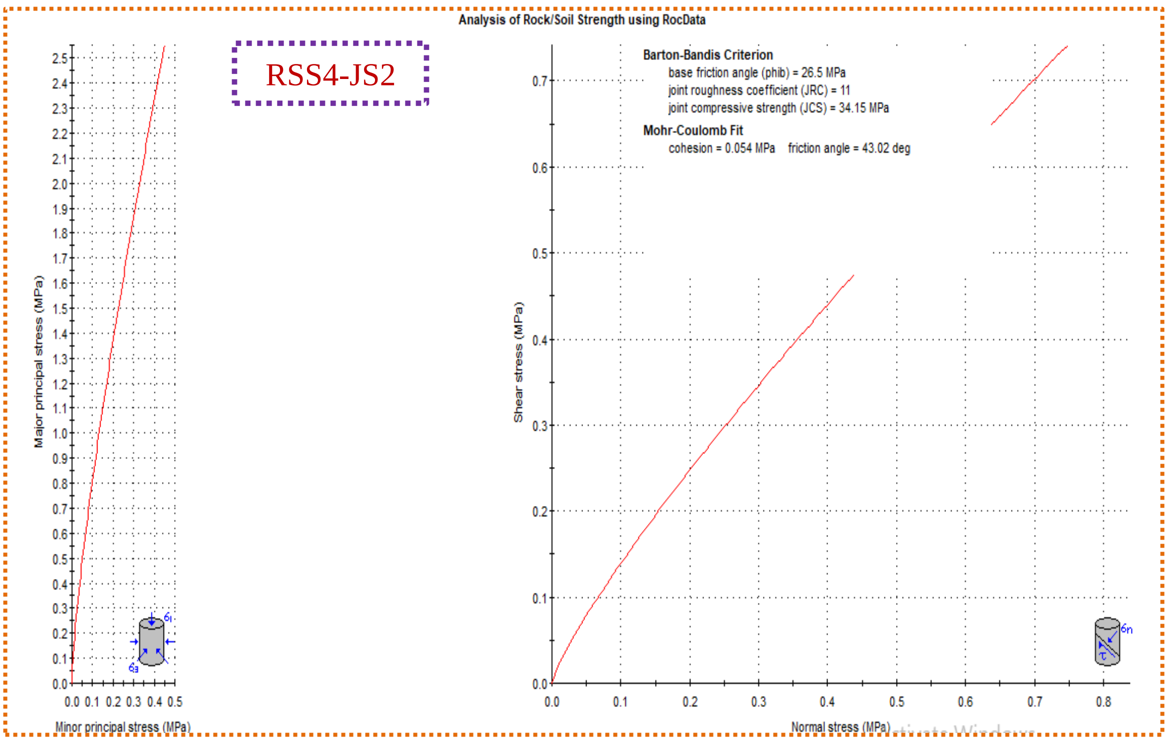
RSS4-JS2
Analysis of Rock/Soil Strength using RocData
Barton-Bandis Criterion
base friction angle (phib) = 26.5 MPa
joint roughness coefficient (JRC) = 11
joint compressive strength (JCS) = 34.15 MPa
Mohr-Coulomb Fit
cohesion = 0.054 MPa friction angle = 43.02 deg
Major principal stress (MPa)
Minor principal stress (MPa)
Shear stress (MPa)
Normal stress (MPa)

Appendix C: Dry unit weight of rock sample collected from a field in laboratory results

Sample Id	Slope section rocks	M (g)	V1(ml)	V2(ml)	V2- V1 (ml)	P= M/V g/cm3	= p*g KN/m3	Average e of dry density
S3-01	RSS3	382.4	520	600	130	2.94	28.81	24.25
S3-02		382.1	505	650	145	2.63	25.77	
S3-03		223.0	566	650	134	1.66	16.26	
S3-04		214.1	520	700	80	2.67	26.16	
S4-01	RSS4	257.7	495	600	105	2.45	24.01	25.1
S4-02		157.7	500	570	70	2.25	22.05	
S4-03		198.6	600	670	70	2.83	27.73	
S4-04		278.1	598	700	102	2.72	26.65	
S5-01	RSS5	217.6	508	600	92	2.36	23.13	23.4
S5-02		284.5	375	500	125	2.28	22.34	
S5-03		203.2	400	480	80	2.54	24.89	

Appendix D: Saturated unit weight of rock sample collected from field in laboratory results

Sample Id	Slope section rocks	M (g)	V1(ml)	V2(ml)	V2- V1 (ml)	P= M/V g/cm3	= p*g KN/m3	Average e of saturated density
S3-01	RSS3	387.2	562	650	130.5	2.96	29.0	26.1
S3-02		382.1	510	650	140	2.73	26.8	
S3-03		227.0	566	700	124	1.83	17.9	
S3-04		220.5	530	600	70	3.15	30.87	
S4-01	RSS4	260.7	500	600	100	2.6	25.5	26.8
S4-02		159.9	500	565	65	2.46	24.1	
S4-03		200.8	600	665	65	3.1	30.4	
S4-04		281.5	600	700	100	2.8	27.4	
S5-01	RSS5	219.9	515	600	85	2.6	25.48	25.5
S5-02		286.5	380	500	120	2.4	23.5	
S5-03		206.4	400	475	75	2.8	27.4	

Appendix E: Geological strength index (GSI) Values estimated in the field based on the weathering condition of discontinuity surface, rock mass structure, and interlocking of rock blocks in successive site visits as proposed by a chart for GSI, Hoek and Marinos, 2000,

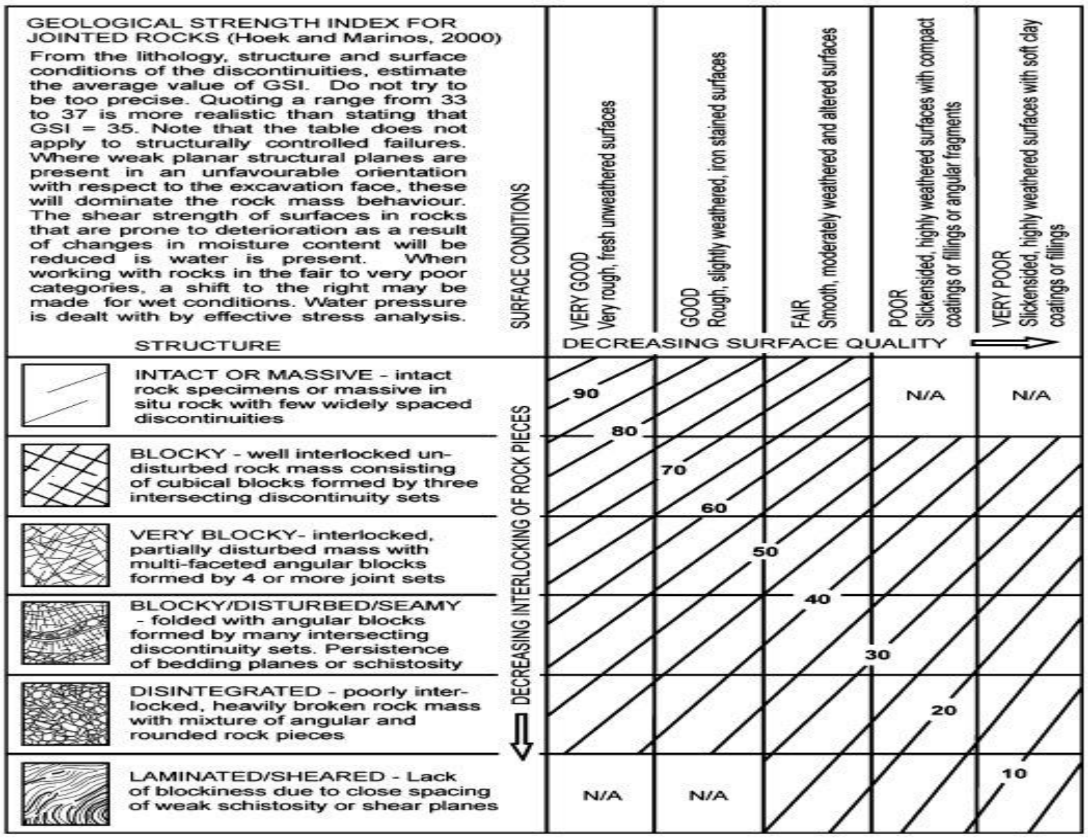

Appendix F: Point Load Test Results

Sample ID	Rock Types	W1(mm)	W2(mm	D(mm)	Ave.w(mm)	De(mm)	De2(mm2)	De/50	A(mm2)	P	Is Mpa	IS(50)	UCS(Mpa)
RSS3-01	Granite	77	56	53	66.5	67	4489	1.34	3524.5	21160	4.7	5.36	139
RSS3-02		78	72	62	75	79.7	6352.1	1.59	4650	24050	3.78	4.66	
RSS3-03		79	100	48	89.5	79.1	6256.8	1.58	4296	28860	4.6	5.65	
RSS3-04		80	67	64	73.5	79.2	6272.6	1.58	4704	38480	6.13	7.5	
RSS4-01	Basalt	69	51	78	60	77.2	5959.8	1.54	4680	14430	2.42	2.94	95
RSS4-02		77	56	45	66.5	61.7	3806.89	1.2	2992.5	17320	4.55	4.94	
RSS4-03		96	85	78	90.5	94.8	8987.04	1.89	7059	24050	2.68	3.57	
RSS4-04		73	55	63	64	71.6	5126.56	1.4	4032	19240	3.75	4.36	
RSS5-01	Rhyolite	81	66	52	73.5	69.8	4872.04	1.4	3822	24050	4.94	5.75	148
RSS5-02		87	75	68	81	83.7	7005.69	1.67	5508	38480	5.49	6.9	
RSS5-03		87	56	32	71.5	50.1	2510.01	1	2288	14430	5.75	5.75	

Appendix G: Soil Particle Size Analysis Result (Sieve)

Sieve No	Test pit location SS1		Test pit location SS2	
	Opening (mm)	% passing	Opening (mm)	% Passing
4	4.75	98.9	4.75	98.2
10	2.00	93.0	2.00	97.7
16	1.18	79.8	1.18	97.3
30	0.6	65.5	0.6	96.6
40	0.425	59.3	0.425	95.9
50	0.3	54.9	0.3	94.9
100	0.15	49.1	0.15	92.2
200	0.075	46.6	0.075	90.7

Appendix H: Soil Particle Size Analysis Result (Hydrometer) for test pit 1

Elapsed Time in (min)	Actual Hyd. Reading (Ra)	Corr.Hydr.Reading (Rc)	Effe. Depth of Hydr. L (cm), from table	Values of K	Diameter of soil Particle D(mm)	% finer insuspension [P]	Adjusted Percen.Finner(%) PA
0.5	40.0	29	9.7	0.0127	0.056	87.293	40.713
1	38	28	10.1	0.0127	0.040	83.261	38.833
2	36	27	10.4	0.0127	0.029	79.229	36.952
4	35	28	10.5	0.0127	0.021	77.213	36.012
8	34	31	10.7	0.0127	0.015	75.197	35.072
15	32	36	11.1	0.0127	0.011	71.165	33.191
30	30	49	11.4	0.0127	0.008	67.133	31.311
60	28	77	11.7	0.0127	0.006	63.101	29.430
120	27	136	11.9	0.0127	0.004	61.085	28.490
240	25	254	12.2	0.0127	0.003	57.053	26.609
480	24	493	12.4	0.0128	0.002	54.432	25.387
960	22.0	971	12.7	0.0128	0.001	50.400	23.507
1440	21	1450	12.9	0.0128	0.001	48.384	22.566
2880	20	2889	13	0.0130	0.001	45.763	21.344

Appendix I: Soil Particle Size Analysis Result (Hydrometer) for test pit 2

Elapsed Time in (min)	Actual Hyd. Reading (Ra)	Corr.Hydr.Reading (Rc)	Effe. Depth of Hydr. L (cm), from table	Values of K	Diameter of soil Particle D(mm)	% finer insuspension [P]	Adjusted Percen.Finner(%) PA
0.5	42.0	46	9.4	0.0129	0.056	92.030	83.453
1	41	45	9.6	0.0129	0.040	90.014	81.625
2	40	44	9.7	0.0129	0.028	87.998	79.797
4	38	42	10.1	0.0129	0.020	83.966	76.141
8	36	40	10.4	0.0129	0.015	79.934	72.485
15	35	39	10.5	0.0129	0.011	77.918	70.656
30	34	38	10.7	0.0129	0.008	75.902	68.828
60	31.5	35	11.1	0.0129	0.006	70.510	63.938
120	30	33	11.4	0.0130	0.004	67.133	60.876
240	28.5	32	11.5	0.0131	0.003	63.806	57.860
480	24	27	12.4	0.0128	0.002	54.432	49.359
960	22.0	25	12.7	0.0128	0.001	50.400	45.703
1440	21	24	12.9	0.0128	0.001	48.384	43.875
2880	20	22	13	0.0134	0.001	45.158	40.950

Appendix J: Atterberg limit test results at SS2 and SS1

Test pit 1= (1m) at SS1	Liquid limit tests				Plasticity limit tests		
Trial no	1	2	3	4	1	2	3
Can code	LT1	LT2	LT3	LT4	PL1	PL2	PL3
No of blows	19	23	28	33			
Weight of can (gm)	24.1	23.9	24.1	24	24.1	24.6	24.1
Weight of can +wet soil	62.7	52.3	57.9	50	28.1	29.8	28.3
Weight of can+ oven-dry soil	49.6	43	47.2	41.9	27	28.3	27.1
Weight of solid soil	25.5	19.1	23.1	17.9	2.9	3.7	3
Weight of water	13.1	9.3	10.7	8.1	1.1	1.5	1.2
Water content (%)	51.37	48.97	46.32	45.25	37.9	40.5	40
	Average of (LL)	=48.23			Average of (PL)=39.49		
PI	PI=8.7%						

Test pit 1= (1m) at SS2	Liquid limit tests				Plasticity limit tests		
Trial no	1	2	3	4	1	2	3
Can code	LT1	LT2	LT3	LT4	PL1	PL2	PL3
No of blows	19	22	26	30			
Weight of can (gm)	24.1	24	24.2	23.6	39.5	26.9	23.4
Weight of can +wet soil	62.7	59.2	59.5	52.4	44.5	30.8	27.1
Weight of can+ oven-dry soil	47	45.4	45.9	41.7	43	29.6	26
Weight of solid soil	22.9	21.4	21.7	18.1	3.5	2.7	2.6
Weight of water	15.7	13.8	13.6	10.7	1.5	1.2	1.1
Water content (%)	68.56	64.48	62.67	59.11	42.86	44.44	42.3
	Average of (LL)	=63.10			Averag of (PL)=43.2		
PI	PI=19.9%						

Appendix K: Natural Moisture contents of soil results (NMC) slope section SS1 and SS2

Determination no for pit 1 at SS1	Test, 1	Test,2	Test,2
Can code	P1T1	PIT2	PIT3
Weight of container(W1) g	23.3	24.4	23.4
Weight of container + wet soils (W2)	94.5	94.2	97.2
Weight of container + oven-dry soil(W3)	85.9	85.8	88.3
Weight of dry soil	62.4	61.4	64.9
Weight of water	8.6	8.4	8.9
Water content(w%)	13.73	13.68	13.71
Average of water contents (W%)	Av(w%) =13.7%		

Determination no for pit 1 at SS2	Test, 1	Test,2	Test,2
Can code	P1T1	PIT2	PIT3
Weight of container(W1) g	23.9	24	23.5
Weight of container + wet soils (W2)	88.6	88	86
Weight of container + oven-dry soil(W3)	72.8	72.2	70.6
Weight of dry soil	48.9	48.2	47.1
Weight of water	15.8	15.8	15.4
Water content(w%)	32.31	32.78	32.69
Average of water contents (W%)	Av(w%) =32.6%		

Appendix L: Specific Gravity test results

Determination no for pit 1 (SS1)	Test 1 (G1)	Test 2(G2)
Container code	1	2
Mass of density bottle + soil+ Water	376.1	372.4
Mass of density bottle + water	344.6	340.9
Weight of dry soil (g)	50	50
Specific gravity	2.7	2.7
Average of Specific Gravity (G1+G2+G3)/3	Ave (Gs) = 2.73	

Determination no for pit 1 (SS2)	Test 1 (G1)	Test 2(G2)
Container code	1	2
Mass of density bottle + soil+ Water	375.6	371.7
Mass of density bottle + water	344.6	340.9
Weight of dry soil (g)	50	50
Specific gravity	2.63	2.60
Average of Specific Gravity (G1+G2+G3)/3	Ave (Gs) = 2.6	

Appendix M: Compaction test results at SS1 and SS2

Pit location at SS1	Test 1	Test 2	Test 3	Test 4	Test 5
Mass of Molds (g)	4321.1	4321.1	4321.1	4321.1	4321.1
Mass of mold + compacted soil (g)	5590.8	5900.8	6273.1	6130.5	5745.6
Mass of compacted soil,g	1269.7	1579.7	1952	1809.4	1424.5
Mass of container	24.3	24.3	24.3	23.6	24.1
Mass of containers + wet soil (g)	54.8	59	62.9	86.9	67
Mass of container +dry soil (g)	52.2	54.3	56.3	72.8	56.1
Mass of water (g)	2.6	4.7	6.6	14.1	10.9
Mass of dry soil,g	27.9	30	32	49.2	32
Water content %	9.3	15.6	20.6	28.6	34.06
Wet Density (g/cm3)	1.35	1.68	2.07	1.92	1.51
Dry Density (g/cm3)	1.23	1.45	1.71	1.49	1.13

Pit location at SS2	Test 1	Test 2	Test 3	Test 4	Test 5
Mass of Molds (g)	4321.1	4321.1	4321.1	4321.1	4321.1
Mass of mold + compacted soil (g)	5587.1	5757.8	5962.5	5901.1	5865.1
Mass of compacted soil,g	1266.2	1406.7	1641.4	1580	1544
Mass of container	24	24.2	24.2	24.5	24.5
Mass of container + wet soil (g)	61.9	80.1	60.9	64.4	73.9
Mass of container +dry soil (g)	58.4	71.9	53.3	54.3	59.1
Mass of water (g)	3.5	8.2	7.6	10.1	14.8
Mass of dry soil,g	34.4	47.7	29.1	29.8	34.6
Water content %	10.17	17.19	26.12	33.89	42.77
Wet Density (g/cm3)	1.34	1.49	1.74	1.67	1.64
Dry Density (g/cm3)	1.22	1.27	1.38	1.25	1.15

Slope sections	Depth (m)	The percentage of soil particles		
		% Gravel	% Sand	% Of Silt and Clay
SS1	1	1.15	52.21	46.64
SS2	1.5	1.75	6	92.19

Appendix N: Direct shear test results at SS1

Horizontal displacement (mm)	Shear load (N) 100kpa	Shear load (N) 200kpa	Shear load (N) 300kpa
0.0	0.0	0.0	0.0
1	7.6	13.2	24.1
1.5	11	18.7	28.5
2	14	23.2	32.4
2.5	17.3	26.8	36.1
3.0	20.4	29.7	41.3
3.5	22.4	33.4	45.2
4	24.6	37.4	47.5
4.5	26	41.2	49.5
5	27.4	44.1	51.3
5.5	28.5	46.5	53.1
6	29.5	48.2	54.9
6.5	31	49.9	57
7	31	50.4	59.9
7.5	31.2	51.3	61.5
8	32	52.2	63.1
8.5	32.3	52.9	64
9	32.7	53.5	64.3
9.5	33	53.9	65.4
10	33.4	53.6	67.3
10.5	34		68.5
11			69.1

Direct shear test results at SS2

Horizontal displacement (mm)	Shear load (N) 100kpa	Shear load (N) 200kpa	Shear load (N) 300kpa
0.0	0.0	0.0	0.0
1	17.3	27.6	30.8
1.5	20.3	34.3	43.1
2	22.4	38.5	53.8
2.5	24.9	43.7	65.6
3.0	28.1	48.5	74
3.5	30.7	53.7	80.4
4	33.3	58	83.7
4.5	35.6	61.4	
5	37.8	64	85.9
5.5	39.3	66.6	87.7
6	39.9	69	88.2
6.5	40.8	71.8	90.1
7	41.6	73.8	91.5
7.5	42.2	75.8	92.8
8	43	77.5	95.9
8.5	43.5	79	97.2
9	44.4	80	100
9.5	45.1	80.7	103
10	45.7	80	
10.5	46.3	80	
11	46.4	79	

SS1

Tests	Normal Stress, kPa	Shear Stress, kPa	Cohesion	Friction angle(ϕ)
1	100	34.05	17	10.07
2	200	53.95		
3	300	69.57		

SS2

Tests	Normal Stress, kPa	Shear Stress, kPa	Cohesion	Friction angle(ϕ)
1	100	47.21	21	15.66
2	200	80.74		
3	300	103.29		

Appendix O:unit weight test results at SS1 and SS2

Sample name	SS-1	
Trial N0	1	2
Mold weight +sample (gm)	3631.2	3629.8
Mold weight (gm)	3339.2	3339.2
Sample weight (gm)	292	290.6
Mold volume (Cm3)	196.25	196.25
Bulk density(g/cm3)	1.49	1.48
Average bulk density	1.48	
Wet unit weight(KN/m3)	14.56	
Moisture content (%)	32.60	
Dry density (g/cm3)	1.12	1.12
Dry Unit weight(KN/m3)	11.00775283	

Sample name	Jinka SS-9	
Trial N0	1	2
Mold weight +sample (gm)	3686.9	3683.7
Mold weight (gm)	3339.2	3339.2
Sample weight (gm)	347.7	344.5
Mold volume (Cm3)	196.25	196.25
Bulk density(g/cm3)	1.77	1.76
Average bulk density	1.76	
Wet unit weight(KN/m3)	17.30	
Moisture content (%)	13.17	
Dry density (g/cm3)	1.57	
Dry Unit weight(KN/m3)	15.35793117	

Appendix P: Temperature recorded in the study area (1970-2021)

NAME	TMPMIN	YEAR	Jan	Feb	Mar	Apr	May	Jun	Jul	Aug	Sep	Oct	Nov	Dec
Jinka	TMPMIN	1970					16.4	15.9	15.6	15.9	15.5	16	12.7	13
Jinka	TMPMIN	1971	14.7	15.3	16.8	16	15.7	15.7	15.2	14.8	15.3	15.6	14	12.2
Jinka	TMPMIN	1972	14.2	15	15.8	16.9	16.3	15	15.6	15.2	15.4	15.8	15	14.1
Jinka	TMPMIN	1973	14.9	15.6	16.7	17.5	16.7	16.4	15.8	15.8	15.4	16.5	14.8	11.8
Jinka	TMPMIN	1974	13.6	14.9	16.6	16	16.2	15.6	15.2	15.8	15.3	15.5	12.6	12.8
Jinka	TMPMIN	1975			16.8	17	16.2	15.2	15.1	15	15.2	15.6	13.9	13.3
Jinka	TMPMIN	1976	14.3	15.9	16.5	16.2	16.4	15.2	15.2	15.2	15.9	16.1	15.8	17.8
Jinka	TMPMIN	1977	19.4	19.2	20.3	19.6	18.8	15.7		15.4	15.5	16.2	14.5	13.8
Jinka	TMPMIN	1978	13.3	15.3	15.9	16.2	16.3	15.8	15.4	15.3		15.6	14.5	14.3
Jinka	TMPMIN	1979	15.7	15.6	16.5	16.9	16.9		15.8	15.7	16.3	17.1	15.1	
Jinka	TMPMIN	1980	16		18.2	17.5	16.8	16.3	16	16.1	16.7	16.8	15.5	14.5
Jinka	TMPMIN	1981	14.8	15.5	17.2	16.5	16	15.1	15.4	15.2	15.2	16.1		14.3
Jinka	TMPMIN	1982	16.1	17	17.1	16.4	16.4	16.1	15.4	14.9	14.9	14	14.2	14.1
Jinka	TMPMIN	1983	14.9	17.2	17.9	17.7	17.2	16.9	15.5	15.2	15.2	15.8	15.7	15.3
Jinka	TMPMIN	1984	16	16.2	18.3	17.8	17.5	16.9	15.7	13.8		14.5	11.5	12.2
Jinka	TMPMIN	1985	14.2	14.9	14.4	15.1	14.4	14.6	14.8	14.2	13.5	13.3	14.5	14.7
Jinka	TMPMIN	1986	14.9	15.5	15.4		15.3	15.3	15.2	15.2			13.7	14.6
Jinka	TMPMIN	1987	14.5	15.8	17.6	17.1	17.3	16.9	16.9	17	17.4	17.7	16.1	15.3
Jinka	TMPMIN	1988	16.6	17.4	18	17.8	17.5	16.8	16.2	16.5	16.6	17.9	14.6	14
Jinka	TMPMIN	1989	14.2	15.4	16.9	16.6	16.2	16.2	15.7	15.6	16.3	16.4	15.6	16
Jinka	TMPMIN	1990	15	17.1	16.6	17	17.1		15.3	16.5	16.1	16.2	14.8	14.3
Jinka	TMPMIN	1991	15.2	16.4	16.4	16.5			15.8	15.9	16.2	16	15.1	13.6
Jinka	TMPMIN	1992	14.3	16.3	16.9	17.1	16.7	16.5	15.6	15.8	16	16.3	14.4	15.4
Jinka	TMPMIN	1993	15.3	15.1	14.8	17.4	16.8	17	15.8	15.7	16.2	16.8	14.5	14.3
Jinka	TMPMIN	1994	14.3	16.1	17.4	17.1	16.9	16	15.7	16.5	16.7	15.6	15.5	14.3
Jinka	TMPMIN	1995	14.1	15.2	16.7	17.2	16.6	16.3	16	16.5	16.7	16.2	14.5	
Jinka	TMPMIN	1996		16.1	16.5	16.8	17.4		15.5	15.9	16.2	15.4	13.3	13.2
Jinka	TMPMIN	1997	14.4	15.8		17.1	17.6	16.1	15.4	15.7	16.1	16.4	16.2	15.3
Jinka	TMPMIN	1998	15.6	15.7	16.7	17.6	17	16	16.5	16.2	16.9	16.4	14	12.9
Jinka	TMPMIN	1999	14.4	14.8	16.4	16.5	16.3	15.9	15.2	15.9	15.9	16.2	14.5	14.1
Jinka	TMPMIN	2000	14.1	14.1	16.7	17.2	17	16.3	15.8	15.4	16.6	16.2	14.4	14.1
Jinka	TMPMIN	2001	14.2	15.2	16.4	16.9	17.1	16.2	15.9	16.2	16.1	16.6	14.9	14.6
Jinka	TMPMIN	2002	15.8	14.7	16.8	17.2	16.7	15.8	16	16	16.3	16.6		

NAME	TMPMIN	YEAR	Jan	Feb	Mar	Apr	May	Jun	Jul	Aug	Sep	Oct	Nov	Dec
Jinka	TMPMIN	2003	14.7	16.2	16.9	17.3	17.4	16.9	16.5	16.6	16.9	16.3	16.1	14.1
Jinka	TMPMIN	2004	15.9	15.7	17.3	17.5	17	17.1	15.9	16.9	16.9	16.4	16.3	15.4
Jinka	TMPMIN	2005	14.9	15.7	17.9	17.9	17	16.7	16.4	16.4	17	16.9	15.3	12.9
Jinka	TMPMIN	2006	15.7	17.2	17.3	17.2	17.6	16.7	16.5	16.8	17.4	17.2	16.2	16.2
Jinka	TMPMIN	2007	15.9	16.6	16.7	17.9	17.9	16.7	16.4	16.5	16.9	16.1	15.6	14
Jinka	TMPMIN	2008	15	15.6	16.7	17.1	17.5	16.7	16.4	16.8	17.4	16.9	15.1	14.2
Jinka	TMPMIN	2009	15	16.9	17.7	18	17.3	16.9	16.6	17.3	17.7	17.3	16	16.4
Jinka	TMPMIN	2010	15.4	17.5	17.2	17.9	18.3	17.2	16.8	16.8	17.2	17.5	15.7	14.8
Jinka	TMPMIN	2011	15.1	16.2	17.6	17.7	18	17.1	16.8	16.9	16.8	16.7	16.4	14.5
Jinka	TMPMIN	2012	14.1	14.1	17.4	17.2	17.2	16.9	16.7	16.2	17	16.8	15.6	15.2
Jinka	TMPMIN	2013	14.9	16.9	18	17.4	17.4	16.9	16.8	16.9	17.3	17.1		14.3
Jinka	TMPMIN	2014	15.8	16.6	17.9	17.4	18.1	17.6	17.7	17	17	17.3	15.7	13.5
Jinka	TMPMIN	2015	13.9	17.5	17.9	17.7	18.2	17.5	17.3	17.6	17.9	18.4	16.8	16.3
Jinka	TMPMIN	2016	16.7	17	18.8	18.9	17.9	17.3	16.8	17	16.4	17.9	14.7	15.1
Jinka	TMPMIN	2017	13.9	17	18.3	18.8	18	18.4	17.6	17.7	17.4	17.9	16.2	13.1
Jinka	TMPMIN	2018	14.5	17.6	17.2	17.2	17.4	16.9	16.9	17	17.4	17.1	16.7	16.2
Jinka	TMPMIN	2019	15.3	16.8	18.5	18.7	18.6	18	17.4	17.1	17.5	17.3	16.9	16.3
Jinka	TMPMIN	2020	16.5	17.3		18	18.1		17	17	17.3	17.4		
Jinka	TMPMIN	2021	15.3	16.7	17.7	17.9	17.6	17.5	17.2		17.9			

NAME	Element	YEAR	Jan	Feb	Mar	Apr	May	Jun	Jul	Aug	Sep	Oct	Nov	Dec
Jinka	TMPMAX	1970					25.7	24.5	24.9	24.1	24.9	25	28.5	29.4
Jinka	TMPMAX	1971	29.3	31	30.4	26.3	25	24.6	24.1	24.2	25.7	25.6	26.8	27.5
Jinka	TMPMAX	1972	29.7	27.9	29.4	26.8	26.4	25	25.2	25.5	26.3	26.3	24.6	27.6
Jinka	TMPMAX	1973	28.6	30.8	31.7	28.3	25.6	25.4	24.7	24.4	25.4	26.5	26.3	29
Jinka	TMPMAX	1974	30.1	30.8	27.9	25.4	24.5	24.9	23.7	25.3	24.5	26.4	28.6	29.9
Jinka	TMPMAX	1975			29.6	25.9	25.9	24.5	24	23.8	25.1	25.1	27.5	30
Jinka	TMPMAX	1976	29.8	29.9	30.1	27	25.6	24.4	24	25.3	25.9	27.5	27	29.5
Jinka	TMPMAX	1977	27.6	28.8	29.3	25.6	25.4	25.6		25.7	26.2	25.3	25.5	27.5
Jinka	TMPMAX	1978	29.2	28.3	25.9	26	25.8	24.6	24.3	24.3		26.3	26.2	27.2
Jinka	TMPMAX	1979	27.8	27.5	27.3	27.3	26.3		26.1	27.1	28	28	27.3	
Jinka	TMPMAX	1980	29.7		29.9	27.9	25.8	26.3	25.9	26.4	28.4	28.7	28.1	30.1
Jinka	TMPMAX	1981	31.1	31.6	28	25.3	25.3	25.7	24.5	26	25.6	27.2		29.8
Jinka	TMPMAX	1982	30.1	30.1	30.9	26.5	25.8	25.9	26.6	26.2	27.1	26.3	25.9	26.4
Jinka	TMPMAX	1983	28.8	29.8	30.8	28.6	26.6	26.6	24.9	23.8	25.1	25.7	26.9	29.3
Jinka	TMPMAX	1984	30.2	31.3	31.5	27.4	26.6	27	26.1	25.3		25.4	24.4	25
Jinka	TMPMAX	1985	27.9	26.4	27.2	24.5	24.6	25.1	25.1	24.2	22.7	26	27	28.8
Jinka	TMPMAX	1986	30	30.3	27.9	24.3	24.7	22.9	25.3	25.2			26.9	26.7
Jinka	TMPMAX	1987	29.3	30.1	28.4	26.7	25.6	24.9	26.1	27	27.7	28.2	28	29.7
Jinka	TMPMAX	1988	28.9	30.8	30.3	27.5	25.4	24.9	24	24.5	24.9	26.1	27.3	28
Jinka	TMPMAX	1989	28.5	27.9	27.8	26.2	25.3	25.6	24.3	25.6	25.3	26.1	27.3	26.3
Jinka	TMPMAX	1990	28	28	26.4	26.6	26.3		25.6	25.3	26.8	26.8	26.4	27
Jinka	TMPMAX	1991	26.4	27.8	28.4	26.7			23.8	25.4	26.2	26	26.7	27.7

NAME	TMPMIN	YEAR	Jan	Feb	Mar	Apr	May	Jun	Jul	Aug	Sep	Oct	Nov	Dec
Jinka	TMPMAX	1992	29.3	29	30.1	27.7	26.4	25.5	24.7	25.3	26.1	25	26.6	25.8
Jinka	TMPMAX	1993	25.7	26.8	29.5	27.3	25.8	24.8	25.4	26.7	28.3	28.1	28.2	29.6
Jinka	TMPMAX	1994	31.2	31.6	29.9	28.4	25.9	25.1	25.1	26	28.1		26.1	27.3
Jinka	TMPMAX	1995	30.7	30	29	27.8	27.8	27.2	25.3	26.6	26	26.3	26.9	
Jinka	TMPMAX	1996		29.2	27.4	26.2	26.9		24.6	25.2	26.7	27.6	28.6	28.9
Jinka	TMPMAX	1997	30.2	30.2		27.2	29.1	26.9	25.3	26.9	29.5	26.7	24.6	25.3
Jinka	TMPMAX	1998	25.6	27.4	28.4	28.1	25.7	25.7	24.8	25.6	27.2	26.6	28.2	30
Jinka	TMPMAX	1999	29.9	31.9	27.8	27.2	27.1	27.5	25.3	26.3	27.3	26.4	28.5	28.2
Jinka	TMPMAX	2000	31.1	32.4	31.7	28.5	27.2	27.1	26.3	25.9	27.9	26.6	28.3	30.2
Jinka	TMPMAX	2001	28.5	30.3	29.1	26.7	27	26	26.2	26.5	27.1	26.7	27.5	29.6
Jinka	TMPMAX	2002	28.9	31.1	28.6	28	26.1	26.5	27.6	27.1	28.6	26.8		
Jinka	TMPMAX	2003	28.3	30.6	29.5	28.2	26	25.8	25.4	25.4	27.3	28	27.9	27.5
Jinka	TMPMAX	2004	28.6	29.5	31	26.9	27.1	27	26.8	26.8	27.3	27.8	26.2	27
Jinka	TMPMAX	2005	28.9	31.7	29.6	28.2	25.7	25.7	25.7	27	27	26.9	27.9	30.8
Jinka	TMPMAX	2006	31.2	30.7	28.4	26.5	26.4	26.7	26.2	25.9	27.2	26.7	25.7	25
Jinka	TMPMAX	2007	26.8	28.4	29.6	27.7	26.6	24.8	25	24.8	26.3	26.9	27.2	29
Jinka	TMPMAX	2008	29.8	30.5	30.1	27.2	27.4	26.4	25.3	26	27	26.1	27.1	29
Jinka	TMPMAX	2009	29.5	31.2	30.8	27.8	27.7	28.2	27.5	28.3	28.1	27.2	28.2	26.9
Jinka	TMPMAX	2010	28.9	29.9	28.2	27.5	26.5	26.4	25.9	26.8	27.4	27.3	29.6	29.6
Jinka	TMPMAX	2011	31.2	32.3	30.7	29.8	27.4	26.2	26.6	26	25.9	26.3	25.1	26.6
Jinka	TMPMAX	2012	29.6	31.5	32	27.6	26.1	25.4	24.8	25.9	25.9	26.9	26.9	27.7
Jinka	TMPMAX	2013	29.3	31.3	29.7	26.7	26.5	26	25.8	26.7	27.1	27.2		29
Jinka	TMPMAX	2014	31.1	30.7	30.6	27.9	27.7	27.3	26.6	26.5	26.7	26.4	27.7	28.8
Jinka	TMPMAX	2015	30.9	32.5	31.4	26.8	27.2	26.5	27.3	28.4	29.8	27.7	26.7	26.4
Jinka	TMPMAX	2016	29.1	31.6	32.4	27.8	26.6	26.6	26.3	27.5	28.6	28.2	28.6	29.8
Jinka	TMPMAX	2017	31.7	30.9	30.9	29.9	27.3	27.7	25.8	26.3	25.9	26.5	26.5	28.9
Jinka	TMPMAX	2018	30.1		27.4	25.8	25.9	25	25.7	26.3	28.1	27.8	28.2	28
Jinka	TMPMAX	2019	31.2	31.9	32.2	29.5	28.5	26	26.1	26.4	27.2	26.1	25.9	26.2
Jinka	TMPMAX	2020	27.5	28.3		27.6	27.1		25.2	26.3	26.7	26.8		
Jinka	TMPMAX	2021	29.7	31.1	32.4	27.6	26.6	27.1	25.3		26.7			

Appendix Q: Rainfall recorded in the study area (1970-2021)

NAME	PRECIP	YEAR	Jan	Feb	Mar	Apr	May	Jun	Jul	Aug	Sep	Oct	Nov	Dec
Jinka	PRECIP	2000	0	0	74.5	183.4	115.3	64.9	83.4	105.3	65.3	257.5	118.2	67.5
Jinka	PRECIP	2001	67.9	39.8	213.5	243.4	180.5	79.9	58.8	35.8	197.2	113.9	162.8	13.3
Jinka	PRECIP	2002	140.6	20.2	177.8	129.1	239.7	23.7	60.6	27.9	97.3	155.1		
Jinka	PRECIP	2003	33.1	42.6	100	216.1	233.4	59.5	62.3	286	80	144.6	132.4	70.6
Jinka	PRECIP	2004	79.3	31.2	56.2	203.7	54.2	60.7	39.5	59.9	127.8	66.5	154.9	92.4
Jinka	PRECIP	2005	62.9	12.5	162.4	154.3	272.8	51.5	56.6	75.5	91.7	105.1	67.2	0
Jinka	PRECIP	2006	17.3	90.4	189.9	189.2	209.2	78.9	19.3	180.7	70.2	279.1	214.9	189.7
Jinka	PRECIP	2007	120.7	102	80.6	241.8	163	374.9	102.4	147.1	126.8	78	117.4	12.7
Jinka	PRECIP	2008	22.8	58.6	81.4	145.1	79.5	126.7	99.1	76.9	178.4	213.6	96.6	20.2
Jinka	PRECIP	2009	65.8	17.8	112.8	188	151.7	39.6	12.2	16.2	140	184.8	85.6	158.2
Jinka	PRECIP	2010	56.5	35.7	211.2	164.8	189.1	83.7	100.6	24.2	78.6	90.2	32.2	37
Jinka	PRECIP	2011	2.1	18.1	80.5	130.3	196.3	97.3	143.5	177.4	157.4	173.3	205.2	58
Jinka	PRECIP	2012	0	5.9	42.4	223.1	194.6	102.7	190.8	172.3	206.5	124.5	138.6	74.5
Jinka	PRECIP	2013	12.4	24	84.1	335.4	58.2	120.4	67.9	80.9	159.1	168.8		20.2
Jinka	PRECIP	2014	19.2	22.2	159.8	159.6	166.6	189.8	133.7	114.2	147	296.9	150.9	5.3
Jinka	PRECIP	2015	0	24.3	72.1	280.6	151.9	97.3	62.2	25.2	62.6	213.9	197.6	182.6
Jinka	PRECIP	2016	24.1	25.8	114.2	288.3	110.6	66	107.5	26.3	27	143.8	111.2	12.2
Jinka	PRECIP	2017	36.1	89.5	70.4	185.9	128.4	11.4	130	183.6	260.1	260.3	166.2	0
Jinka	PRECIP	2018	2.7	128.3	137.8	362.8	243.5	201.5	27.9	111.8	102.6	123.6	63.5	108.4
Jinka	PRECIP	2019	0	14.2	74	211.6	140.1	225.3	145.5	104.1	105.1	218.6	252.3	206
Jinka	PRECIP	2020	89	81.4		259.6	116.4		105.9	158	171	194.7		
Jinka	PRECIP	2021	0.2	45.2	28.1	378.7	188.8	71.6	119.1		138.1			

NAME	PRECIP	YEAR	Jan	Feb	Mar	Apr	May	Jun	Jul	Aug	Sep	Oct	Nov	Dec
Jinka	PRECIP	1970					179.7	153.8	57.2	118.7	143.9	202.5	14.1	20.9
Jinka	PRECIP	1971	33.1	0	52.3	176.8	148	56.9	168.1	166	57.2	133.7	73.2	44.3
Jinka	PRECIP	1972	32.5	87.7	58.2	155.3	233.2	117.8	64.4	171.3	120.4	228.1	277.2	23.3
Jinka	PRECIP	1973	59.4	63	42.2	153.3	149.9	68.7	93.6	125.5	158.9	137.8	194.2	2.8
Jinka	PRECIP	1974	6.7	7.6	174.2	287.3	186.4	68.3		170	136.7	155.6		25.6
Jinka	PRECIP	1975			112.1	182.7	109	142.4	145.3	76.9	121.5	127.2	37.6	16.8
Jinka	PRECIP	1976	23.4	84.5	48.2	236	256.8	126	118.2	129.2	110.9	124.7	74.2	24.6
Jinka	PRECIP	1977	156.1	62.2	98.2	204.5	151.9	116.7		57.8	169.3	342.4	132.6	17.4
Jinka	PRECIP	1978	24.3	209.3	170.3	159	44.2	118.4	155.1	144.2		110.3	187	127
Jinka	PRECIP	1979	56.7	147.1	205.5	122.3	132.9		15.7	37.9	77.6	78.1		
Jinka	PRECIP	1980	10.5		84.6	151.2	193.7	104.7	14.7	25.6	51.8	76.6	130.7	6
Jinka	PRECIP	1981	48.1	44	278.5	232.5	153.9	93.9	162.4	43.7	187.3	184.7		7.3
Jinka	PRECIP	1982	35.5	37.7	86.5	171.3	193.6	71.8	28.9	120.1	174.7	211	266.7	149.8
Jinka	PRECIP	1983		43.7		127.2	120.6				74.8	89.8	120	0
Jinka	PRECIP	1984	0	15	35.9	157.7	104.1	26.9		51.1		34	160.8	
Jinka	PRECIP	1985	26.1	4.3	116.5	268.7	176.8	47	72.5	26.5	38.5	15.5	22	8.2
Jinka	PRECIP	1986	0	13.4	60.1	128.9	216.7	131.8	100.3	161.7			63	91.1
Jinka	PRECIP	1987	15.4	36.5	78.8	164.4	242.2	119.6	34.8	25.6	74.6	55.9	63.1	46.5
Jinka	PRECIP	1988	93	49	71.5	313.9	106.1	218.3	379.1	156.4	142.2	112.7	51.6	5
Jinka	PRECIP	1989	14.2		137.8	173.6	152.2	101.5	234.7	61.8	289.2	155.2	169.6	201.1
Jinka	PRECIP	1990	17.2	238.3	273.2	122.3	130.9		25.2	98	76.7	185.9	128.6	90.1
Jinka	PRECIP	1991	166.9	89.5	122.5	151.6			60.9		118.7	290.9	50.8	29.2
Jinka	PRECIP	1992	16.3	30.9	95.1	190.6	107.3	67.2	87.7	84.8	108.6	221.5	69.6	229.1
Jinka	PRECIP	1993	121.1	46.3	33.2	173.2	259.3	139.9	16.6	12.1	33.8	141.6	55.7	4.4
Jinka	PRECIP	1994	7	4.7	113.5	98.4	249.2	165.5	72.3	92	89.3		247.2	47.8
Jinka	PRECIP	1995	0	63.9	129.2	161.3	108.3	118.1	114.9	33.2	134.2	152.8	115.6	88.1
Jinka	PRECIP	1996	91.7	68.2	218.2	242.2	115.6		178.6	98.3	89.9	82.3	43.3	33.3
Jinka	PRECIP	1997	26.6	10.2			41.3	28.6	173.1	27	37.4	249.4	249.3	199.8
Jinka	PRECIP	1998	201	77.2	83.9	183.6	184.5	207.4	137.4	86.1	50.4	159.1	96.4	17.5
Jinka	PRECIP	1999	35.5	4.2	128.8	171.5	121.4	19.2	74.3	101.6	92.8	151.5	60	33.3

RESEARCH FUND ACKNOWLEDGMENT

This research project is funded by Adama Science and Technology University under grant number ASTU/SM-R/702/23, Adama, Ethiopia.